NASA CR-167,891

NASA CR-167891
MTI 83TR55

NASA

T55 POWER TURBINE ROTOR MULTIPLANE-MULTISPEED BALANCING STUDY

by Michael R. Martin

MECHANICAL TECHNOLOGY INCORPORATED

Prepared for

NATIONAL AERONAUTICS AND SPACE ADMINISTRATION

NASA Lewis Research Center
Contract NAS3-19408

1. Report No.	2. Government Accession No.	3. Recipient's Catalog No.
NASA CR-167891		

4. Title and Subtitle	5. Report Date
T55 POWER TURBINE ROTOR MULTIPLANE-MULTISPEED BALANCING STUDY	February 1982
	6. Performing Organization Code
7. Author(s)	8. Performing Organization Report No.
Michael R. Martin	MTI 83TR55
	10. Work Unit No.
9. Performing Organization Name and Address	
Mechanical Technology Incorporated 968 Albany-Shaker Road Latham, NY 12110	11. Contract or Grant No. NAS3-19408
	13. Type of Report and Period Covered Contractor Report
12. Sponsoring Agency Name and Address National Aeronautics and Space Administration Washington, DC 20546	14. Sponsoring Agency Code

15. Supplementary Notes

Project Manager, David P. Fleming, Structures and Mechnaical Technologies Division, NASA Lewis Research Center, Cleveland, Ohio

16. Abstract

A rotordynamic analysis of the T55-L-11C engine was used to evaluate the balancing needs of the power turbine and to optimize the balancing procedure. As a result, recommendations were made for implementation of a multiplane-multispeed balancing plan.

Precision collars for the attachment of trial weights to a slender rotor were designed enabling demonstration balancing on production hardware. The quality of the balance was then evaluated by installing a high speed balanced power turbine in an engine and running in a test cell at the Corpus Christi Army depot. The engine used had been tested prior to the turbine changeout and showed acceptable overall vibration levels for the engine were significantly reduced, demonstrating the ability of multiplane-multispeed balancing to control engine vibration.

17. Key Words (Suggested by Author(s))	18. Distribution Statement
Balancing High Speed Balancing Rotordynamics	Unclassified - Unlimited

19. Security Classif. (of this report)	20. Security Classif. (of this page)	21. No. of Pages	22. Price*
Unclassified	Unclassified		

* For sale by the National Technical Information Service, Springfield, Virginia 22151

MTI-17983

N83-33894#

TABLE OF CONTENTS

1.0 SUMMARY

This report relates the work accomplished under NASA contract NAS3-19408. The scope of work comprised seven technical tasks with initial efforts beginning in 1975. All work involved the Avco Lycoming T55-L-11C engine. The following items highlight the major areas of work accomplished:

- A Rotordynamic Analysis of both the T55 engine power turbine and gas generator rotor-bearing systems was performed. Lateral critical speeds were calculated for both systems and unbalance distributions in the rotating elements, determined from manufacturing tolerances, were used to investigate the sensitivity of the power turbine to residual unbalance. Standard engine balancing and assembly procedures were reviewed and recommendations were made for implementation of a multi-plane-multispeed balancing procedure.

- Precision balance collars for addition of temporary weights to uniform shafts were designed and tested. A flexible rotor was balanced with the use of two collars for operation through and above two critical speeds. Rotor balance remained satisfactory after equivalent weights were added to the rotor and the collars were removed.

- The ability of multiplane-multispeed balancing procedures to balance production hardware was demonstrated. An existing balancing system was used to acquire and store power turbine response data, calculate influence coefficients and calculate size and location of the required correction weights.

- The analytical model used to calculate the critical speeds and mode shapes was updated based on observations made during the testing. The refined mathematical model was then used to analytically evaluate shaft end and third turbine stage balance planes.

- The quality of the balance achieved in the high speed balancing rig was evaluated by running two power turbine rotors in a test cell engine, and monitoring engine case vibration. The first power turbine was high speed

balanced only prior to testing. It was installed in an engine that had run acceptably with a different (low speed balanced) turbine. The engine was then rerun with the high speed balanced turbine installed and showed a significant decrease in overall vibration, confirming the conclusion of the analytical phase - that high speed balancing is more effective at controlling vibration at the design speed than low speed balancing techniques.

- The effect of drive shaft to power shaft spline fit on the rotordynamic response was experimentally determined. The spline showed no signs of instability or tendency for a dynamic offset.

2.0 INTRODUCTION

Shaft speeds in many gas turbine designs are above one or more critical speeds at which bending of the shaft elastic axis is expected. Such designs are very sensitive to unbalance. This is particularly true when rolling element bearings are utilized because of low system damping. Excessive vibration arises because the rate at which vibration energy is produced is not adequately counterbalanced by the rate at which it is dissipated in the engine. The science which permits this energy balance to be understood and controlled in a complex structure such as a gas turbine is rotordynamics. A rotordynamic analysis of the T55-L-11C engine performed under this contract was used to evaluate the balancing needs of the T55 power turbine and to optimize the procedure. The analytical evaluation of the benefits of high speed balancing as adapted to T55 power turbines formed the basis for the second phase of the program in which the balancing procedures were tested in the laboratory on actual engine hardware which was then given a final evaluation by running in a T55 engine.

The objective of the program was to evaluate both analytically and experimentally the benefits of high speed balancing over low speed balancing as applied to T55 power turbines. The following sections describe the basic techniques used during the analytical and test efforts of this contract.

2.1 Critical Speeds and Mode Shapes

The objective of task 1 was to use a rotordynamic analysis to evaluate power turbine sensitivity to unbalance and to analytically investigate balancing techniques, including the choice of speeds, planes & sensors. After gathering the necessary engine design data (including rotor and bearing assemblies and detailed drawings) a rotor is analytically modeled to depict its mass and elastic characteristics. The analytical effort for the T55-L-11C included identification of lateral critical speeds, unbalance response and balance plane evaluation. A rotor lateral critical speed is the condition in which the rotor speed matches the natural frequency of the rotor bearing system. At such a frequency, the system's mass and elastic properties combine to form a resonant condition in which relatively large amplitudes are possible at low input energy levels.

When the rotor speed is near one of its critical speeds, the rotor will vibrate with amplitudes in a particular mode of vibration. The shape of the elastic axis of the rotor at the critical speed is calculated in terms of relative amplitudes to examine the rotor displacement. This analysis shows the amount of rotor bending, which is an indication of rotor flexibility.

2.2 Rotor Response to Unbalance

While the information obtained from the undamped critical speed map is very useful for evaluating the dynamic behavior of a rotor bearing system, the calculated mode shapes and critical speed map are only intermediate results in a comprehensive vibration analysis. Actual engine vibration results when the rotor is subjected to excitational forces. These forces may be aerodynamic, magnetic, mechanical, etc. By far the most common of such excitations are the unbalance forces present in the rotor, which are distributed along and about the rotor axis based on machining tolerances and rotor assembly procedures. Rotation of the unbalance masses at the speed of the rotor gives rise to forces acting radially outward from the rotor's axis which are proportional to the mass of the unbalance, and to the square of the rotor speed. As a result of these forces, the rotor whirls about the bearing axis. By analyzing the rotor's response to unbalance, these forces and their corresponding bearing loads can be analyzed as the rotor increases in speed. Rotor deflections can be calculated as critical speeds are traversed.

Just as deflections can be calculated for unbalances by this approach, effectiveness of correction weights can also be evaluated. This is done by analyzing the reduction in amplitudes achieved when calculated correction weights are mathematically installed in the model. To mathematically evaluate alternative balancing techniques for the T55, a random distribution of unbalance was included all along the rotor model. The unbalance was modeled using random numbers representing both magnitude and phase. Different methods of calculating the correction weights can be compared:

1. A simple summing of unbalances (which simulates a low speed balance machine)
2. The influence coefficient technique

To calculate T55 influence coefficients using the unbalance response program, a series of rotor response runs was made which sequentially placed a 71.8 gm.cm. (1 in. oz.) unbalance as a trial weight at each balancing plane. The amplitudes and phase at each vibration sensor location and at each balance speed were the input for the influence coefficient program. Once the influence coefficients were determined, amplitude and phase data from the response program were input to the balancing program which calculated the balance correction weights. The calculated balance weights were then added to the unbalance model and their effectiveness evaluated by the corresponding decrease in rotor response amplitudes.

2.3 Testing

The analytical results discussed in this report are only useful when they duplicate both experimental hardware and actual engine characteristics. During the demonstration balancing phase of the project, rotor response data was taken to determine actual rotor critical speeds and mode shapes. This information was then used to tune the mathematical model.

For the balancing demonstration, the power turbine modules were operated in a test rig consisting of a two speed constant speed electric motor, eddy current (variable speed) clutch, step-up gearbox and associated couplings and spindles. Precision collars were utilized for temporary weight addition enabling the development of influence coefficients. A known trial weight was installed successively in each balance plane to determine the sensitivity to unbalance at each plane. The sensitivity or influence coefficients are complex numbers, representing both phase and magnitude. Once they have been determined, balance corrections can be calculated from a single run of the rotor. Five candidate T55-L11C rotors were balanced, demonstrating the ability of multiplane-multispeed balancing to balance production engine hardware.

The following section presents the detailed results of the rotordynamic evaluation and the balancing experiments.

3.0 DISCUSSION

This section relates the results of work accomplished in each technical task authorized under this contract.

3.1 TASK 1 DEVELOPMENT OF CRITERIA FOR MULTIPLANE-MULTISPEED BALANCING

In Task 1, an analytical study was conducted of the dynamics of the T55 engine power turbine and gas generator rotor bearing system. Details of the mathematical model used in the analysis are presented on Figures 3.4.1 thru 3.4.3. Lateral critical speeds were calculated for both systems. Unbalance distributions, determined from manufacturing tolerances, were used to investigate the sensitivity of the power turbine to residual unbalance. Combined support stiffness (bearing in series with structure) of 1.75×10^7 N/M (100,000 lb/in) was used for each of the ball bearings between the power turbine stages, and 1.75×10^8 N/M (1,000,000 lb/in) was used for the roller bearing.

The first critical speed was calculated at 12,070 RPM and the second critical speed at 21,090 RPM. The critical speed map is shown in Figure 3.1.1 and the calculated mode shapes of the power turbine rotor at the first and second critical speeds are presented in Figures 3.1.2 and 3.1.3. At the first critical speed the rotor exhibits maximum amplitudes at the fourth turbine stage. The mode shape for the second critical speed shows significant bending with peak amplitudes at the rotor midspan.

The sensitivity of the power turbine rotor was next investigated using unbalance combinations derived from manufacturing tolerances. Resulting calculated maximum rotor amplitudes are shown for the power turbine on Figure 3.1.4.

The unbalance distribution used was determined using an 0.05mm radial eccentricity between shaft section and bearing centerline, and with .05 mm wall thickness variations. The resulting unbalance masses were then distributed with random phase angle. Next, it was assumed that standard two plane balancing was performed on each rotor segment, and calculated correction weights for these unbalances were applied to the balancing locations. Unbalance representing the

fourth stage residual unbalance was included to simulate assembly of that stage in the final configuration.

Rotor mode shapes derived from the response calculations for the two critical speeds and for the operating speed are shown in Figures 3.1.5 through 3.1.7. The modes shapes in Figures 3.1.5 and 3.1.6 are associated with the first and second critical speeds, respectively. At those resonances considerable amplitudes are indicated because essentially no damping was modeled at the bearings. The rotor mode shape at operating speed (Figure 3.1.7) indicates a maximum amplitude of approximately 0.2 mm (peak-to-peak) at the rotor mid-span location. Such predicted amplitude appears reasonable, considering the likelihood that most power turbine shafts will probably be of better machined quality than that assumed (at tolerance limits) for this study. A reduction to half of the eccentricity limits used in the calculations would yield a like reduction in rotor amplitudes. It may be noted that the calculated rotor mode shape at its operating speed resembles that of the second critical speed. It is apparent, from the result shown in Figure 3.1.4 that the assumed rotor support stiffness is very nearly optimum. Thus, if the actual value is greater than assumed, vibration amplitudes at the design speed would be larger than those predicted because of an upward shift in the first critical. Similarly, softer supports would bring the second critical down closer to the operating speed.

The proximity of the power turbine rotor operating speed to two critical speeds with distinctly different mode shapes influences the selection of the most effective balancing procedure. Should it prove feasible to traverse the first critical speed with an initially unbalanced rotor (which depends on manufacturing tolerances) a two speed two plane balance procedure would suffice. Alternatively, if large initial amplitudes are encountered at the first critical, the two speed balancing step should be preceded by a single plane step aimed at reducing rotor amplitudes associated with the first critical speed.

3.2 TASK 2: EVALUATION OF PRECISION COLLAR FOR ATTACHING TRIAL WEIGHTS

The experimental evaluation of two precision collars for the attachment of trial weights to a slender rotor had three objectives:

1. Design of a precision collar suitable for high speed operation typical of modern turboshaft engine power turbine rotors.

2. Evaluation of balancing requirements of the collar itself and its effect upon the state of balance achievable in a balance sensitive rotor.

3. Evaluation of general handling characteristics of the collars such as ease of installation, susceptability to misapplication, alignment and holding problems, etc.

The design evaluation of the removable collar concept led to a two-piece configuration machined from solid material and held together by two high strength socket head screws. Precise axial alignment between the two halves is guaranteed by two precision locating pins. Two collars fabricated for evaluation on the engine rotor simulator are shown in Figure 3.2.1. Clearly visable on each of the collars in Figure 3.2.1 are four tapped holes which are intended to accept the trial weights during multiplane-multispeed balancing.

Low speed balancing of the individual collars was accomplished through single plane balancing on a commercial balancing machine. Each collar was balanced on a pre-balanced drill-rod shaft. The roundness tolerance of the shaft which was determined to be approximately 0.003 to 0.005 mm was probably the determining factor of the minimum residual unbalance remaining with each collar. There were no further or special attempts made to reduce residual unbalance levels.

Experience with handling of the collars showed that mounting and dismounting of the collars could be improved by shortening of the alignment pins. No other problems were experienced in repeated balancing operations to 31,000 RPM. A general view of the engine rotor simulator, which served as the test rig for the collar evaluation, is shown in Figure 3.2.2 and a close-up view of both collars mounted on the shaft is given in Figure 3.2.3. The location and numbering of displacement sensors on the rotor is shown in Figure 3.2.4. A detailed description and dynamic analysis of this rig may be found in Reference 1. Balance planes available on the rig include threaded holes, for the addition of

weights allowing the rotor to be balanced (or unbalanced) independent of the collars being tested.

When this rig is operated, large undamped rotor vibration can be observed near the second critical speed which occurs at 21,500 RPM. Rotor response sensitivity at the second critical speed is much higher than that observed at the first critical speed (around 8,000 RPM), and previous balance steps were halted intentionally to leave significant rotor amplitudes at the second critical speed. In evaluation of the balancing collar, emphasis in the experimental tests was on rotor operation through and beyond the second system critical speed.

Test rig rotor amplitudes were recorded as a means of demonstrating that:

- The addition of the two collars to the rotor will not significantly affect rotor balance.

- The intentionally unbalanced test rig rotor can be balanced through two critical speeds with two collars used for the addition of trial weights.

- The rotor will remain satisfactorily balanced when permanent corrections are made and the trial weight collars removed.

Abstracted test results are presented here as before and after amplitudes recorded from displacement sensors located on the rotor (see Figure 3.2.4). Only vertical amplitudes are presented, since rotor orbits were generally circular.

The residual balance condition of the test rig and the change due to the addition of the collars was first investigated. The results are shown in Figure 3.2.5 in which rotor amplitudes at the turbine location are plotted with no collars on the shaft (curve A) with both collars installed (curve B). Addition of the collars increased rotor amplitudes slightly at the critical speed. The difference in amplitudes between test runs with and without balance collars are not considered significant and both conditions were acceptable. Additional

tests indicated the rotor response at the undamped critical speed is not completely repeatable regardless of the presence or absence of the trial weight collars. After these tests the rotor was deliberately unbalanced.

With collars in place, the rotor was balanced twice by the multiplane-multispeed method. For the first balancing run, four balancing planes were utilized on the rotor (Nos. 1, 3, 4, and 5) with data obtained from three sensors (Nos. 1, 4 and 6) at two rotor speeds (19800 and 20500 RPM) by the addition of trial weights in the temporary collars. The obtained rotor balance was satisfactory (Curve B, Figure 3.2.6). and showed some deterioration when the trial collars were removed (Curve C, Figure 3.2.6). The results from this test series serve very well the purpose of demonstrating the maximum expected range of deviation that may appear to be the result of removing the trial weight collars. Variations in shaft and bearing temperatures can cause amplitude variations at resonance that exceed those shown in Figure 3.2.6.

A second independent balance run was conducted from the same initial balance condition, this time using three balance planes (Nos. 3, 4, and 5) with data obtained from probes 3, 4 and 6 at one speed (20500 RPM). The effectiveness of this balance run, shown in Figure 3.2.7, is attributable to the selection of balancing planes, probe locations and balance speed, all of which were chosen as optimum for balancing at the second critical. Upon removal of the balance collars practically no deterioration of rotor balance was observed.

The experimental evaluation of the precision collars intended for temporary weight placement on slender or thin walled shafts during balancing operations has proven the concept practial and convenient to apply. Rotor balancing has been successfully demonstrated with the help of two collars for operation through and above two critical speeds. Rotor operation remained satisfactory after removal of the two collars.

3.3 TASK 3 MULTIPLANE-MULTISPEED BALANCING DEMONSTRATION OF T55 POWER TURBINES

3.3.1 Introduction

The objectives of this task were: to multiplane balance T55 power turbine rotors for operation to the maximum service speed, record rotor influence coefficients, to calculate mean and standard deviation for each influence coefficient, and document times required for various stages of balancing.

Five power turbines were available for testing purposes. Three of the modules were composed of components that were prebalanced as subassemblies. Components of the remaining two were not prebalanced.

The power turbine modules were operated in a specially designed test rig. Vibration was measured by displacement probes located along the length of the power turbine module and associated drive couplings and components. Special balance collars (developed in Task 2) were installed along the length of the power shaft. These collars permitted trial and correction weights to be easily added to the rotor without grinding. An MTI owned Multiplane-Multispeed Balancing System was used to calculate the amount and angular location of balancing weights. All vibrations signals were also tape recorded for later playback, analysis, and plotting.

3.3.2 Balancing Summary

Five power turbine modules were operated in the test rig. Various degrees of success were achieved with each module. These results are outlined as follows:

Rotor No.	Serial Number	Prebalanced ?	Results (max synchronous amplitude, peak to peak)
1	U00257	yes	.064 mm reduced to .051 mm 2.5 mils reduced to 2.0 mils
2	268922	yes	.051 mm reduced to .038 mm 2.0 mils reduced to 1.5 mils
3	268975	yes	.089 mm reduced to .038 mm 3.5 mils reduced to 1.5 mils
4	265503	no	.254 mm reduced to .114 mm 10 mils reduced to 4.5 mils
5	U00559	no	.254 mm reduced to .114 mm 10 mils reduced to 4.5 mils*.

Sections 3.3.4 through 3.3.8 discuss the results of the balancing tests in detail.

The marked influence of the test rig on the vibration signals (see Section 3.3.3) and variability in the vibration signals hindered efforts to combine influence coefficient data from the balancing runs to determine combined influence coefficients. Section 3.3.9 contains a detailed discussion of these efforts.

---

*Seal failure in test rig and prior commitments of the high-speed balancing facility to other NASA projects halted testing.

Extraneous effects from the test rig and drive system also hindered attempts to define various times for balancing. However, some estimates have been made and are presented in Section 3.3.10.

3.3.3 Drive System and Test Rig

The high speed drive system consists of a two speed (1800/3600 RPM) constant speed electric motor, eddy current (variable speed) clutch, step-up gearbox (1:5.5 increase) and associated couplings and spindles. The drive system is fully described in Reference 2.

Although not used during these tests, the facility is capable of 900 Nm (8,000 lb-in) of torque. The drive shaft and couplings are, therefore, very much oversized for use in the T55 application. The large masses of these components proved to be a hindrance to effective high speed balancing of the dynamically sensitive T55 power turbine.

The locations of spin up hardware instrumentation, used to measure vibration, are shown in Figure 3.3.1. Sensors 7 thru 12 were used to measure vibration on drive system components. Balance planes 4 and 5 were used to reduce unbalance vibrations in these components.

The balancing tests were conducted in two phases. Rotor number 3 was run in the first phase. Although the balancing effort for this rotor was successful a number of rig related problems were encountered. Prior to beginning the second phase of balancing tests, the rig hardware was revised to eliminate one spline connection and simplify the drive system. However, problems in the test rig and drive system continued to plague the balancing efforts. Although in retrospect, many of the phenomena witnessed during the tests can be attributed to the rig and drive system, it was very difficult to extract true rotordynamic data from the overall vibration signature while the actual tests were being run. Although much time and effort was expended deciphering the rather confusing data, it is the intent of this report to document only the results as they relate to the task requirements.

Overheating in the drive system clutch limited operation to 10,000 RPM during the second phase of the balancing test. It is suspected that insufficient cooling water to the clutch caused the clutch to overheat. Schedule restraints and prior commitments of the test facility to other NASA projects prohibited investigation and correction of the heating problem. However, the results obtained in the first phase of the balancing efforts demonstrated that effective high speed balancing at the 7,500 RPM critical speed also reduced vibration at the 16,000 RPM operating speed. Therefore, the modules balanced at 7,500 RPM in the second phase should be expected to perform acceptably at operating speeds as well.

3.3.4 Rotor No. 1

Initial unbalance response plots for this power turbine (Serial Number U00257) are shown in Figures 3.3.2 and 3.3.3 for vertical probes at both ends of the turbine module.

Initial trial weight runs indicated that unbalance at the drive coupling was very high, especially in the horizontal direction. Further investigations concluded that unbalance in the coupling caused the entire turbine module to respond. Effective correction weights were applied to the drive coupling.

Trial weights were next installed on the spline end of the output shaft to check for any influence of unbalance at this location on a possible spline shift or other turbine rotor behavior. No appreciable changes were detected. It should be noted however, that because of the large mass of the output shaft (rig hardware) or the transmission shaft (engine hardware), any eccentricity or wear-related unbalance can significantly affect vibration of the power turbine.

Analysis of test data gathered to this point showed that the vibration data from the horizontal probes indicated a large amount of variability and unexpected vibration signatures. These phenomena were perhaps due to non-uniform rig stiffness in the horizontal direction or possibly a probe bracket resonance, although these possibilities have not been analyzed in detail. It was concluded that balancing efforts would be conducted using vibration data from vertically mounted sensors only.

Attention was next directed towards the original goal of balancing the power turbine. A correction weight (calculated from data at 7500 and 8500 RPM) of 21.6 gm-cm at plane 3 and 20.1 gm-cm at plane 1 resulted in the residual response shown in Figures 3.3.4 and 3.3.5.

3.3.5 Rotor No. 2

This power turbine rotor module (Serial Number 268922) showed initial response as indicated in Figure 3.3.6. Note that these curves relate displacement sensor data that have been compensated for run-out. Thus they represent only net, or truly dynamic rotor vibration. Runout compensation was required for these plots due to the larger than normal runouts measured along the rotor. A correction weight (calculated at 8700 RPM) of 13.0 gm-cm at plane 3 resulted in the residual response shown in Figure 3.3.7.

3.3.6 Rotor No. 3

Curve "A" on Figures 3.3.8 and 3.3.9 show the as-received balance condition of this rotor (Serial Number 268975). This rotor was operated prior to the clutch damage that limited operation to 10,000 RPM. High speed balancing at 7800 RPM resulted in the unbalance response shown by curve "B" on these figures. It should be noted that unbalance response at the operating speed was sigificantly reduced by balancing at a lower speed, near the rotor's critical speed.

3.3.7 Rotor No. 4

This power turbine module (Serial Number 265503) was the first module tested that had not been previously low speed balanced. The initial spin-up of this rotor showed substantial vibration which increased with speed. The rotor could not be run above 9000 RPM without excessive vibration levels. Figure 3.3.10 shows the as-received vibration response. Although the same trend in vibration was detected in successive accels, the amplitudes and phase angles of vibration were not considered to be repeatable enough to assure accurate balancing.

Initial trial and correction weights confirmed that rotor nonrepeatability limited the use of routine methods of data gathering and weight calculation.

Engineering judgement was used in scaling and applying calculated correction weights. It soon became apparent that this rotor would require larger correction weights than had been used on the modules that had been previously low speed balanced. Installing a large trial weight resulted in the calculation of an effective 99 gm-cm correction at plane 3. Applying this correction resulted in a dramatic improvement and permitted a speed increase to 10,000 RPM.

Rotor nonrepeatability continued to prevent strict adherence to a routine balancing procedure. A combination of calculated influence coefficients, engineering judgement and analysis of on-the-spot test data resulted in weight additions of 94 gm-cm at plane 1 and an additional 12.7 gm-cm at plane 3. The results of these balancing efforts are presented in Figure 3.3.11.

It was concluded that this rotor was balanced to an acceptable degree, especially given the large amount of initial unbalance. The cause of the nonrepeatable nature of this rotor response was not investigated but may have been attributable to excessive wear, shifting components in the turbine or drive train, or perhaps as yet undetected damage to the labyrinth vacuum seal at the splined end of the power shaft (see discussion in next section).

3.3.8 Rotor No. 5

This power turbine module (Serial Number U00559) was the second module tested which had not been previously low speed balanced. Initial spin up of this rotor showed high vibrations which limited speed to 7800 RPM. Figure 3.3.12 shows as-received vibration plots for this rotor.

This rotor also showed a degree of nonrepeatability. As a result, a combination of computer calculations, engineering judgement and data analysis resulted in installing correction weight of 43.2 gm-cm at plane 1 and 25.4 gm-cm at plane 3. Unbalance vibration was significantly reduced, permitting operation through the critical speed to 9,000 RPM. Figure 3.3.13 shows the results of this balance.

Data was being gathered for a trim balance when overcurrent in the test facility drive motor aborted the test. Initial investigations disclosed both magnetic and non magnetic metal filings in the test rig lubricant. Teardown of the rig

revealed a damaged rig labyrinth vacuum seal at the splined end of the power shaft. It was concluded that contact between the seal and runner probably caused thermal expansion and further rubbing of the seal. The increased friction destroyed the seal and caused the overload to the drive motor.

Prior scheduling of the test facility for other NASA projects precluded any attempts to repair the test rig. The power turbine was removed from the test rig and the test fixture was disassembled.

In later balancing runs using the high speed balancing facility developed under NASA contract NAS3-20609, this rotor was balanced to 16,000 RPM and was then successfully run in an engine at CCAD. Consistent data was acquired with no repeatability problems. This information supports the liklihood that the problems at this phase of the program were related to the balancing test fixture.

3.3.9 Consolidation of Influence Coefficients

Because of the wide variability in response characteristics, rotor nonrepeatibility and the necessity to depart from routine balancing procedures, a comprehensive set of influence coefficients could not be obtained for all five rotor modules.

Since most of the balancing efforts occurred at two distinct speed ranges (7000 and 9000 RPM), the influence coefficient data has been grouped accordingly. Figure 3.3.14 shows the spread of the consolidated influence coefficient data and the mean and standard deviation of each data set.

Because of the limitations outlined above, extrapolating these influence coefficients to T55 power turbine modules in general is not recommended. The small data sample further limits their meaningfulnes. As a result, it can be concluded that, although influence coefficient balancing was effective in reducing unbalance vibration, establishing a comprehensive set of influence coefficients requires a larger data sample drawn from rotor modules with similar dynamic performance. This was demonstrated under NASA contract NAS3-20609 in which a comprehensive set of influence coefficients were developed which were

effective in balancing T55 power turbines without the need for trial weight runs.

3.3.10 Documentation of Balancing Times

Many of the problems discussed in previous sections of this report also prevented the formulation of accurate estimates of times for various stages of balancing.

It was initially envisioned that estimates of balancing times would be established in the following categories:

- Rotor Installation - after basic rig set-up and debug
- Trial Weight Data Gathering - including "as is" and all trial weight runs
- Correction Weight Calculation & Installation
- Check Run
- Rotor Removal

However, during the actual balancing effort, the drive system and test rig anomalies, rotor variabilities and nonrepeatabilities and other phenomena as described in this report affected the balancing times in each of the above categories.

Rotor Installation and Removal times were almost entirely contingent upon the "ease of access" of the balancing fixture. The present test rig is very cumbersome and was not designed for quick change-out of power turbine modules. Alignment checks and vacuum sealing also compounded the complexity of rotor installation and removal. Estimates of installation times varied from 20 to 60 manhours per rotor while removal times ranged from 2 to 20 manhours per rotor.

Times estimates for trial weight data gathering were very difficult to extract from the considerable amounts of time spent in resolving the extraneous vibration and equipment-related difficulties. Although total manhours expended in this phase of testing range from 60-120 manhours per rotor, actual time spent gathering useful trial weight data is estimated to have been less than 5 percent of this amount, or 3-6 manhours per rotor.

Correction weight calculation and installation typically constituted the smallest amount of balancing time. Computer-assisted calculations only require several seconds. Installation of correction weights took somewhat more time, but was facilitiated by use of the special balance collars attached to the power shaft. The largest time segment involved the engineering judgement and on-the-spot data analysis used to place weights for the nonrepeatable rotors discussed in sections 3.3.7 and 3.3.8. Estimates of manhours expended in calculating and installing correction weights ranges from 2-8 manhours per rotor.

True check runs of the balanced rotors involved only a small amount of time. However, because more than one balance was required for each rotor, many of the check runs actually became trial weight or "as is" runs for additional balancing efforts. These runs amounted to approximately 4-20 manhours per rotor, with true check runs amounting to less than 1 manhour per rotor.

Extrapolating these estimates of balancing time to T55 power turbines in general is not recommended. Access to the test rig, rig and drive train vibration and other extraneous influences have caused the demonstration balancing tests to consume much more labor than would be expected under more production-oriented balancing conditions. For example, using the prototype balance rig developed for balancing T55 and T53 power turbines under NASA contract NAS3-20609 a typical installation time for T55 power turbine was only 20 minutes and removal time only 15 minutes. Similar reductions were also seen in balancing times.

3.4 TASK 4: REVISION & CORRELATION OF THE ANALYTICAL MODEL

3.4.1 Background

The objective of task 4 was to tune the mathematical model used for the rotordynamic analysis due to the dissimilarity between observed test rig behavior and original rotordynamic analysis. This was accomplished by adding the effect of engine static structure and bearing support flexibility to the existing power turbine model and revising the bearing and spline stiffness based on observation made during the experimental work of task 3.

These topics were addressed by creating four mathematical models:

ROTOR #1 - Engine Casing Model

ROTOR #2 - Engine Rotor Model

ROTOR #3 - Balancing Rig Model, previous

ROTOR #4 - Balancing Rig Model, current

Detailed drawings were made for the four rotor systems identifying rotor mechanical and dynamic properties at each modeling station. (see Figures 3.4.1 - 3.4.3).

The entire engine static structure is represented in Figure 3.4.1. The gas producer rotor is included in the static structure mass since the objective was to analyze power turbine behavior.

The previous version of the test rig is shown in Figure 3.4.2. The drive train (not shown) provides torque to a coupler, a spindle supported on bearings 1 and 2, the aircraft transmission shaft on bearings 3 and 4, and the engine power turbine rotor on bearings 4 and 5. Modeling stations for the balancing rig are denoted by circles. Triangles indicate positions where the geometric model is indentical to locations within the engine.

The current version of the test rig is shown in Figure 3.4.3. Positions to the left of station 21 and right of station 47 (these stations are denoted by circles) are the same as the early test rig (Figure 3.4.2). Positions 21 thru 46 (denoted by hexagons) reflect changes made to the early test rig for current tests.

Materials typically used in turbine engines were assumed where actual types were not known. Support stiffnesses and damping were based on previous experience. All other values were calculated. Splined joints were modeled either as a rigid connection or as a hinge having no lateral moment generating capability.

3.4.2 MTI Rig Analysis

The previous rig rotordynamics analysis is presented in Table 3.4.1. The first lateral critical speed is a disk end, conical mode of the power turbine at 9500

RPM. The second lateral critical speed is a bending of the shaft at 23000 RPM. Spline flexibility has only a small effect on critical speeds of the rotor. A critical response of the drive spindle appears at 20400 RPM for a "rigid" spline and at 18700 RPM for a "hinged" spline. There is no cross talk between rig and drivetrain. Therefore, any beginning traces of the rig critical at the 16000 RPM maximum rotor speed should not affect turbine vibration.

The current rig rotordynamics analysis is also presented in Table 3.4.1. Changes in the hardware included elimination of the spline joint in plane A as well as the inclusion of a coupler for parallel and angular misalignment. The analysis predicted that critical speeds should be essentially the same as the previous rig.

A comparison of the mode shapes for previous and current rig models also indicated similarities in rotordynamic behavior. Figures 3.4.4 through 3.4.9 show the mode shapes for the hinged spline case. It is important to note that there is no cross-mode influence between the rig mode and the rotor modes.

The critical speed map in Figure 3.4.10 shows the calculated sensitivity of the turbine mode critical speed as a function of bearing stiffness. The rig critical speed is relatively insensitive to change in support stiffness at the power turbine.

3.4.3 Engine Analysis

The T55 engine was analyzed using a two level model to determine relative motion between the engine case (static structure) and the power turbine rotor, as well as case/inertial ground motion. Figure 3.4.11 is a schematic representation of rotor interconnection modeling details. Since the objective of this task was to gain insight into power turbine behavior only, the gas producer rotor mass was included in the static structure mass.

The engine rotordynamics analysis is presented in Table 3.4.2 for an assumption of no hinges (locked spline joint). The casing and turbine are considered separately in order to identify which rotor is responsible for total engine vibration. The engine is predicted to have casing related vibration response at

about 900 RPM, 4500 RPM, and 8800 RPM. Vibration at about 11000 RPM is due to the turbine disk conical mode. Vibration at the 16000 RPM service speed is caused by proximity to the 23000 RPM rotor flexible critical speed.

The mode shape analysis for each critical speed provides further insight. The 905 RPM casing response (Figure 3.4.12) indicates a rigid casing driven by the turbine disks. The 4461 RPM casing response (Figure 3.4.13) shows casing bending driven by the disks. The 8804 RPM casing response (Figure 3.4.14) reveals forward casing motion driven by the forward end of the turbine. The cause for the discontinuity at the transmission shaft is unknown but is believed to be caused by an anomaly in the modeling technique. The 11007 RPM engine vibration (Figure 3.4.15) is caused by the power turbine disk mode. The 22087 RPM engine vibration (Figure 3.4.16) is above the service speed of the engine. The casing shows no response to rotor bending at this speed. Although this calculated critical speed is well above the rotor's 16,000 RPM service speed, it is important to note that some amount of rotor bending is detected within the rotor operating speed range.

3.4.4 Correlation of Experiment with Analysis

The previous analysis was conducted with the belief that the rigorous identification of mechanical parameters would result in the prediction of observed behavior, i.e., bimodal turbine response below 10000 RPM. When the result of the analysis showed only the single turbine "bounce"mode another explanation was sought. The shaft orbits (Figure 3.4.17) showed a mode shape with motion at both the forward (spline) and aft (disk) end at about 9000 RPM, although the analyses predicted only disk end whirl. The mode near 8000 RPM was not predicted at all. Also note that the orbits were strongly elliptical. The analysis predicted only circular orbits as symmetric bearings were assumed.

Several possibilities for lack of experimental/analytical correlation were evaluated. Bearing/support stiffness was strongly implicated because of the spline end motion as well as orbit ellipticity. A simplified "desk-top" analysis was used to estimate the support stiffness required to produce forward turbine whirl. Observed amplitudes and speeds were used as input. The "desk-top" solution for support stiffness was input to the rotordynamic model

for the Current MTI Rig and the resulting mode shapes determined. For a forward support stiffness of 1,925,000 N/M (11000 lb/in) and an aft support stiffness 29,750,000 N/M of (170000 lb/in) the model did predict spline end motion at 7879 RPM and 8712 RPM with some motion at the turbine (Figure 3.4.18).

Even closer agreement of test and analytical data was achieved when assymetric support stiffnesses were used in the model. The forward bearing was selected at 1,400,000 N/M (8000 lb/in) and 1,925,000 N/M (11000 lb/in) with 1,137.5 N sec/m (6.5 lb sec/in) damping. The aft bearing was selected at 21,000,000 and 35,000,000 N/M (120000 and 200000 lb/in) with 17.5 N sec/m (0.1 sec/in) damping.

The mode shape was cylindrical at 9280 RPM with 70° phase difference from one end of the rotor to the other. The mode shape at 9305 RPM had the turbine end amplitude twice that of the spline end and 100° phase difference end-to-end.

The actual data from the rig in Figures 3.4.19 & 3.4.20 indicates an excellent comparison with the analysis, but the existence of such a soft support did not seem possible. The rig was instrumented to determine static case deflection when known amounts of force were applied. The result was essentially uniform stiffness in excess of 87,500,000 N/M (500,000 lb/in) for both forward and aft casing. The forward measurement included structure up to the bearing housing.

Although not examined in detail, any of a number of phenomena could result in the large difference in support stiffness between the amount indicated by static measurement and the amount needed to result in agreement with test data. One possiblility is the presence of localized resonances in the test-rig which react with the driving force to create a "dynamic" stiffness that is significantly lower than the measured "static" stiffness. Other phenomena capable of generating the observed bimodal behavior include the following:

- Spline shift (However, there is no abrupt increase in amplitude at the forward end.

- Clearance in the forward bearing. (Unlikely because the clearance was measured at .076 mm (3 mils) and peak-to-peak rotor deflections exceeded .127 mm (5 mils) peak-to-peak for a balanced condition)

- Coupler and transmission shaft weight exceeded 15.9 kg (35 lbs). (However, vibration never exceeded .051 mm (2 mil) peak-to-peak and reached a maximum consistently at 8850 RPM, while the unexplained vibration was always below 8000 RPM).

These and other possibile causes of the difference between statically measured and analytical/test data were not further explored because of funding limitations.

3.5 TASK: 5 EFFECTIVENESS OF THIRD TURBINE STAGE BALANCING CORRECTIONS

The objective of this task was twofold. The first objective was to analytically evaluate the T55 rotor sensitivity to fourth turbine stage unbalance and determine if this unbalance can be effectively corrected at the third turbine stage. The second objective was to analytically subject the power turbine rotor to a random unbalance and optimize the balancing method to effectively reduce rotor amplitudes throughout the speed range. At its 16000 RPM design speed, the rotor exhibits a significant degree of bending that cannot be compensated for by balancing at low speed. High speed multiplane balancing is capable of reducing these vibrations to an acceptable level.

3.5.1 Fourth Turbine Stage Sensitivity

Tables 3.5.1-3.5.3 present a summary of the rotor response analysis concerning fourth turbine stage unbalance and the effects of third turbine stage corrections on power turbine vibration levels. Table 3.5.1 shows power turbine amplitudes at various stations along the shaft for a 71.8 (1 in oz.) unbalance at the 4th stage and for a 3rd stage correction. At the 11500 RPM first critical, which is a rigid rotor mode, the introduction of the couple substantially reduced the peak amplitude. However, at the 16000 RPM design speed the rotor is no longer rigid, and the couple resulted in drastically increased vibration levels.

3.5.2 Randomly Distributed Unbalance

The second phase of the analysis concerned a random distribution of unbalance along the rotor. The unbalance was modeled using random numbers representing both magnitude and phase angle. The range of values chosen was 0 - 10 grams at 0 - 360° phase at each of the 50 stations. The resulting net rotor unbalance was 99gm cm (1.38 in. oz). at -83.2°.

A two plane low speed balance was evaluated by calculating static correction weights at the third turbine stage and one of three arbitrarily chosen balance planes on the output shaft (stations 29, 33, 36). This was accomplished by solving a force and moment equation simultaneouly to give correction weights which were then included in the model for rotor response runs. Table 3.4 summarizes the results at 11500 RPM and at 16000 RPM for the static correction weights. The balance plane furthest away from the third stage turbine (station 29) was the only one that showed any reduction in amplitude at 16000 RPM. For the other two cases correction weights resulted in increased vibration at the 16000 RPM design speed due to the flexible nature of the shaft.

The final balancing technique evaluated was a two speed influence coefficient balance. For computational ease, four balance planes were initially chosen since this resulted in a square matrix. These were then combined to simulate a two plane balance for the rotor response. The two balance planes coincided with the existing balance plane on the output shaft and the third stage turbine. The probe locations for data acquisition were chosen at stations showing peak amplitudes at each of the balancing speeds.

The input for the influence coefficient program was obtained from a series of rotor response runs that sequentially placed one inch ounce unbalance as a trial weight at each of the balancing planes. The amplitude and phase at each probe location for 11500 and 16000 RPM were input to the influence coefficient program. Table 3.5 presents the results for this balancing method.

Figure 3.5.1 shows the mode shapes at the 11500 RPM first critical speed and at the 16000 RPM design speed for the random unbalance. Also shown on this figure is the resulting amplitudes after the addition of correction weights at the

existing balance planes on the output shaft and the third stage turbine for static correction weights and for the influence coefficient balancing technique. The influence coefficient balance effectively reduced the peak amplitudes at both speeds. The results of this analysis indicate that the presently established balance planes are sufficient to reduce unbalance vibration.

3.6 TASK 6: VERIFICATION OF POWER TURBINE BALANCE QUALITY

The objective of task 6 was to evaluate the quality of the high speed balancing by running two of the rotors balanced in task 3 in engines at Corpus Christi Army Depot (CCAD).

With the concurrence of the NASA program manager, the high speed balancing of two power turbine rotors for operation in an engine was conducted utilizing facilities developed under NASA contract NAS3-20609. Rotor SN268922 (prebalanced at low speed) was high speed balanced using precision balance collar on the shaft foward end and by attaching safety wires to third stage turbine blades. The initial top speed of 14000 RPM allowed balancing data to be gathered at 8265, 12000, and 14000 RPM. The balance weights were installed permitting operation to 16000 RPM where additional balance data was acquired for trim balancing which further reduced the vibration response Figure 3.6.1 shows the final balance condition for this rotor.

Rotor SNU00559 (not prebalanced at low speed) was installed and run to the 16000 RPM service speed. Trim balancing data was gathered at 8265, 15000, and 16000 RPM. The balance condition after the trim balancing is shown in Figure 3.6.2.

Permanent correction weights were ground into both rotors and the trial weight balance collars removed. This completed the preparation of these two rotors for engine testing at CCAD.

The first of the two power turbines was successfully run in an engine during a visit to CCAD by MTI personnel. The engine had been run in the test cell earlier in the week and then the power turbine was replaced with one incorporating high speed balancing (SNU00559). This power turbine was not low speed balanced. The engine test showed a decrease in overall vibration as measured by the case

mounted sensors after the turbine changeout (see Figure 3.6.3) and was considered by the operators to be extremely smooth running engine.

Figure 3.6.4 represents a vibration spectrum plot taken from the engine test with the high speed balanced power turbine operating at 15600 RPM (97.5%). It is clear from this plot that the contribution of the compressor rotor (N1) now dominates the overall engine vibration. Any further reduction in the vibration levels measured by test cell instrumentation (which measure overall vibration) would require improving the balance on the compressor rotor to a level comparable with the high speed balanced power turbine. It is important to note that the high speed balanced turbine now contributes very little to the engines vibration signature.

The reduction in overall engine vibration achieved by the installation of the high speed balanced power turbine (SNU00559) clearly shows the ability of high speed balancing to improve operation at design speed. The engine vibration levels were significantly reduced from a level already below the vibration criteria prior to turbine changeout.

MTI personnel were not present at CCAD for the testing of the second power turbine in the test cell due to scheduling delays at CCAD. CCAD personnel indicated a suspected faulty waterbrake caused high vibration during the test. Test data forwarded to MTI supports this conclusion. Table 3.6. presents the test data for this run as recorded by standard test cell instrumentation. The high vibration is predominantly on the V3 sensor which in on the waterbrake. Unfortunately the test was not rerun with a repaired or alternate waterbrake.

3.7 TASK 7: EXPERIMENTAL STUDY OF SPLINE DYNAMICS

3.7.1 Introduction

Previous studies of rotor vibration response have identified spline joints as a potential source of excessive vibration. Balancing experiments in previous tasks of this contract showed a significant change in vibration response as a function of engagement position of the power shaft spline to the transmission shaft spline. Test cell operation of an AVCO Lycoming T53 under NASA Contract

NAS3-20609 showed a large increase in engine vibration as a result of dynamic spline offset. During test cell qualification of engines, it is common practice to re-index spline joints in an effort to reduce vibration. This information formed the basis of the work accomplished under this task.

The primary objective of this task was to experimentally study the dynamic environment of the power shaft-transmission shaft spline on the AVCO Lycoming T55 engine. Spline fits for the units tested were documented and correlation made between spline fit, observed dynamic response and balance achieved.

The existing NASA owned Drive Train Test Facility at MTI was used for the experimental tests. The balancing rig used for previous tasks was modified to permit detailed monitoring of shaft motion across the spline joint.

Vibration response tests were conducted for two power turbine modules. Shaft amplitudes and phase angle were monitored for a number of spline indexes.

3.7.2 Test Set-Up

The test facility used for the vibration test was constructed at MTI under NASA Contract NAS3-16824 (Ref 2). Designed to accomodate rotors up to 20 feet long to speeds of 20,000 RPM, the system is well suited for the spline study.

The test rig used for the vibration tests had been designed and constructed under previous tasks of this contract. The facility was set up as shown in Figure 3.7.1. The vacuum enclosure incorporated engine hardware to provide bearing support and also provided low ambient pressure for reduced windage losses. Eight non-contacting displacement probes permitted observation of orbits in three turbine planes and one drive shaft plane. Probes 5 and 7 were oriented in a vertical plane and were located to span the spline joint. Thermocouples were used to insure a proper temperature environment for the probes. An optical tachometer sensed the rotational speed of the high speed spindle for phase determination. A synchronous tracking filter and phase meter were connected to probe outputs for real time display of shaft vibration. A special design drive shaft minimized drive line elements and permitted the use of a lightweight 339 gm (12 oz) coupler. The coupler could be easily removed, thus permitting spline

indexing without altering alignment of the rotating system. Spline clearance measurements were made in place with the rig in an operable condition.

3.7.3 Testing Procedures

Because of its importance in measuring any effects of spline dynamics, the test procedure for the vibration test emphasized gathering of repeatable data. A vacuum of 71 cm (28") Hg was supplied by a continously running vacuum pump. A warm-up run and starting temperature of 49°C (120° F) were established. Constant drive torque was applied by setting the speed controls for top speed and allowing the drive system to accelerate at its own rate (about 90 rpm/sec). If top speed was not achieved when probe temperatures reached 149°C (300°F), the run was terminated. Synchronous vibration amplitude response was generated during the acceleration and was used to verify playback of information recorded on magnetic tape. Drive shaft indexing included positions of 0°, 90°, 180°, 270°, and 0°. The index was made by backing off the light weight coupler allowing indexing of the spline without requiring any motion of the drive system or power turbine and therefor not affecting shaft alignment.

Spline clearance measurements were made by moving the transmission shaft back and forth and noting the change in position with a dial indicator. Motion was checked for several positions.

Spline fit measurements were based on over-the-pins measurements of the internal and external splines. Two precision diameter pins were placed 180° apart between spline teeth. A micrometer was used to check the dimension over the two pins.

3.7.4 Data Analysis

Data recorded on magnetic tape was used to compile vibration response information. Synchronous vibration amplitude and phase for each of the eight probes was plotted. Plots from each index position were overlayed to determine differences in response. The repeat data at the 0° index position was compared with the four overlays to assess data repeatability.

Spline fit data was generated from over-the-pins measurements of the splines. The external spline measurements (transmission shaft) were displayed in schematic form as the runout of a pitch circle. The internal spline data (power shaft) was subtracted from journal measurements and a similar pitch circle schematic created. By overlaying the internal and external pitch circle schematic, the point of closest approach of the pitch circles was identified. The external spline schematic was placed so that closest approach points were equally spaced. This is shown in figs. 3.7.2 and 3.7.3 for four index positions. The centerline seperation (parallel misalignment) of the two splines was noted. It was expected that a larger misalignment would impose a larger unbalance force on the turbine shaft giving a larger at speed vibration.

Actual spline clearance data was noted after the rotating hardware was installed in the test rig. With the spline shafts in a ready-to-run condition, the drive shaft was moved laterally and the displacement recorded. This was repeated for each index condition.

3.7.5 Results

As expected, power turbine vibration response magnitude and phase did vary as a function of spline engagement position (see Figures 3.7.4 to 3.7.9). No dynamic offset or shift in the spline joint was observed and the spline did not show any signs of instability. The high and low vibration test results, however, did not agree well with predictions based on the measured spline data. For turbine SN 265503 the spline vertical probes vibration was generally highest at 270° and lowest at 0°. This data is shown in Figures 3.7.4 & 3.7.5*. Using the pitch circle techniques outlined above, essentially equal vibration was predicted at 90°. 180°, 270° with somewhat lower vibration at 0° (see Figure 3.7.2). For turbine SN U00257 the power shaft vibration was generally higher at 0° and lower at 180° (see Figures 3.7.7 & 3.7.8). Pitch circle measurements predicted high vibration for the 270° position and uniformly lower vibration at 0°, 90°, and 180° (see Figure 3.7.9). The probable cause for this lack of correlation is

---

*The vertical probes were considered to be most representative because the horizontal probes direction has historically acted as if it were softly sprung.

nonrepeatability. The change in response from one run to the next with no change in spline index were in some cases as large as the change in response observed after indexing the spline.

Table 3.7.1 presents the spline clearance measurements made after each index. Comparing those measurements with vibration data did not result in a direct correlation between available clearance and vibration response. It should be noted, however, that the variation in spline clearance was typically .05 mm (.002 in) or less. Measurement error, along with the inconsistent repeatability between 0° check runs, may have combined to obscure whatever changes may have been related to the change in spline clearance.

The vibration response for the two modules tested was compared to their response when previously run in the Task 3 balancing demonstration. As Figure 3.7.10 shows, the response of SN U00257 is very comparable, while SN 265503 showed some change in response. Possible reasons for the differences in SN 265503 include:

- Intentional change in unbalance - After the Task III balancing demonstration, both rotors were trim balanced in the High Speed Balance Facility developed under NASA Contract NAS3-20609. This balance was necessary because during Task III the test facility top speed was limited to 10,000 rpm even though balancing was required through 16,000 rpm.

- Degradation in rotor mechanical condition - In the interim between Task III test and the current spline evaluation, it is possible that a turbine disk has become loose or some inadvertent damage has occured. Similar response peaks were detected on this module when it was operated in the high speed balance facility under NAS3-20609. A loose disk or damage bearing are possible causes for the non-repeatable vibration observed for this rotor. No disassembly checks or other inspections were made to determine the cause of this change in vibration.

- Differences in the demonstration rig between tests - Changes to the mechanical configuration of the rig were made between Task III and the current work in order to make spline indexes without disrupting

alignment. A lighter drive shaft, lighter coupler, and new alignment were the most significant changes.

4.0 CONCLUSIONS

The evaluation of the rotordynamic analysis of the two rotor system in the T55-L11C concluded that the multiplane-multispeed balancing procedure could be effectively applied to the power turbine rotor. The mode shape at the 16,000 RPM service speed has the shape of the second system critical and exhibits significant bending of the rotor.

Experimental evaluation of a precision collar intended for temporary trial weight placement on slender or thin-walled shafts during balancing operation has proven the concept practical and convenient to apply.

Five T55 power turbine modules were balanced using the multiplane - multispeed technique in a specially designed test rig. Balance collars were installed to permit trial and correction weights to be easily added to the rotor without grinding. An existing multiplane-multispeed balancing system was used to calculate balance weights. It is concluded that multiplane-multispeed balancing techniques are effective in reducing unbalance caused vibration in T55 power turbine modules.

The effect of engine static structure and bearing support flexibility were included in an engine analytical model. The power turbine rigid critical speed causes engine vibration at 11,000 RPM. The power turbine bending critical speed at 23,000 RPM is beyond the 16,000 RPM service speed. Vibration at 900 RPM, 4,500 RPM, and 8,800 RPM, is peculiar to the engine because of casing resonant response.

The effect of the test rig static structure was included in a revised rig analytical model. The power turbine rigid critical speed mode shape at 9,500 rpm compares well with the engine critical speed at 11,000 rpm. The rotor bending critical speed at 22,000 rpm compares well with the engine critical speed at 23,000 rpm.

At the 16,000 rpm service speed, the T55 power turbine rotor exhibits a significant degree of bending. For this reason a single plane correction in the third turbine stage to compensate for fourth turbine stage unbalance is ineffective at

design speed. Similarly, two plane low speed balance results in either a minor decrease in vibration or a significant increase in vibration at 16,000 RPM depending on the location of the balance planes. The multiplane-multispeed influence coefficient balancing technique effictively reduces the peak amplitudes at both the 11,500 RPM critical speed and the 16,000 RPM design speed.

The effectiveness of the multispeed-multiplane balancing procedure was confirmed when a high speed balanced power turbine rotor was run in an engine at the Corpus Christi Army Depot. The engine showed a significant decrease in overall vibration levels when its power turbine was replaced with one that was high speed balanced. A frequency spectrum plot of the overall vibration for the run with the high speed balanced power turbine installed showed conclusively that the contribution from the compressor rotor dominated the overall vibration level. To improve vibration levels futher it would be neccessary to balance the compressor rotor to a level comparable with the high speed balanced power turbine rotor.

The spline dynamics study concluded that the power shaft-transmission shaft spline connection showed no signs of instability, nor was there a tendency for a dynamic offset or shift to occur in the spline joint.

4.1 General Conclusions

The following conclusions are more of a generic nature and are applicable to other turbine engines as well as other rotating equipment that operates near a bending critical speed.

- Low speed balancing techniques become decreasingly effective as the transition from rigid rotor to flexible rotor is made. In the flexible regime low speed balancing can adversely effect the vibration levels at operating speed.
- It is essential to run the rotor to be high speed balanced in the test fixture before final formulation of the balance plan in order to optimize the balance speeds used based on actual response.

5.0 RECOMMENDATIONS

Additional analysis of engine vibration as measured in the overhaul faciltiy test cells is needed for the T55 and other engines. Presently only overall vibration is measured which gives CCAD personnel little information on which to base corrective measures on. In addition, better understanding of the vibration measurements would enable CCAD engineers to detect any weakness in the balancing procedures used during overhaul that might be resulting in rejected engines.

High speed balancing needs to be introduced into the overhaul cycle due to the continuing development of more flexible shaft engines. On the T55, an engine developed more than 25 years ago, improvements can be achieved with high speed balancing but the technique is not essential fo acceptable engines. If current design trends continue toward more horsepower with lighter engines high speed balancing will become a required procedure for the overhaul centers to produce smooth running engines.

REFERENCES

1. Cundiff, R.D.; Badgley, R.H; and Reddecliff, J. "Pneumomechanical Critical Speed Control for Gas Turbine Engine Shafts", Air Force Aero Propulsion Laboratory, Technical Report AFAPL-TR-73-101, November 1973.

2. Darlow, M., and Smalley, A.; "Design and Application of a Test Rig for Super Critical Power Transmission Shafts", NASA Contractor Report 3155, 1979.

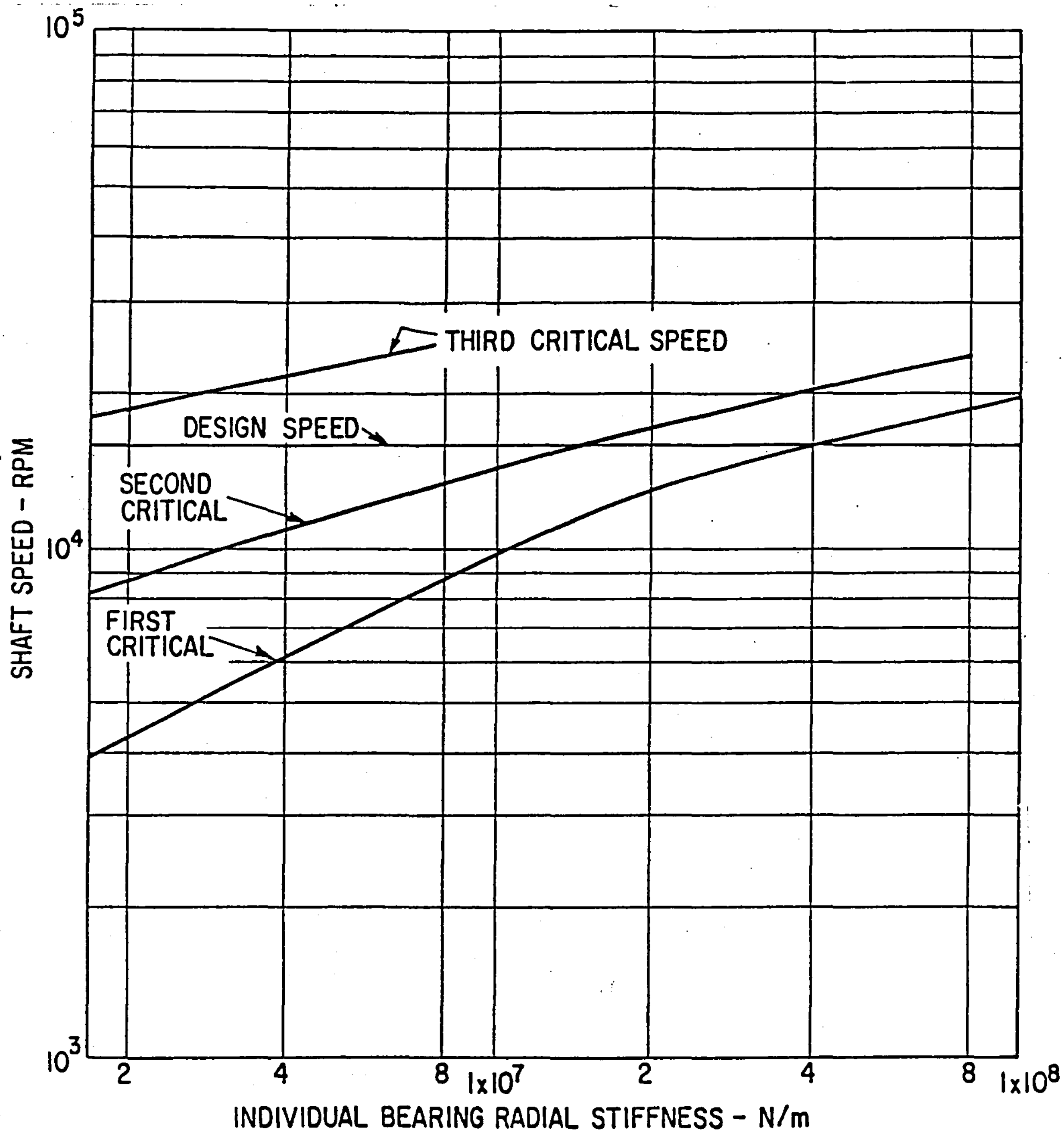

FIG. 3.1.1 CRITICAL SPEED MAP - POWER TURBINE ROTOR OF T55-L-11A ENGINE

82726

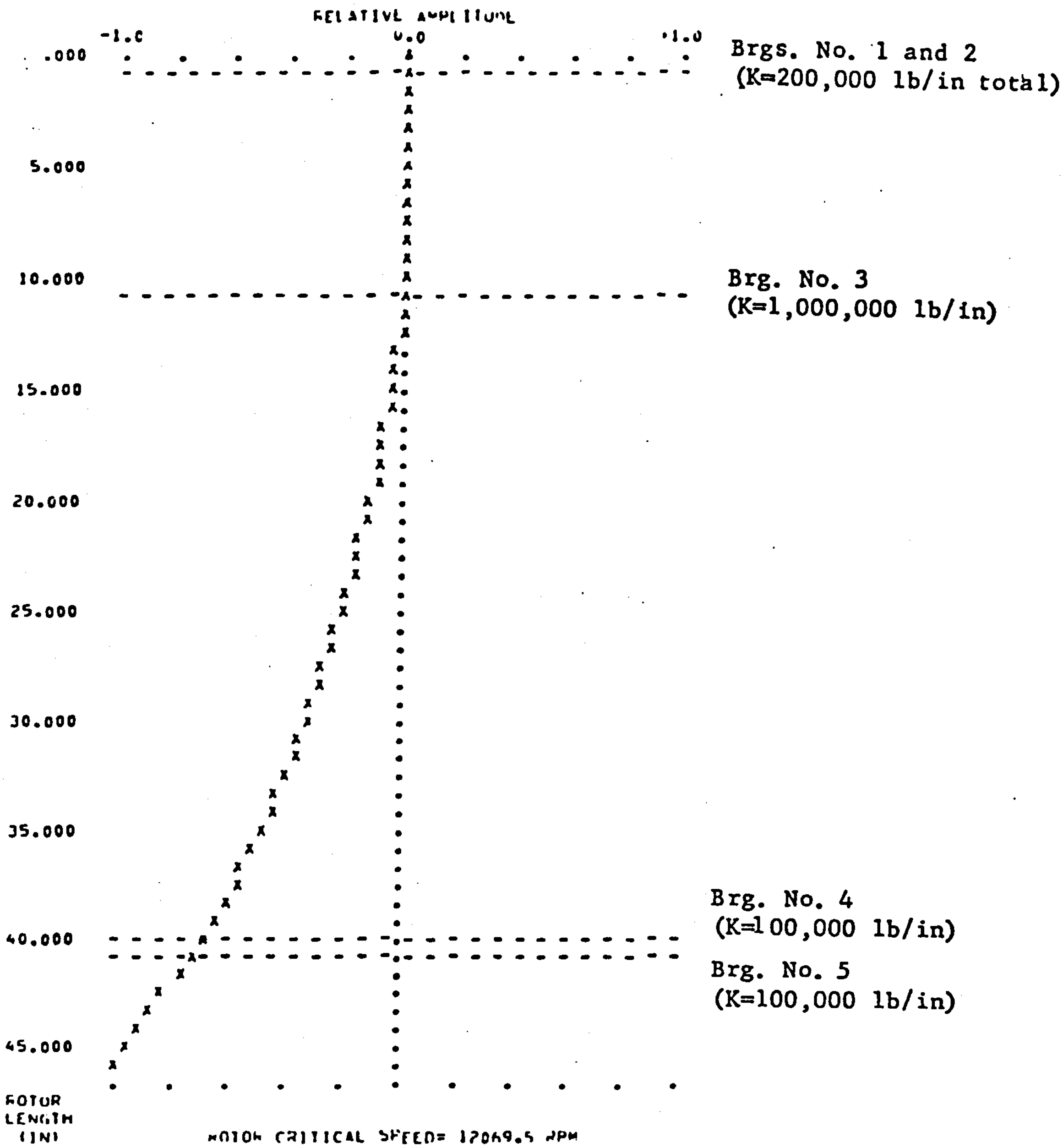

82715

FIG. 3.1.2 UNDAMPED MODE SHAPE AT FIRST CRITICAL SPEED FOR T55-L-11A POWER TURBINE ROTOR ASSEMBLY

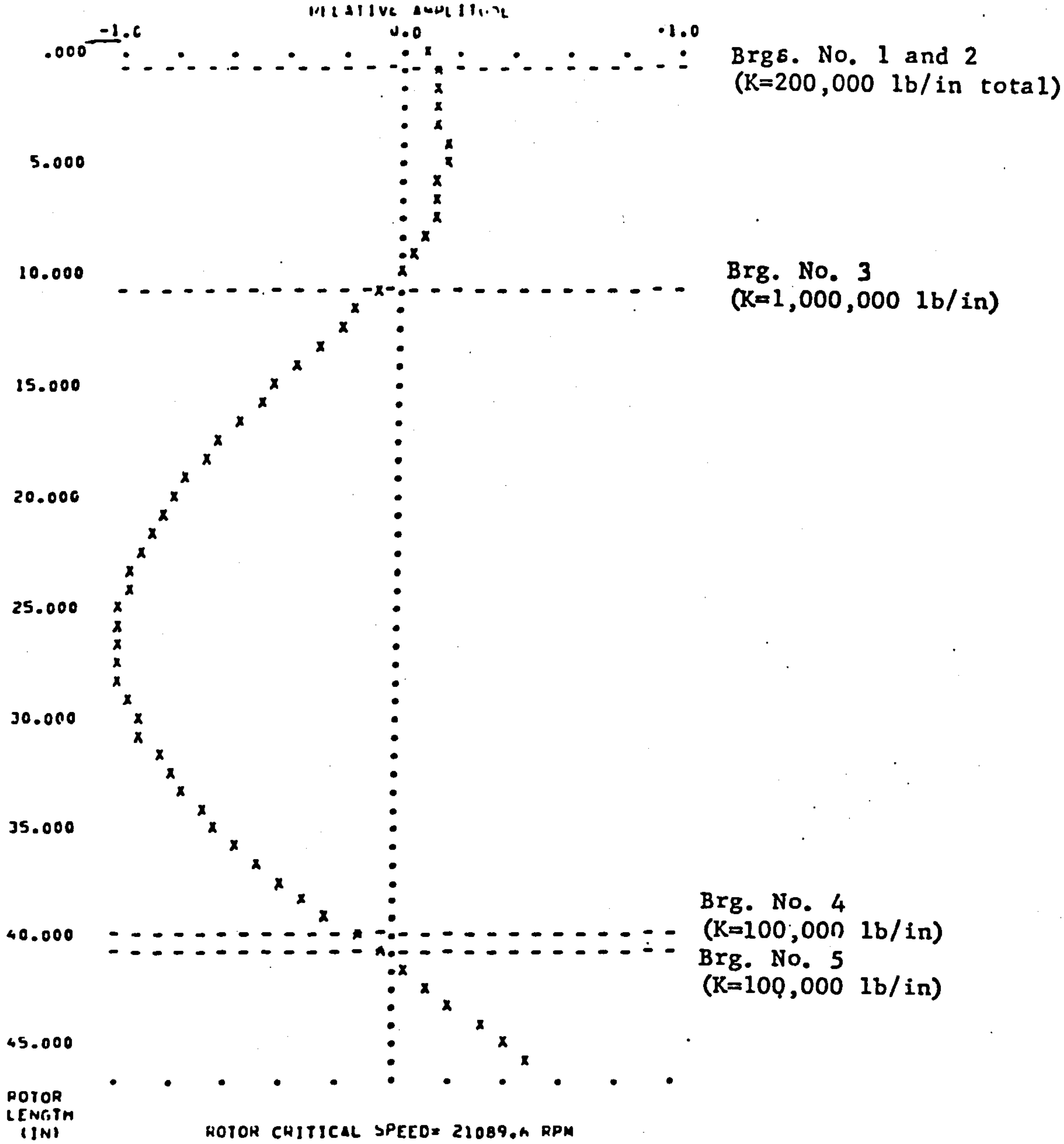

82714

FIG. 3.1.3 UNDAMPED MODE SHAPE AT SECOND CRITICAL SPEED FOR T55-L-11A POWER TURBINE ROTOR ASSEMBLY

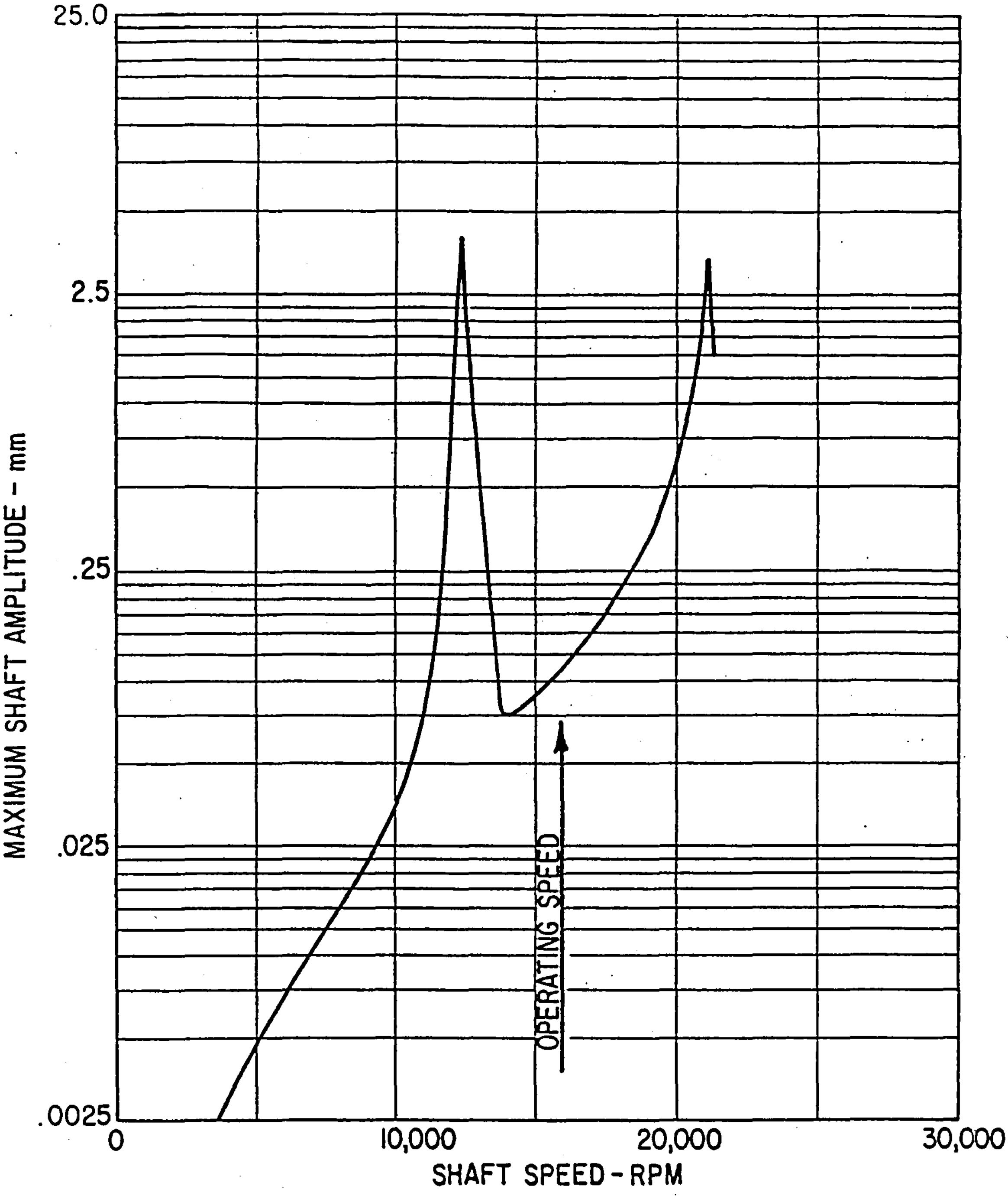

FIG. 3.1.4 CALCULATED MAXIMUM ROTOR AMPLITUDES
FOR T55-L-11A POWER TURBINE ROTOR

82725

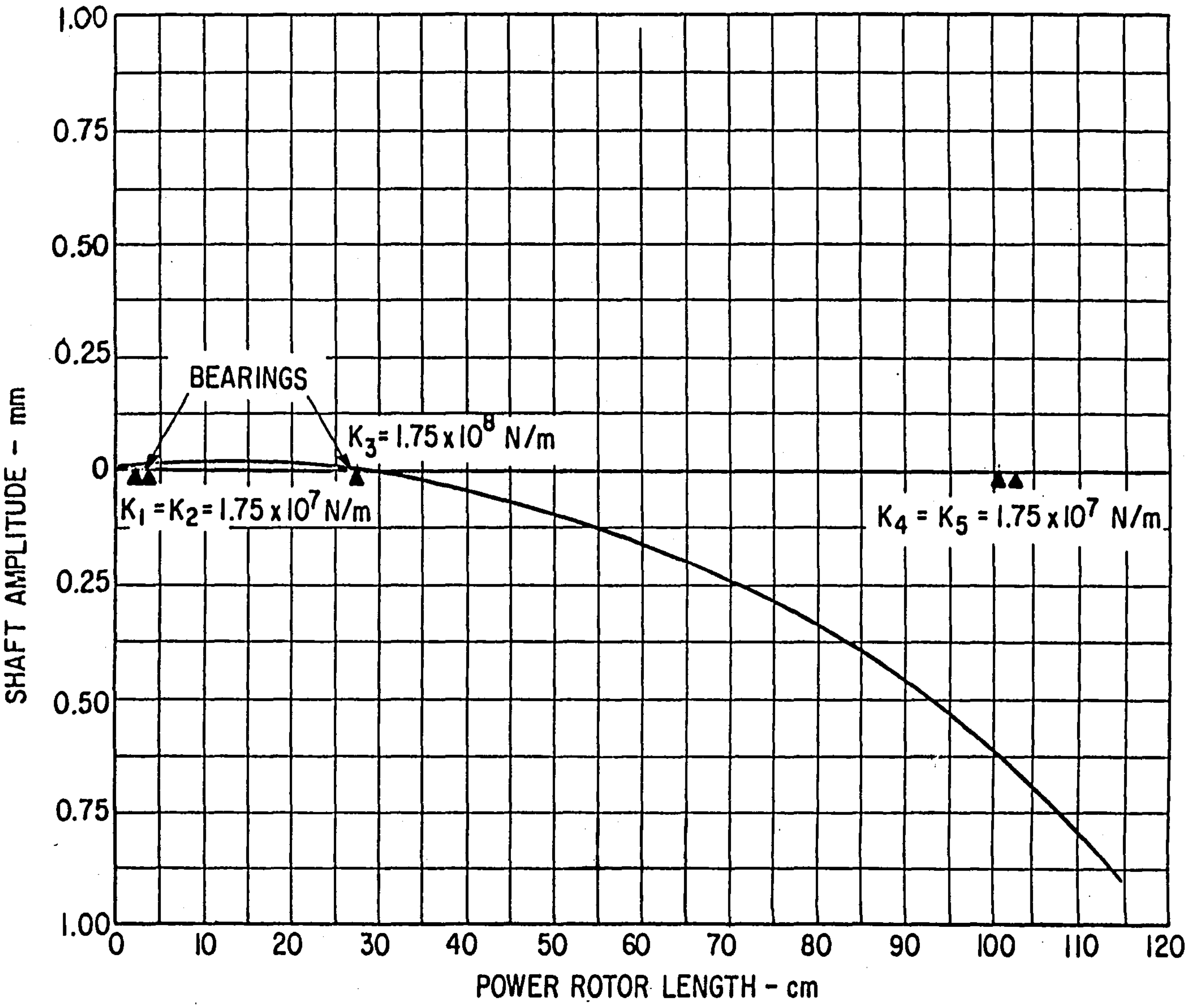

82724

FIG. 3.1.5 CALCULATED AMPLITUDES FOR T55-L-11A POWER TURBINE ROTOR ASSEMBLY AT 12,070 RPM <u>(FIRST CRITICAL SPEED)</u>

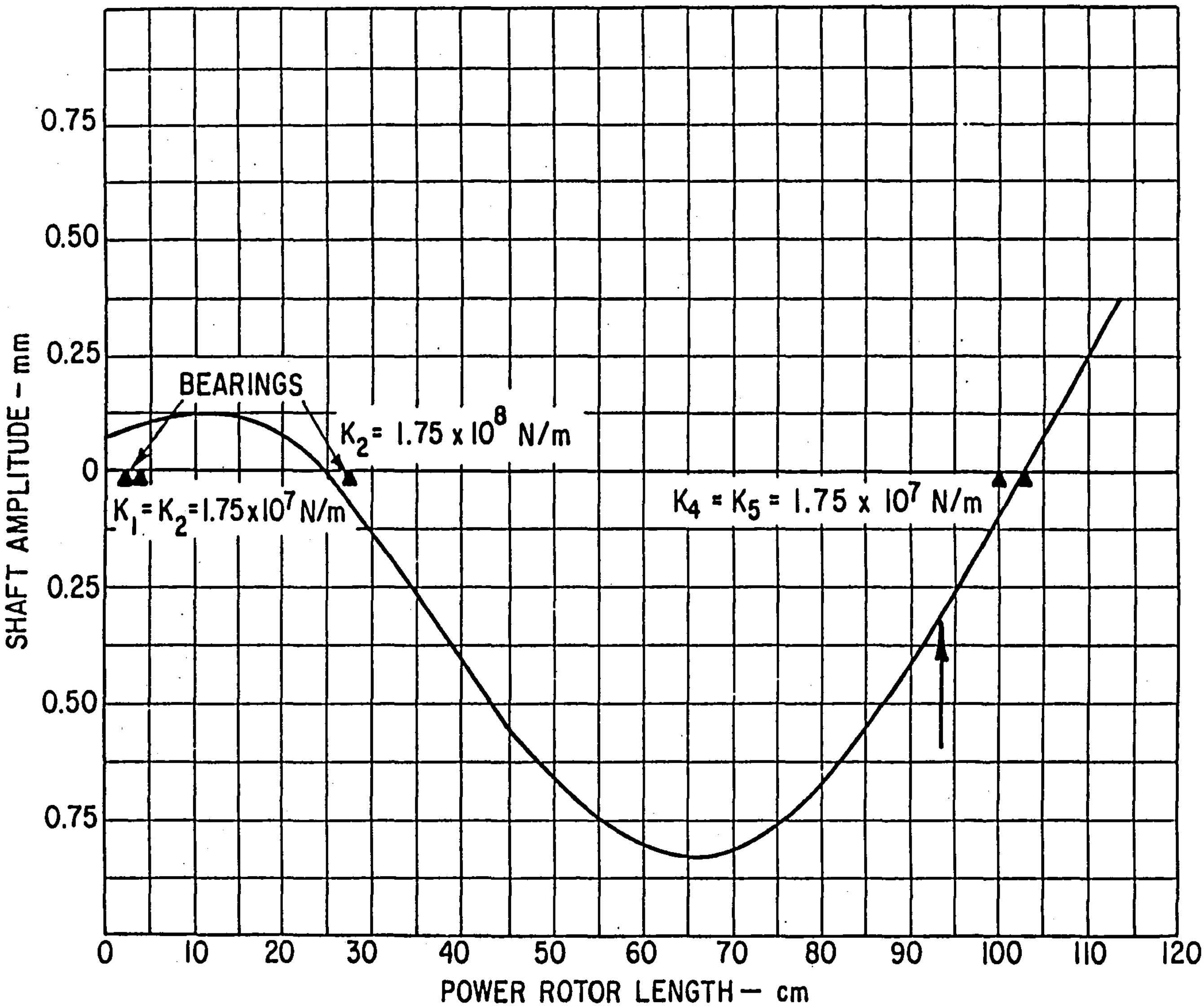

82723

FIG. 3.1.6 CALCULATED AMPLITUDES FOR T55-L-11A POWER TURBINE ROTOR ASSEMBLY AT 21,000 RPM (SECOND CRITICAL SPEED)

MECHANICAL TECHNOLOGY INCORPORATED

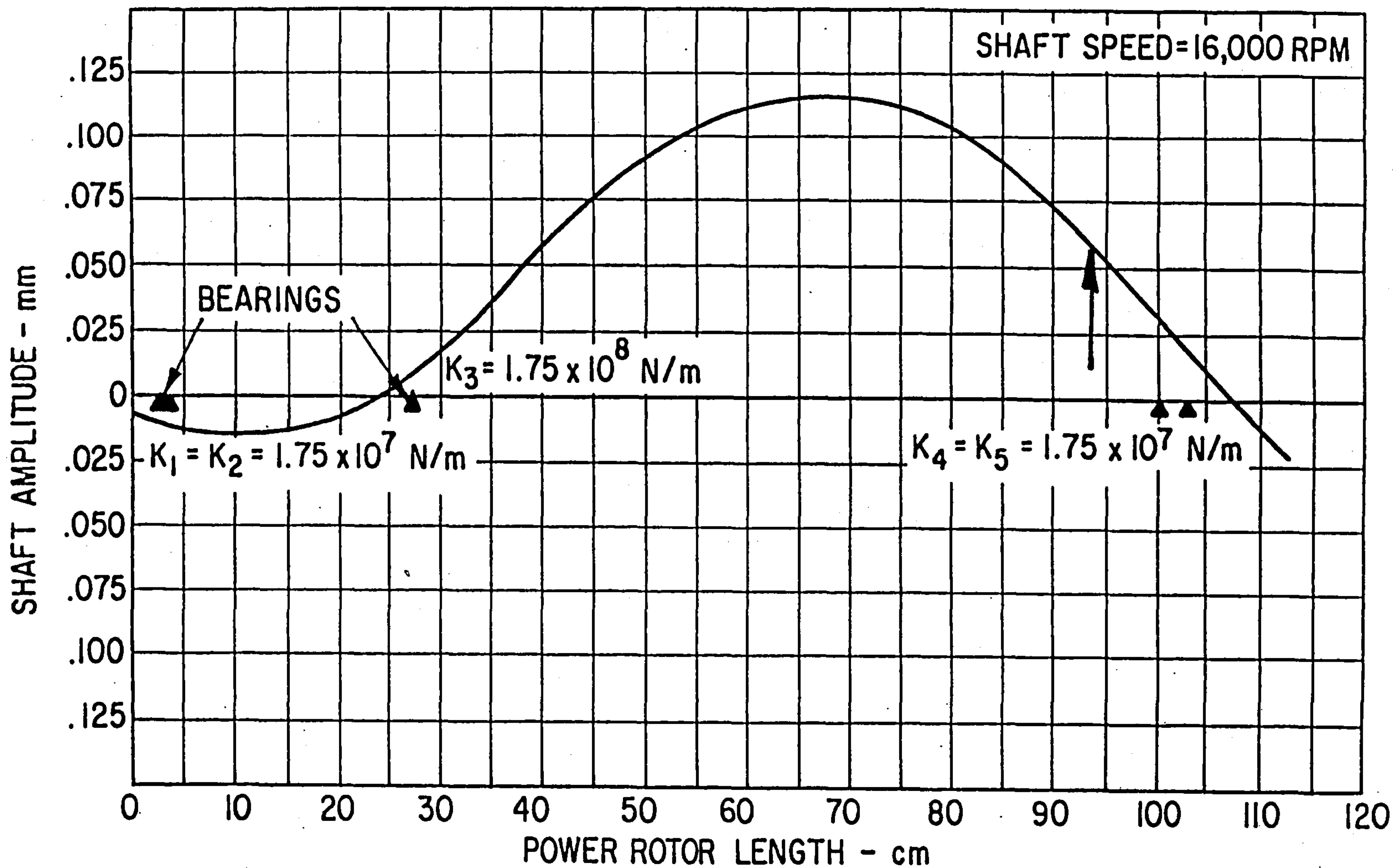

FIG. 3.1.7 CALCULATED AMPLITUDES FOR T55-L-11A POWER TURBINE ROTOR ASSEMBLY AT 16,000 RPM <u>(OPERATING SPEED)</u>

82713

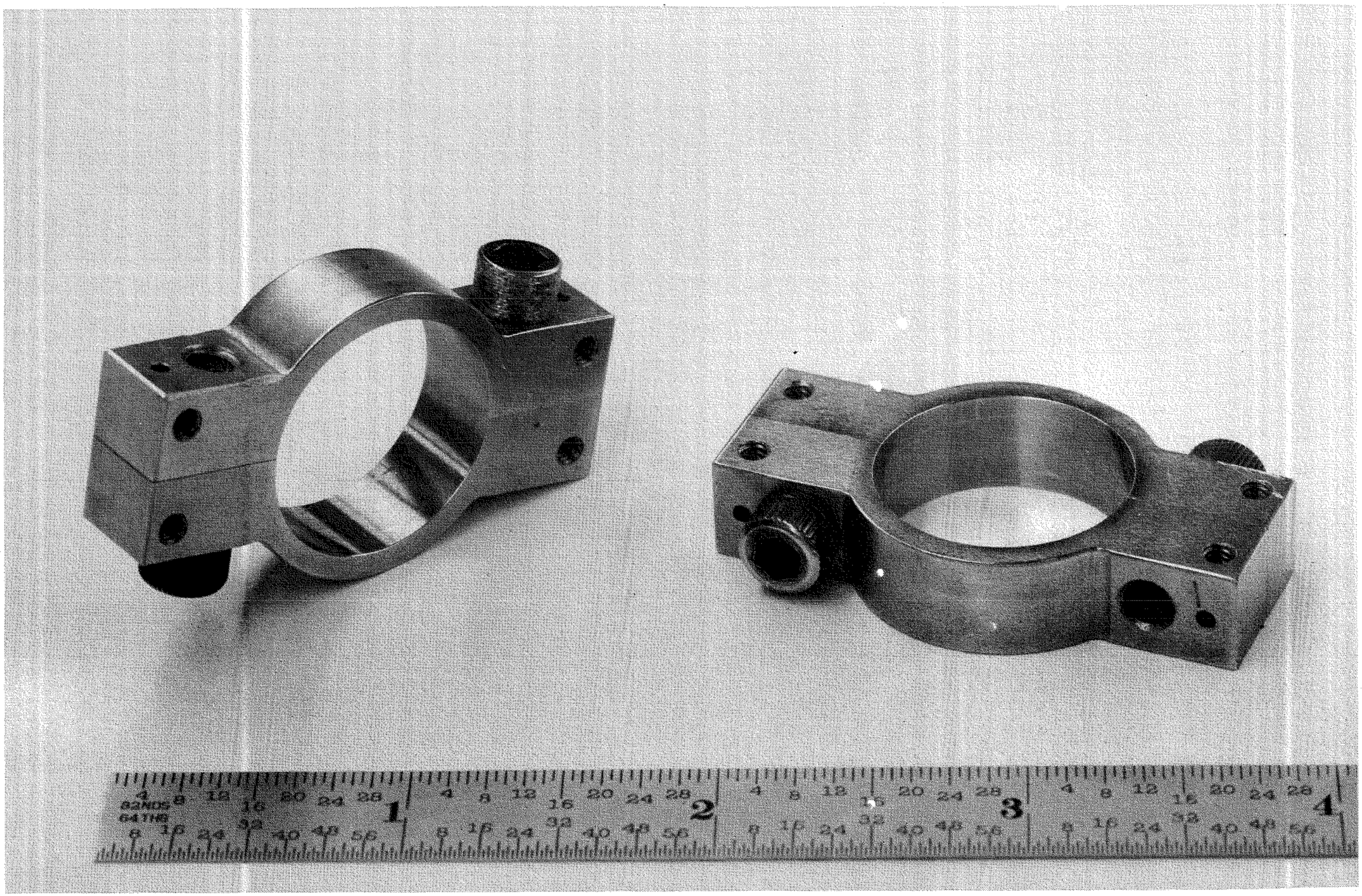

FIG. 3.2.1 PRECISION BALANCING COLLARS FOR ENGINE ROTOR SIMULATOR

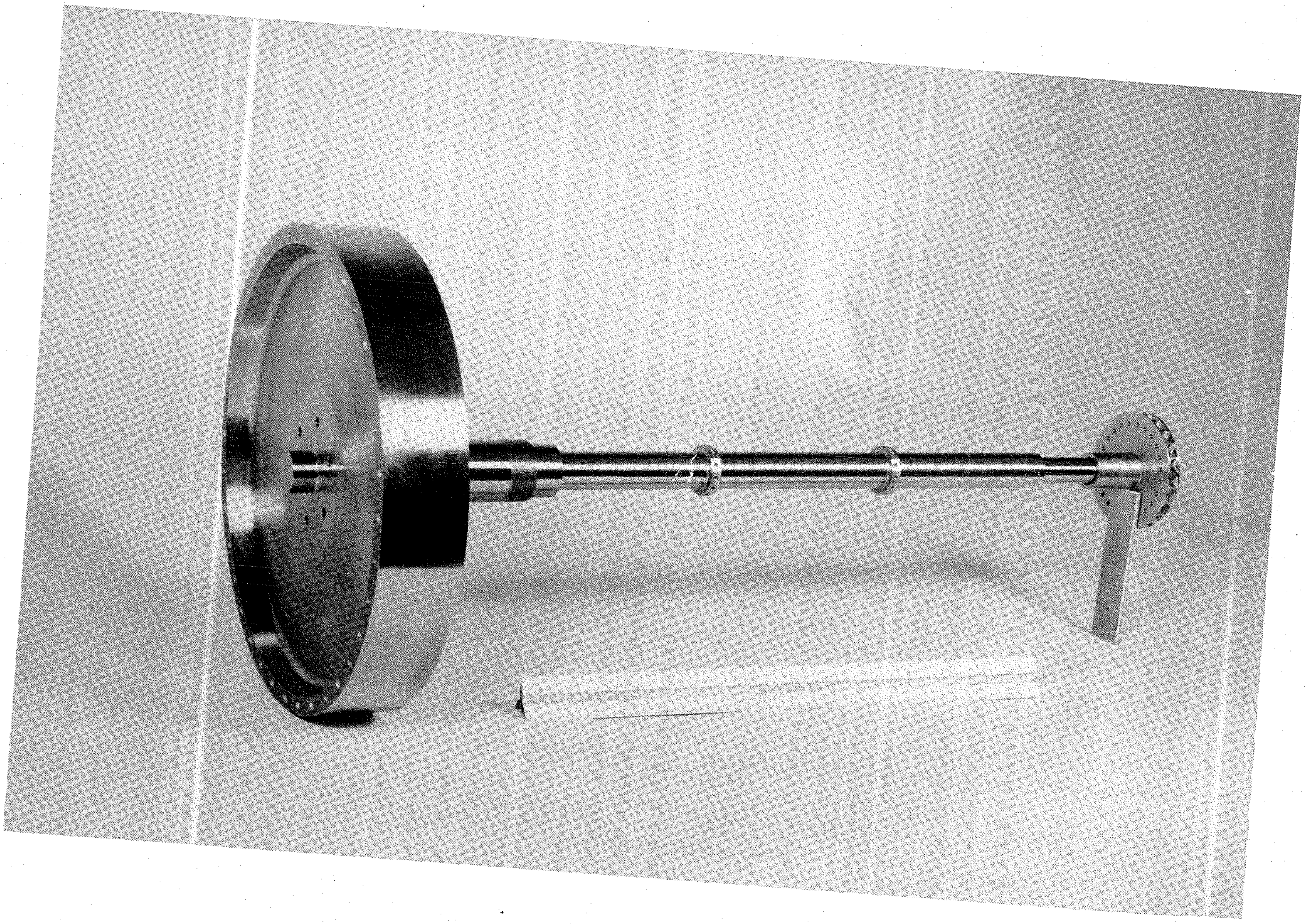

FIG. 3.2.2 ENGINE SIMULATOR ROTOR

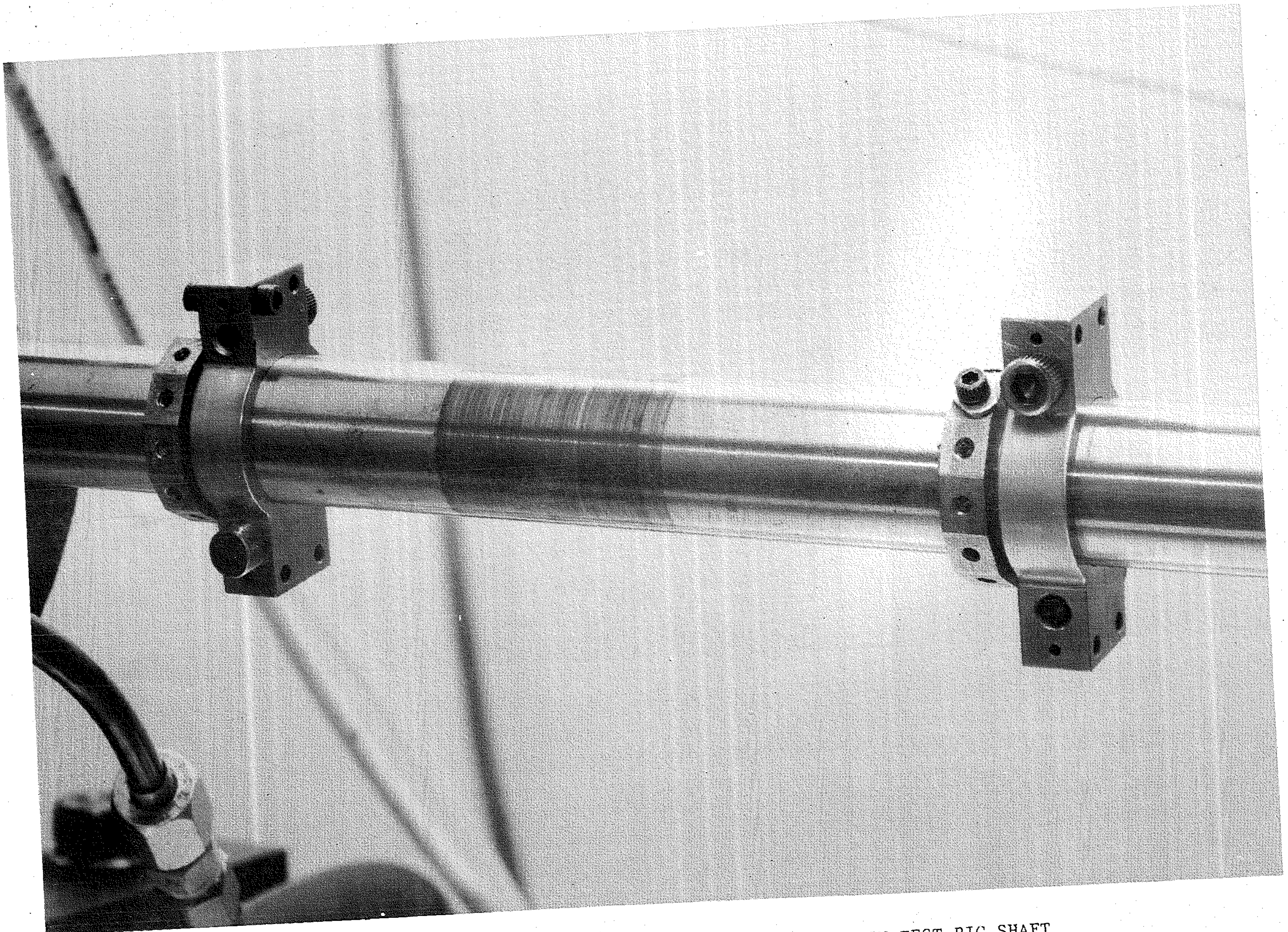

FIG. 3.2.3 CLOSE-UP VIEW OF BALANCING COLLARS MOUNTED ON TEST RIG SHAFT

MTI-16458

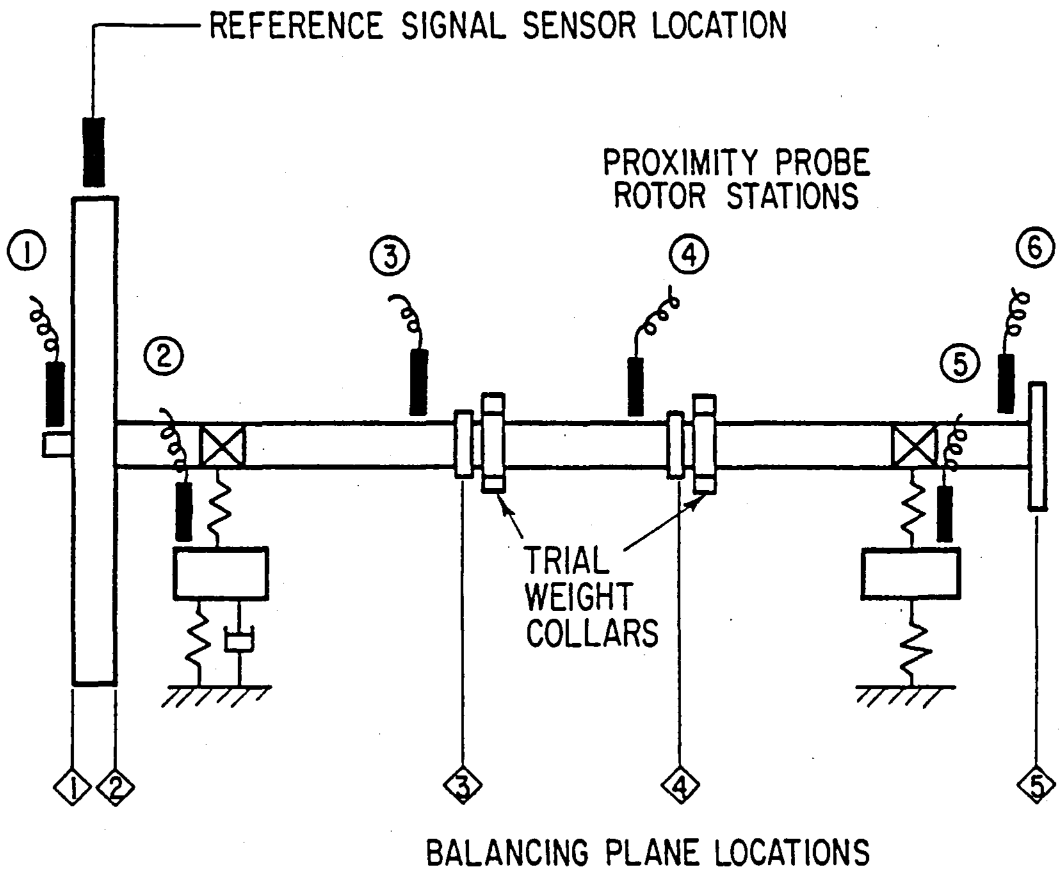

FIG. 3.2.4 PROBE AND BALANCING PLANE LOCATIONS ALONG TEST ROTOR USED FOR PRECISION BALANCING COLLARS EVALUATION

82712

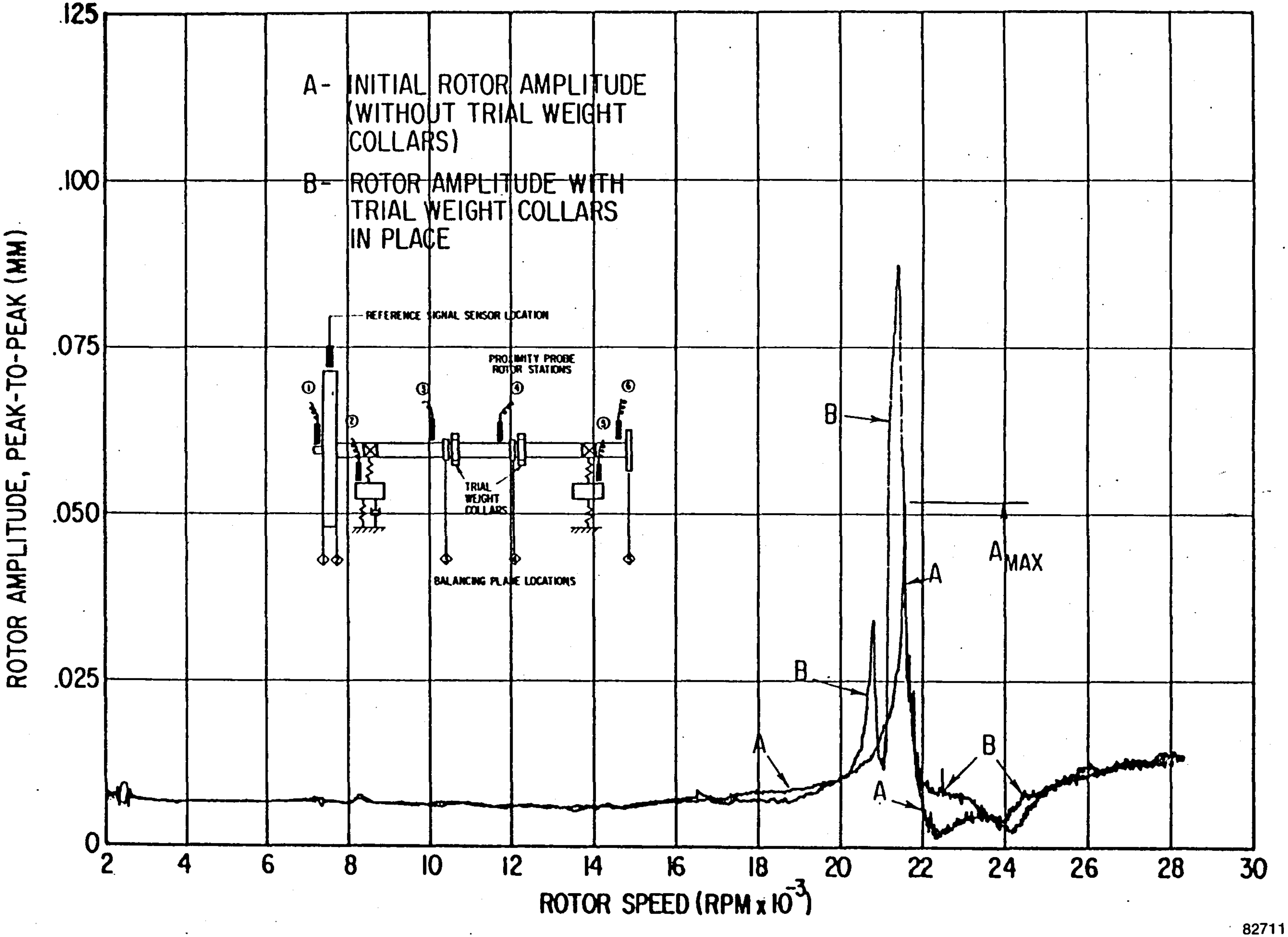

FIG. 3.2.5 ROTOR AMPLITUDES AT STATION 4 – WITH AND WITHOUT COLLARS ON SHAFT

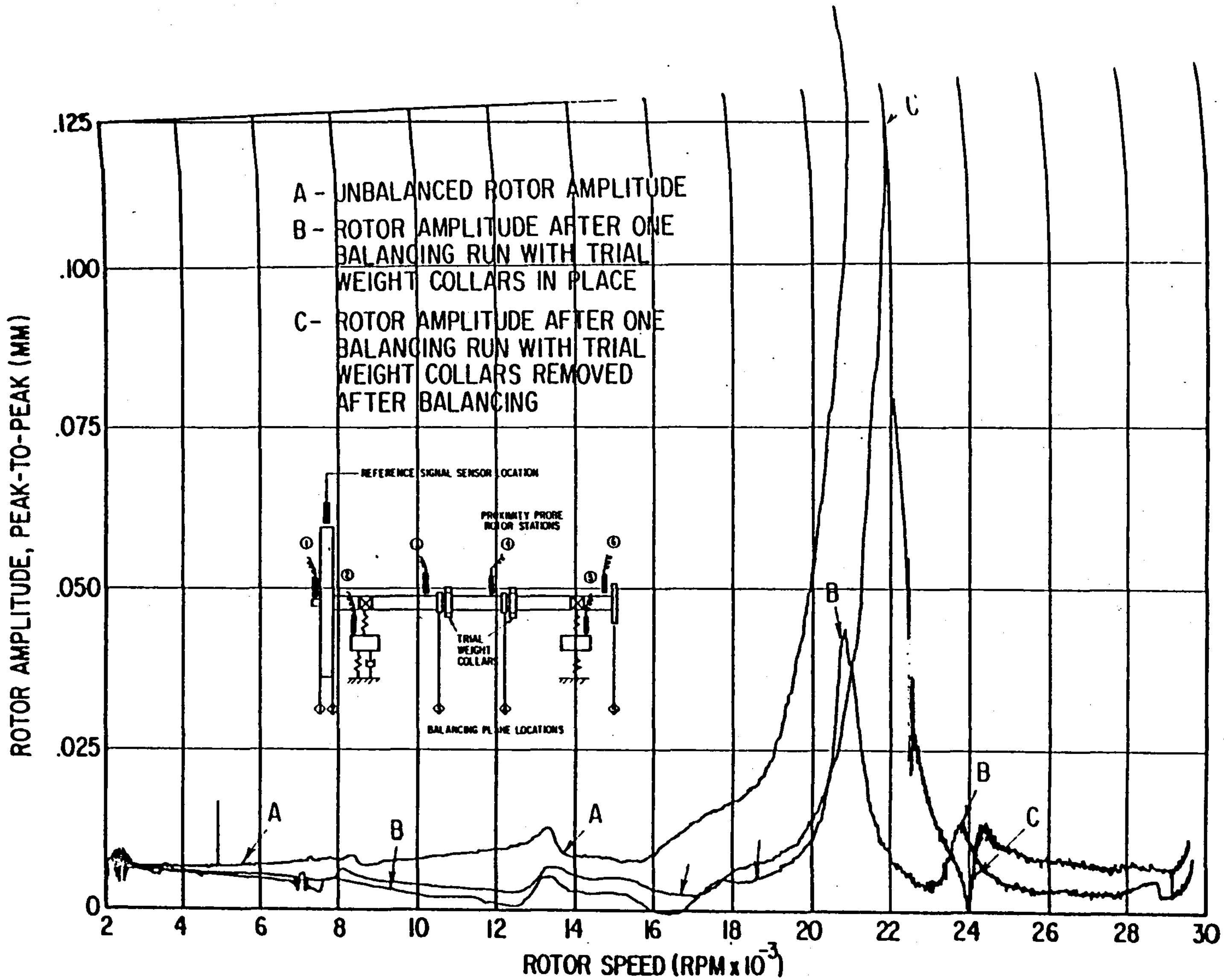

82722

FIG. 3.2.6 ROTOR AMPLITUDES AT STATION 4 - INITIAL CONDITION AND AFTER ONE BALANCING RUN, WITH AND WITHOUT COLLARS ON SHAFT

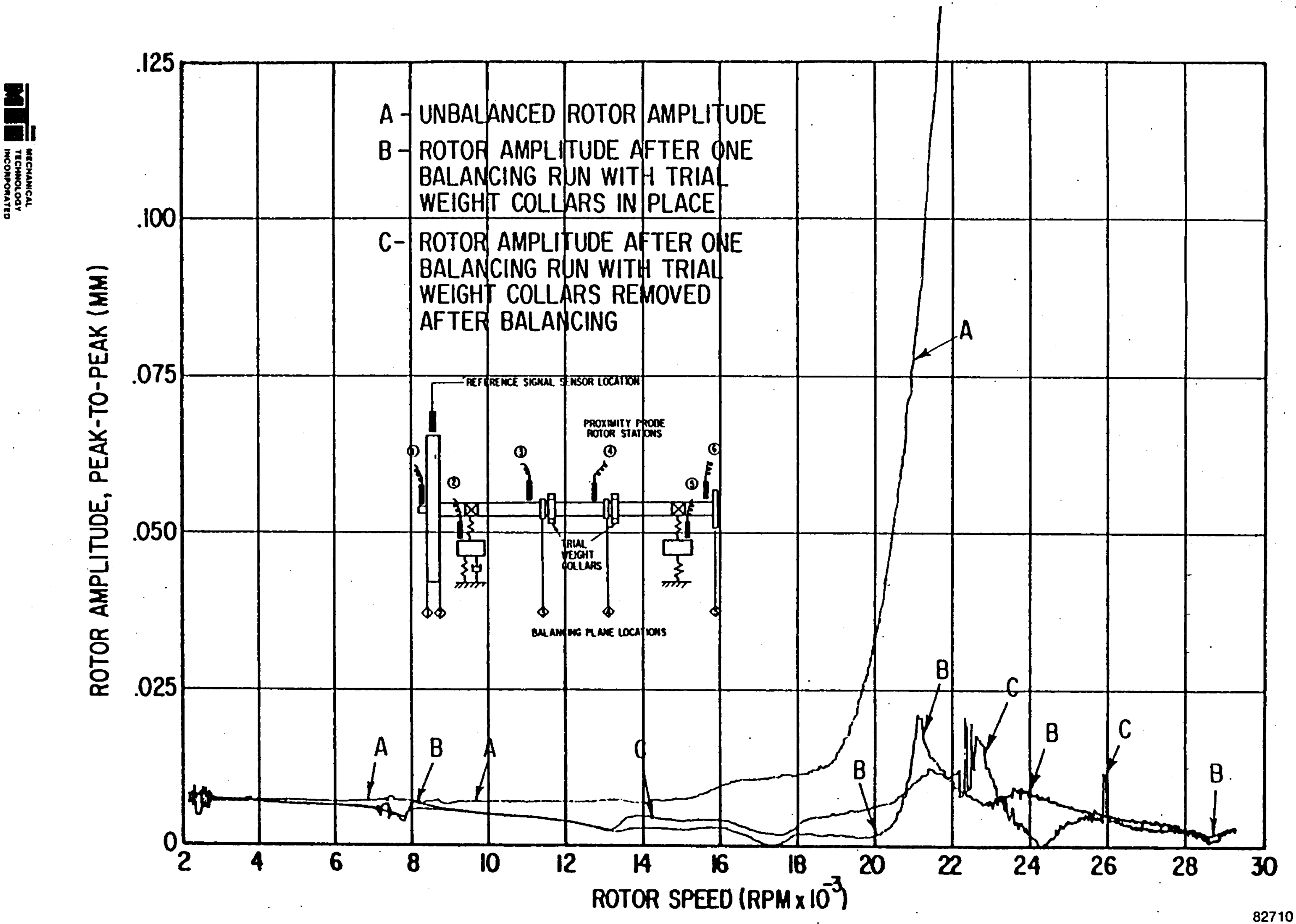

FIG. 3.2.7 ROTOR AMPLITUDES AT STATION 4 - INITIAL CONDITION AND AFTER ONE BALANCING RUN (REPEAT), WITH AND WITHOUT COLLARS ON SHAFT

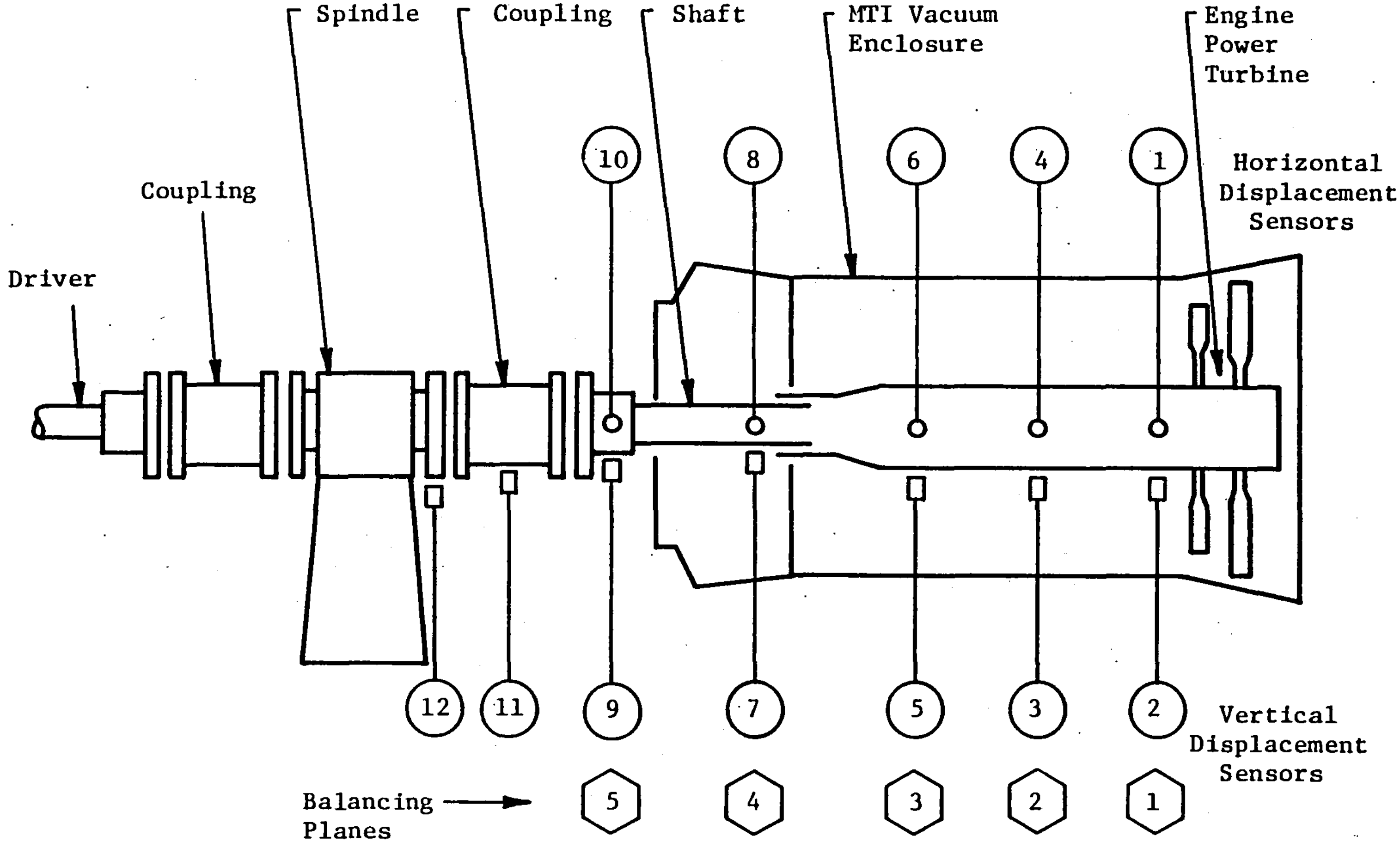

FIG. 3.3.1 SPIN-UP HARDWARE & INSTRUMENTATION LOCATIONS - T55 POWER TURBINE

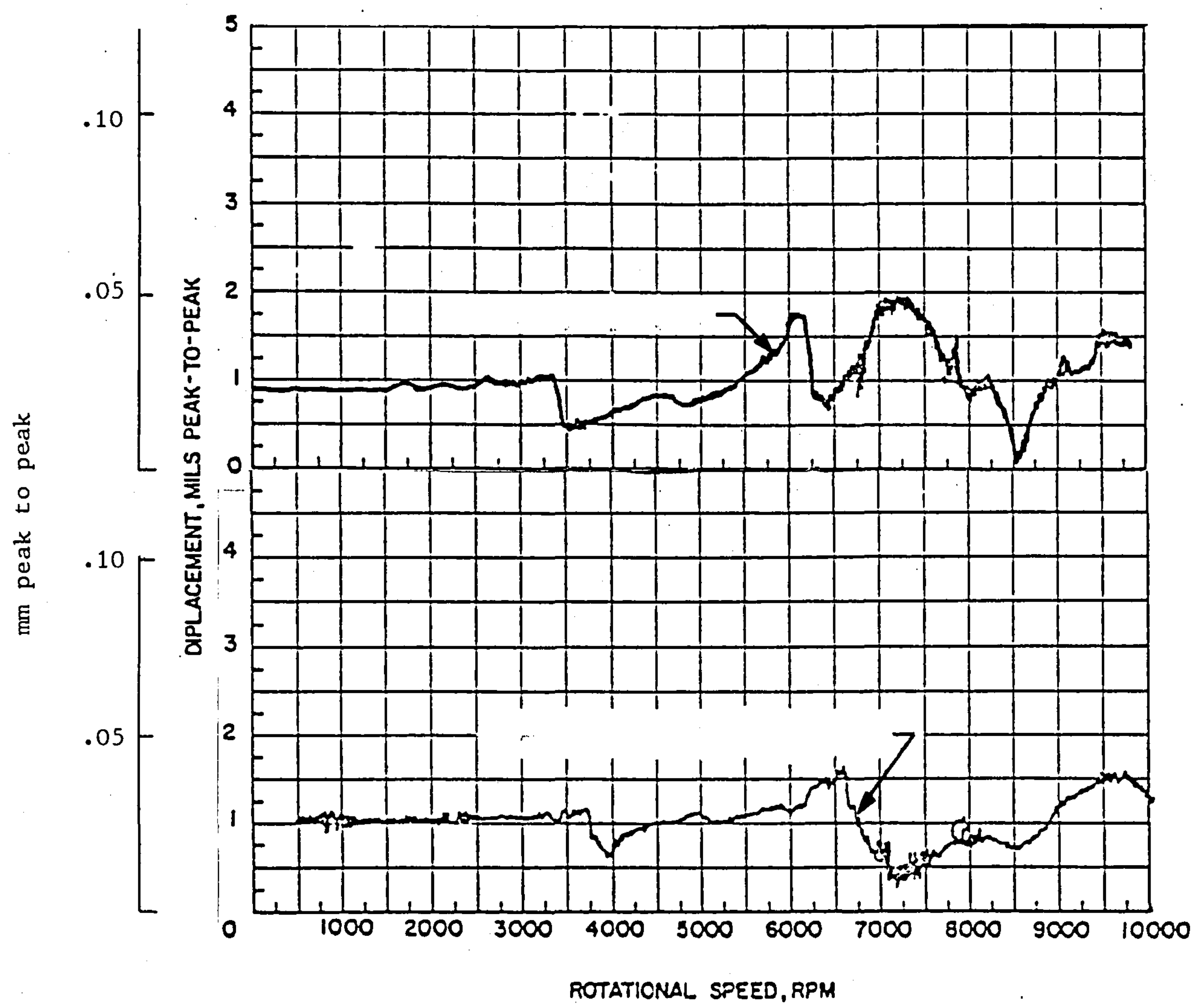

82708

FIG. 3.3.2 ROTOR 1 - AS RECEIVED - PROBES 2 & 5

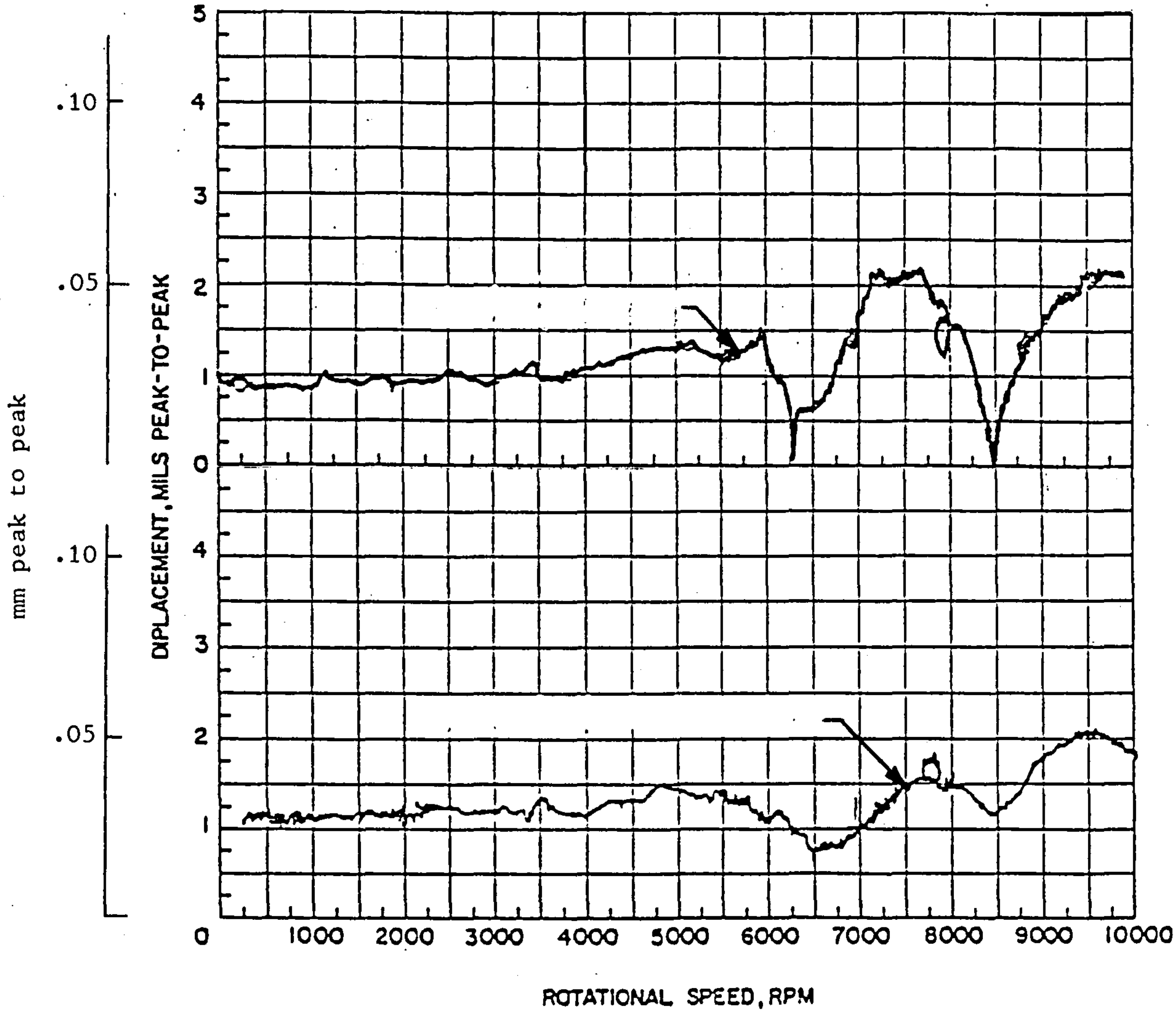

82709

FIG. 3.3.3 ROTOR 1 - AS RECEIVED AND AFTER HIGH SPEED BALANCE - PROBES 2 & 5

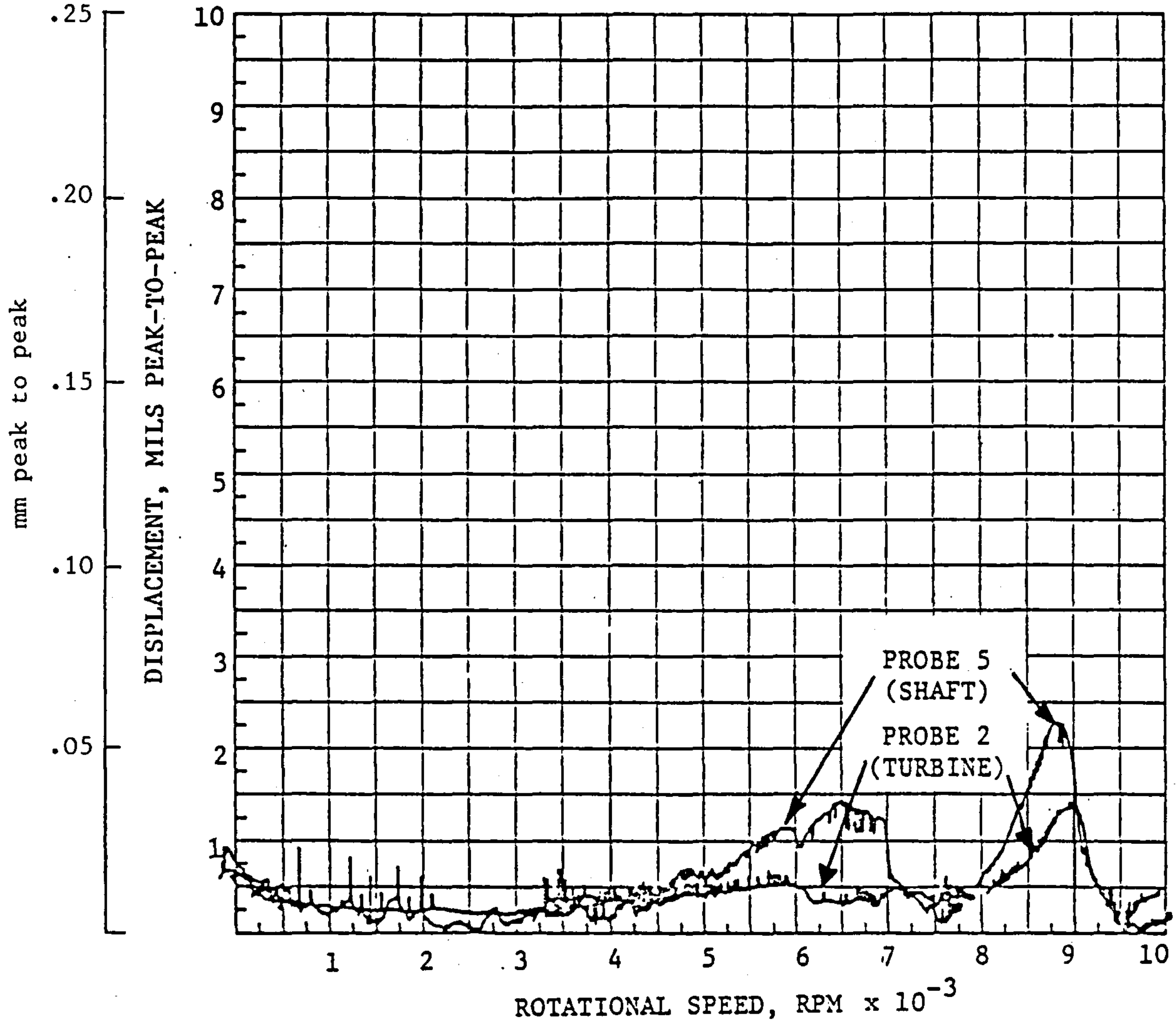

82705

FIG. 3.3.4 ROTOR 2 - AS RECEIVED - PROBES 2 & 5

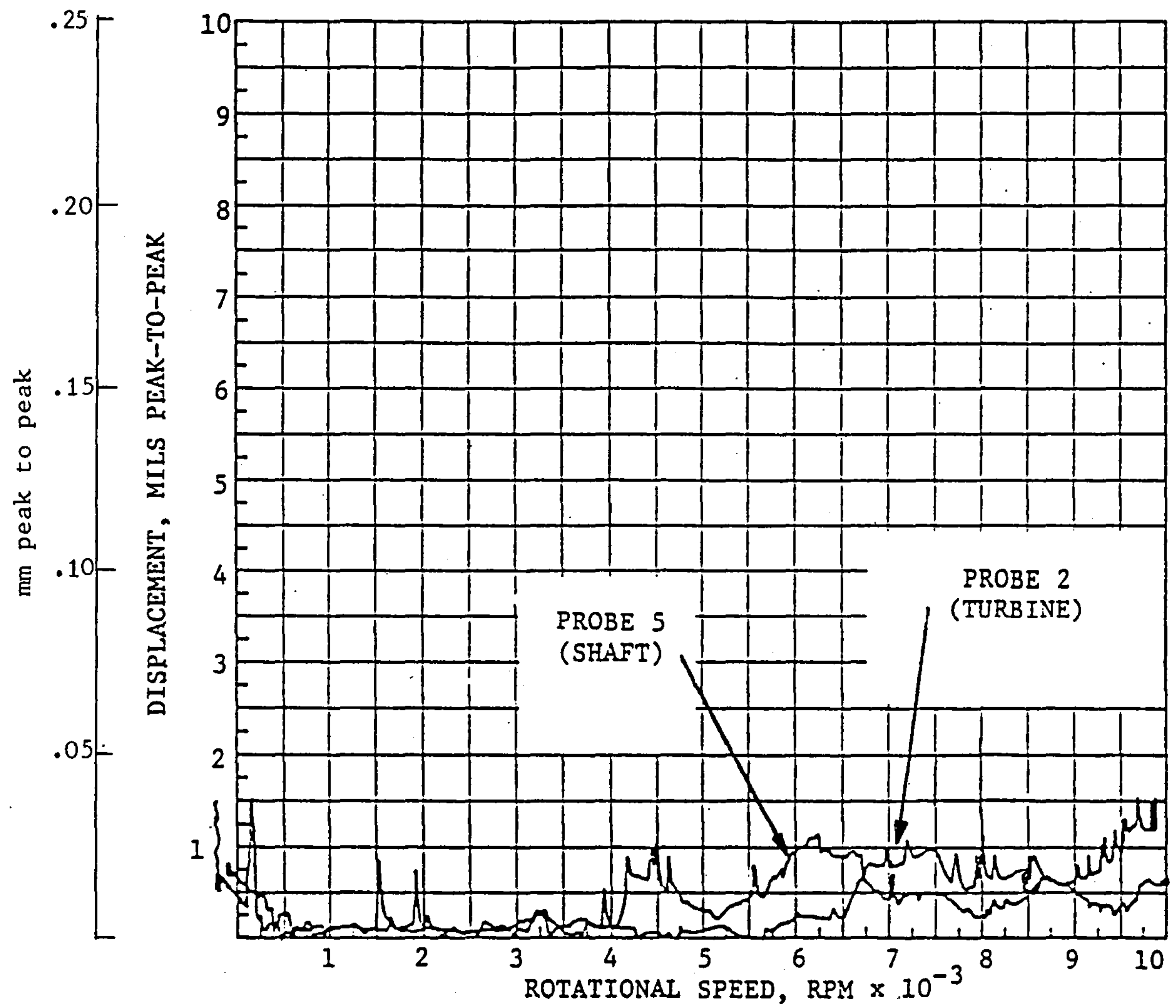

82704

FIG. 3.3.5 ROTOR 2 - AFTER HIGH SPEED BALANCE - PROBES 2 & 5

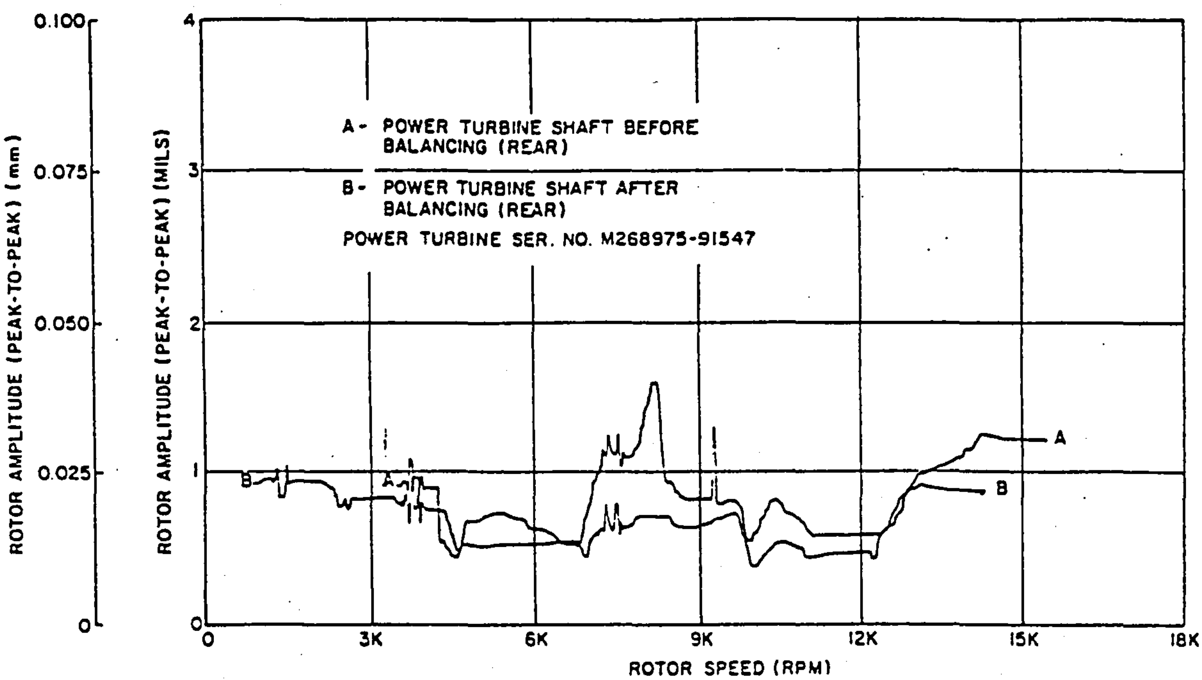

82703

FIG. 3.3.6 ROTOR 3 - BEFORE & AFTER HIGH SPEED BALANCE - PROBE 2

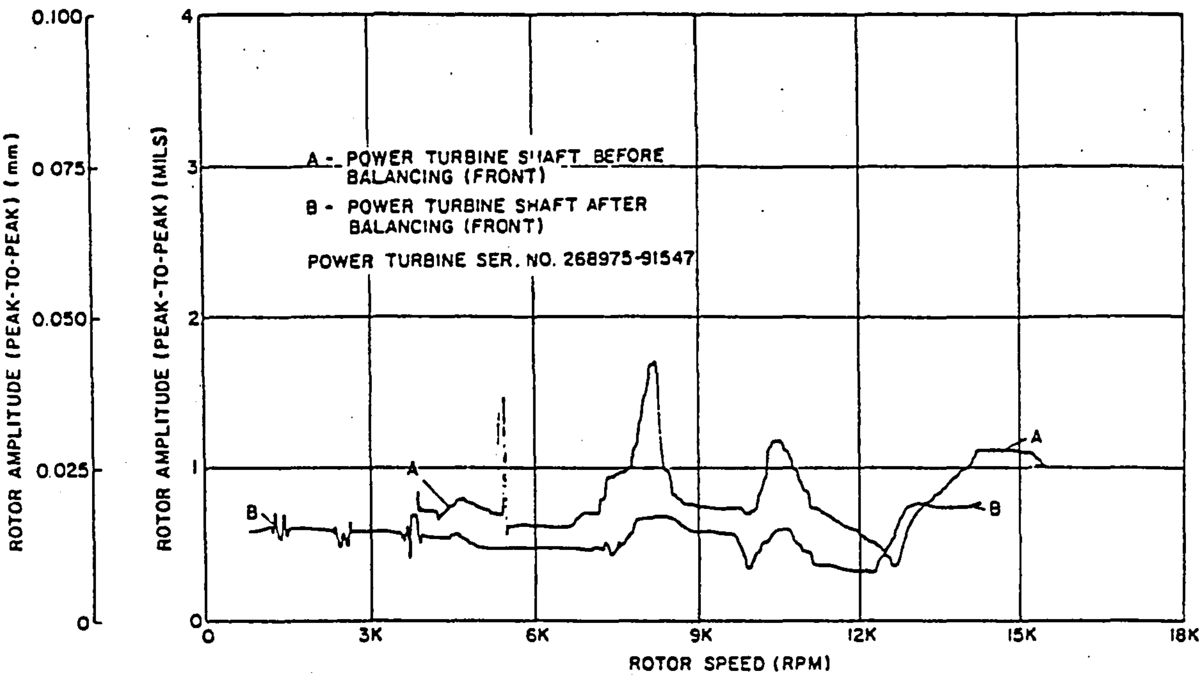

82702

FIG. 3.3.7 BEFORE & AFTER HIGH SPEED BALANCE - PROBE 5

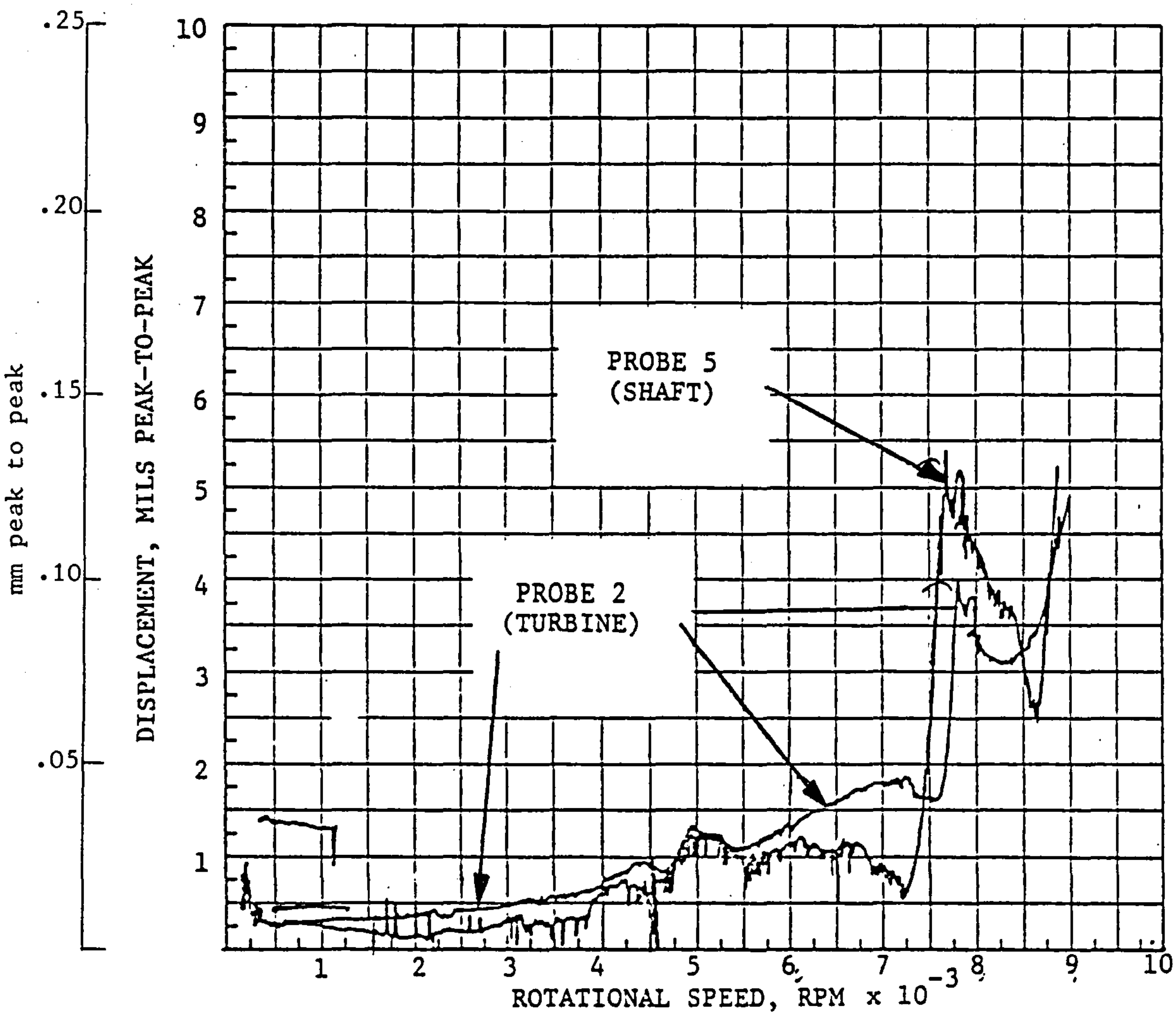

82701

FIG. 3.3.8 ROTOR 4 - AS RECEIVED - PROBES 2 & 5

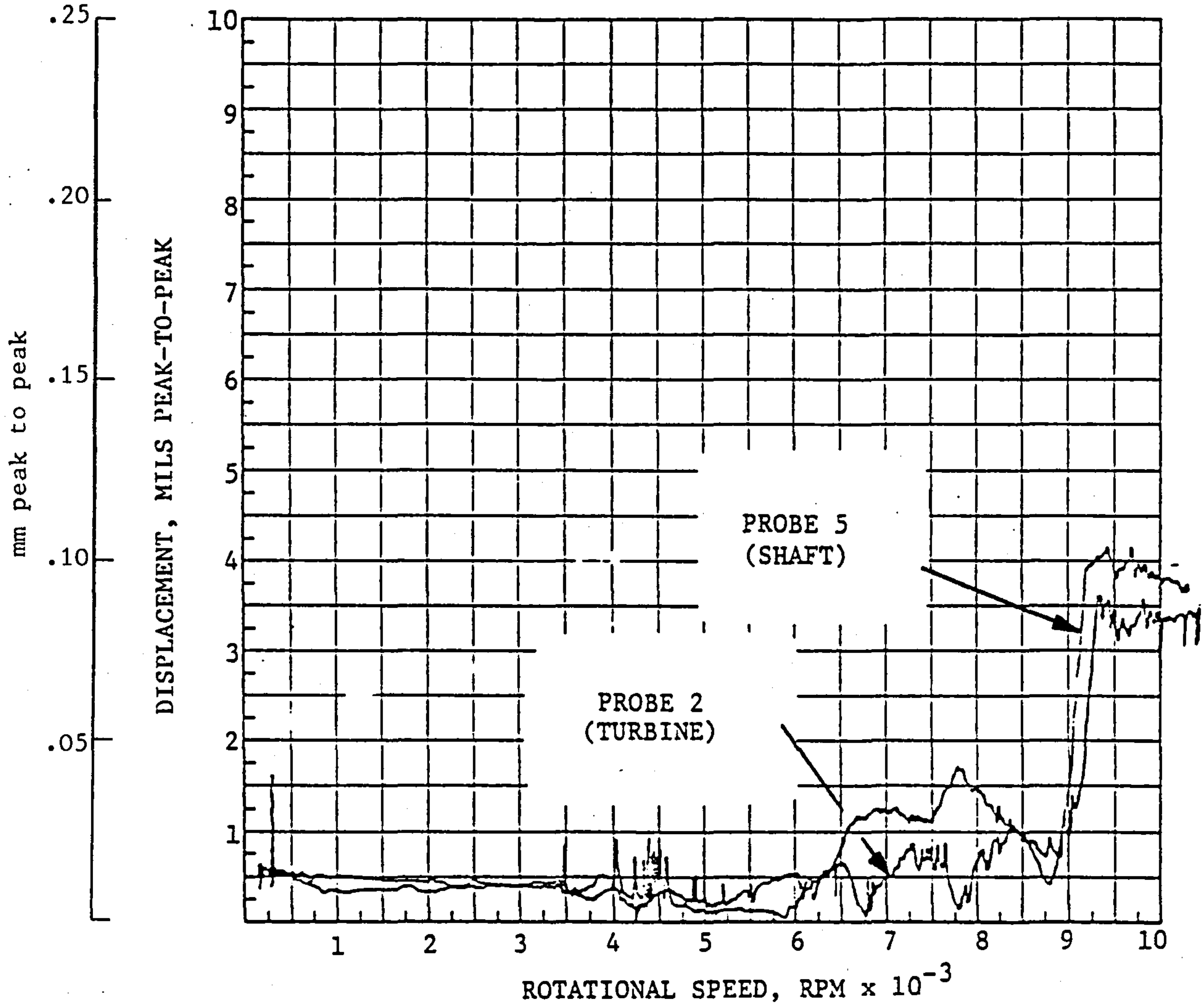

82700

FIG. 3.3.9 ROTOR 4 - AFTER HIGH SPEED BALANCE - PROBES 2 & 5

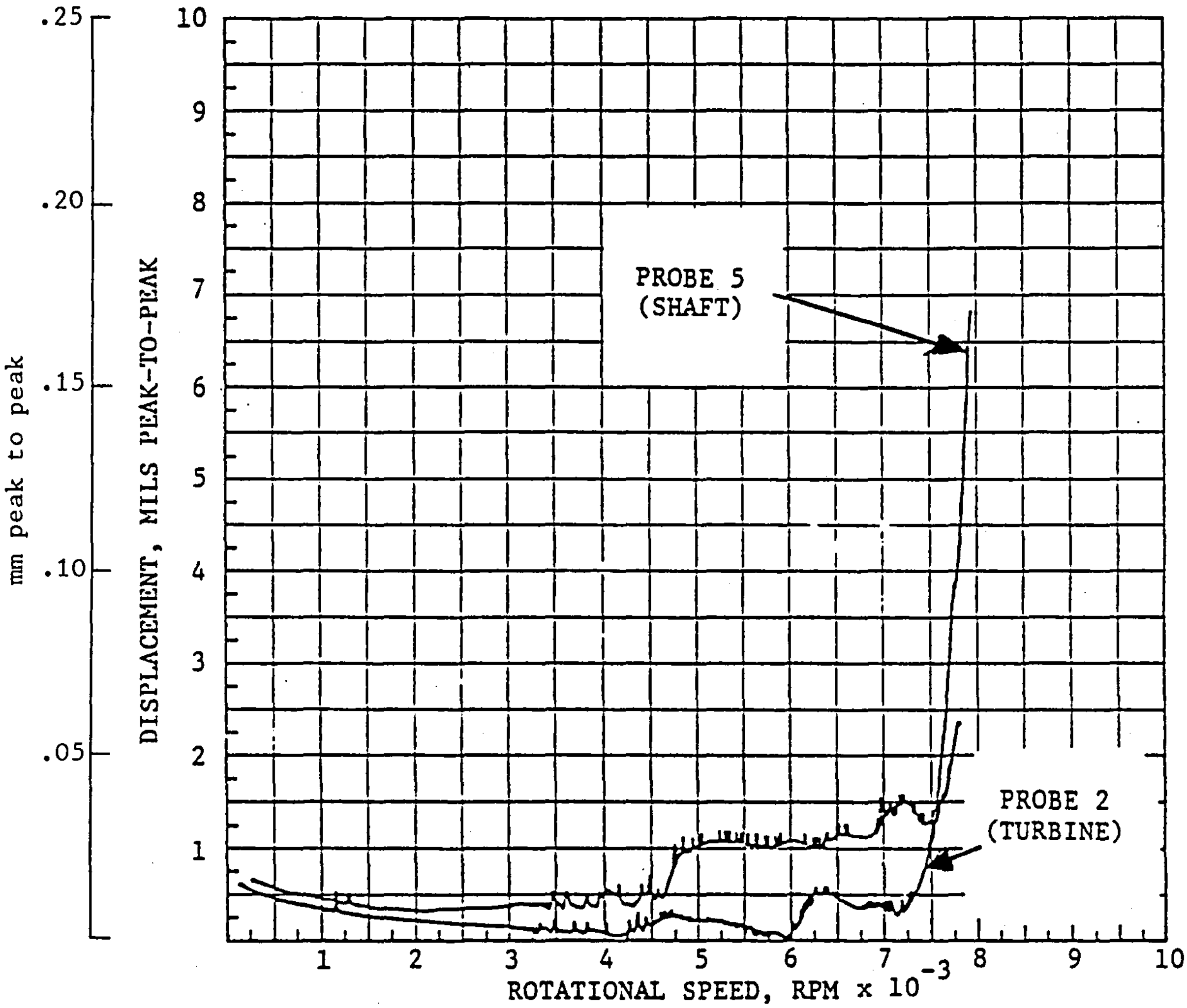

82699

FIG. 3.3.10 ROTOR 5 - AS RECEIVED - PROBES 2 & 5

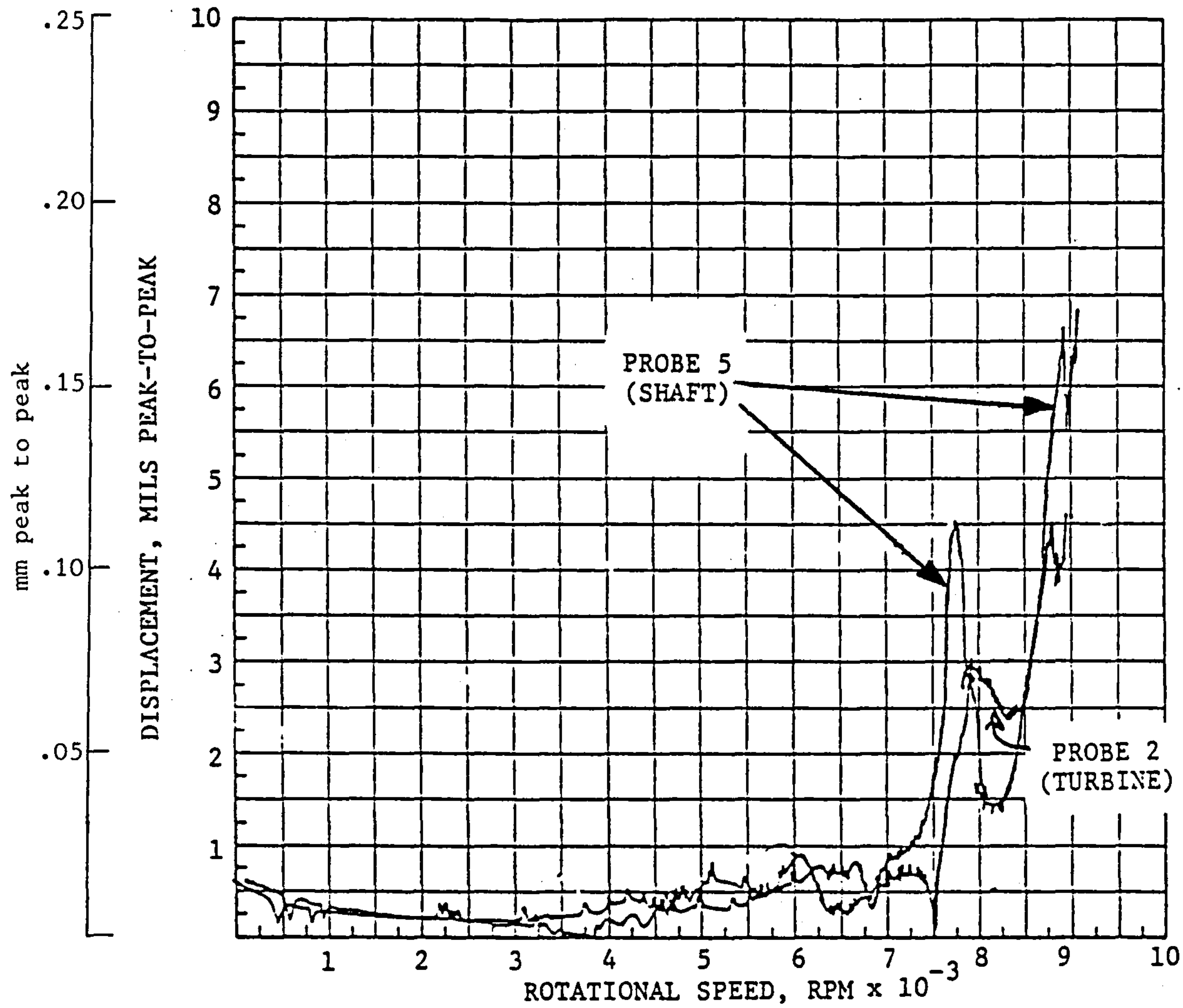

82698

FIG. 3.3.11 ROTOR 5 - AFTER INITIAL HIGH SPEED BALANCE - PROBES 2 & 5

MECHANICAL TECHNOLOGY INCORPORATED

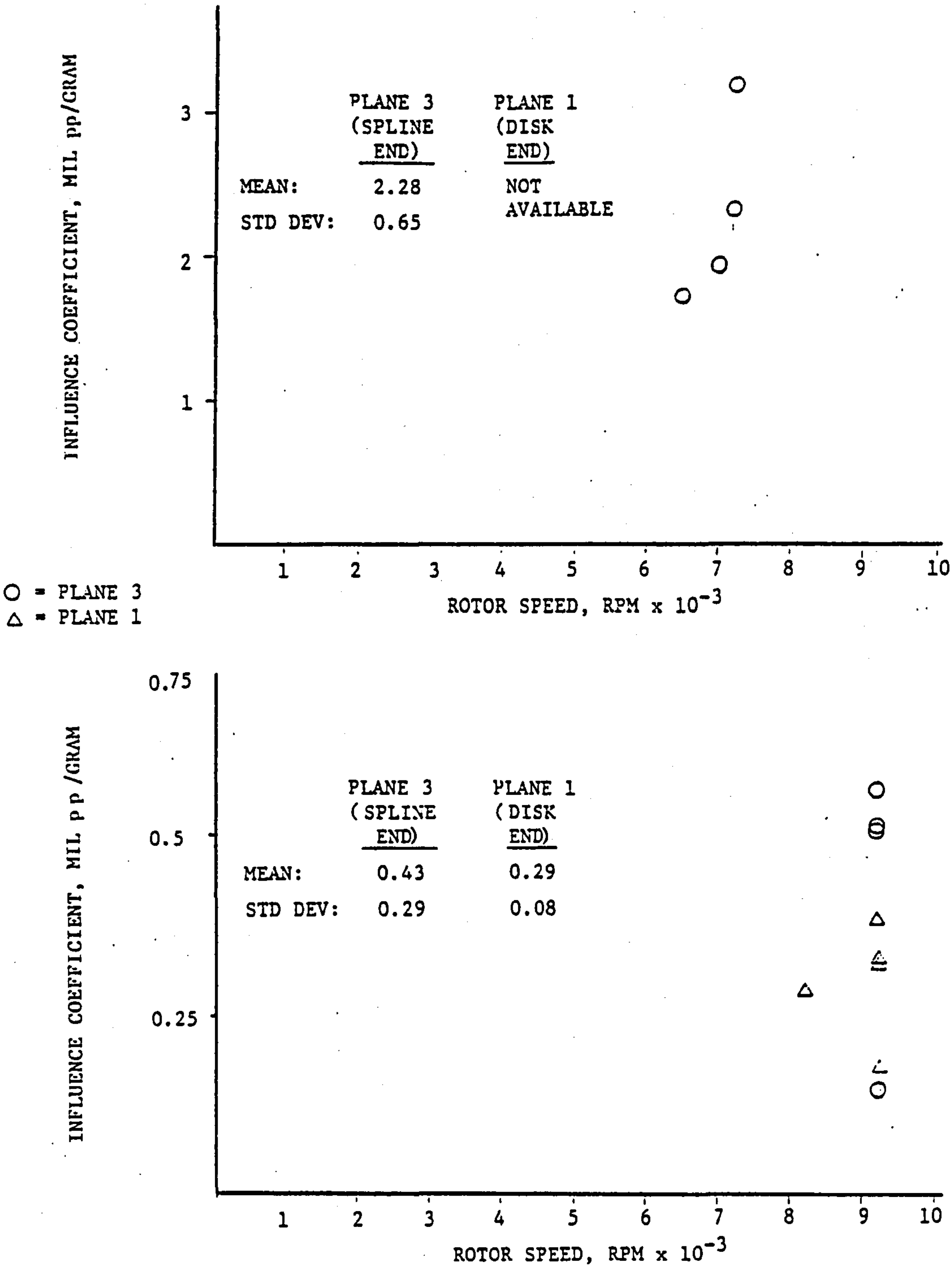

82721

FIG. 3.3.12 CONSOLIDATED INFLUENCE COEFFICIENT DATA

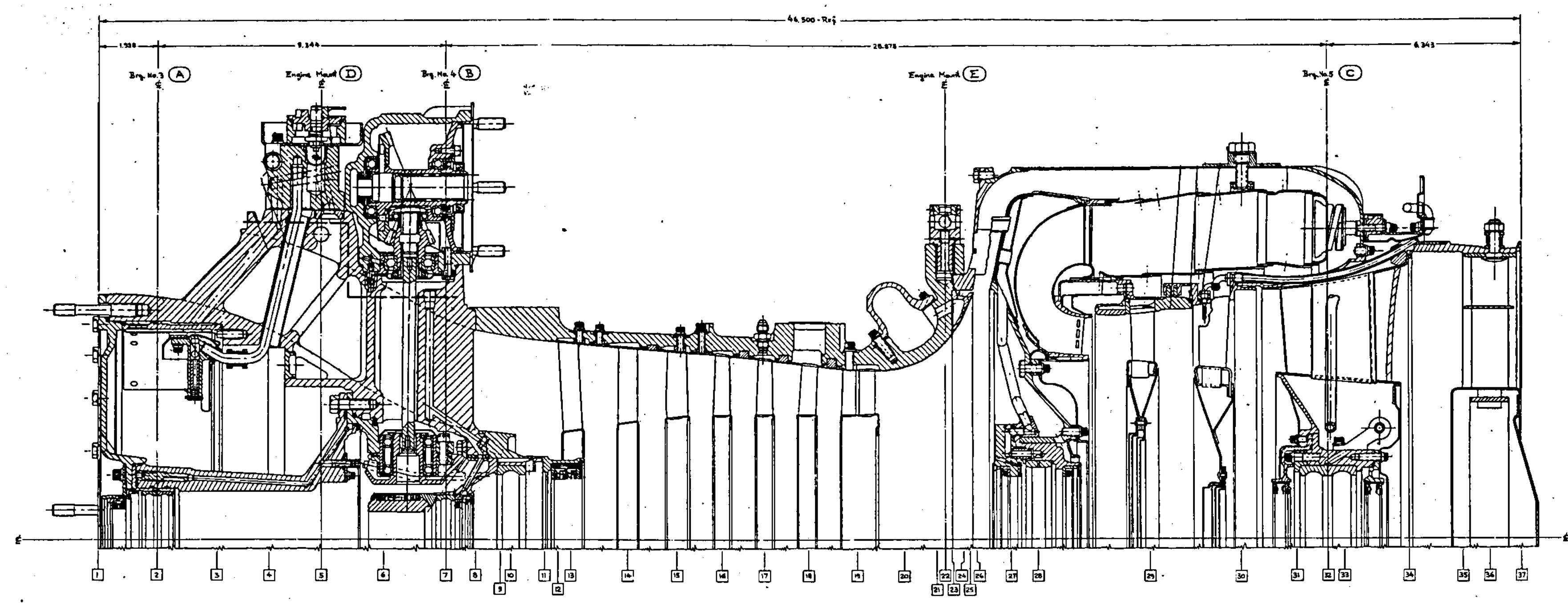

<table>
<tr><th>1</th><th>2</th><th>3</th><th>4</th><th>5</th><th>6</th><th>7</th><th>8</th><th>9</th><th>10</th><th>11</th><th>12</th><th>13</th><th>14</th><th>15</th><th>16</th><th>17</th><th>18</th><th>19</th><th>20</th><th>21</th><th>22</th><th>23</th><th>24</th><th>25</th><th>26</th><th>27</th><th>28</th><th>29</th><th>30</th><th>31</th><th>32</th><th>33</th><th>34</th><th>35</th><th>36</th><th>37</th><th></th></tr>
<tr><td>9.2</td><td>—</td><td>5.0</td><td>19.2</td><td>—</td><td>17.4</td><td>—</td><td>14.9</td><td>—</td><td>—</td><td>—</td><td>—</td><td>3.9</td><td>4.5</td><td>3.4</td><td>3.2</td><td>3.3</td><td>2.5</td><td>4.4</td><td>—</td><td>—</td><td>—</td><td>—</td><td>—</td><td>—</td><td>126.8</td><td>—</td><td>—</td><td>—</td><td>16.0</td><td>81.9</td><td>—</td><td>33.9</td><td>—</td><td>—</td><td>21.1</td><td>—</td><td>Concentrated W — lbs.</td></tr>
<tr><td>—</td><td>—</td><td>—</td><td>—</td><td>—</td><td>—</td><td>—</td><td>—</td><td>—</td><td>—</td><td>—</td><td>—</td><td>—</td><td>—</td><td>—</td><td>—</td><td>—</td><td>—</td><td>—</td><td>—</td><td>—</td><td>—</td><td>—</td><td>—</td><td>—</td><td>—</td><td>—</td><td>—</td><td>—</td><td>—</td><td>—</td><td>—</td><td>—</td><td>—</td><td>—</td><td>—</td><td>—</td><td>Concentrated Ip - lbs.in.²</td></tr>
<tr><td>—</td><td>—</td><td>—</td><td>—</td><td>—</td><td>—</td><td>—</td><td>—</td><td>—</td><td>—</td><td>—</td><td>—</td><td>—</td><td>—</td><td>—</td><td>—</td><td>—</td><td>—</td><td>—</td><td>—</td><td>—</td><td>—</td><td>—</td><td>—</td><td>—</td><td>—</td><td>—</td><td>—</td><td>—</td><td>—</td><td>—</td><td>—</td><td>—</td><td>—</td><td>—</td><td>—</td><td>—</td><td>Concentrated It - lbs.in.²</td></tr>
<tr><td>1.938</td><td>1.969</td><td>1.669</td><td>1.669</td><td>2.018</td><td>2.019</td><td>0.580</td><td>0.775</td><td>0.350</td><td>1.120</td><td>0.450</td><td>0.400</td><td>1.872</td><td>1.596</td><td>1.487</td><td>1.487</td><td>1.446</td><td>1.616</td><td>1.511</td><td>1.050</td><td>0.275</td><td>0.230</td><td>0.370</td><td>0.200</td><td>0.230</td><td>1.100</td><td>0.850</td><td>3.600</td><td>3.020</td><td>1.800</td><td>1.000</td><td>0.500</td><td>2.140</td><td>1.780</td><td>0.875</td><td>1.049</td><td>—</td><td>Distance between Stations - in.</td></tr>
<tr><td>14.040</td><td>15.560</td><td>14.800</td><td>12.960</td><td>18.960</td><td>16.900</td><td>15.430</td><td>15.280</td><td>15.280</td><td>15.280</td><td>14.800</td><td>14.040</td><td>13.680</td><td>13.540</td><td>13.420</td><td>13.320</td><td>13.150</td><td>12.700</td><td>12.380</td><td>12.760</td><td>13.900</td><td>14.400</td><td>17.000</td><td>17.440</td><td>0.960</td><td>23.700</td><td>24.400</td><td>24.400</td><td>24.400</td><td>24.400</td><td>1.790</td><td>16.538</td><td>17.500</td><td>19.040</td><td>19.040</td><td>19.080</td><td>—</td><td>O.D. for Stiffness - in.</td></tr>
<tr><td>16.040</td><td>15.560</td><td>14.800</td><td>12.960</td><td>18.960</td><td>16.900</td><td>15.420</td><td>15.280</td><td>15.280</td><td>15.280</td><td>15.280</td><td>14.040</td><td>13.760</td><td>13.540</td><td>13.850</td><td>13.540</td><td>13.900</td><td>13.250</td><td>13.700</td><td>15.960</td><td>18.800</td><td>18.800</td><td>19.680</td><td>18.100</td><td>0.960</td><td>24.000</td><td>24.400</td><td>24.400</td><td>24.400</td><td>24.400</td><td>—</td><td>16.538</td><td>17.500</td><td>19.400</td><td>19.160</td><td>19.080</td><td>—</td><td>O.D. for Weight - in.</td></tr>
<tr><td>14.300</td><td>14.250</td><td>13.630</td><td>12.160</td><td>17.700</td><td>15.300</td><td>14.080</td><td>14.300</td><td>13.440</td><td>13.220</td><td>13.040</td><td>13.240</td><td>13.130</td><td>12.860</td><td>12.640</td><td>12.420</td><td>12.100</td><td>11.920</td><td>11.480</td><td>11.750</td><td>12.680</td><td>13.200</td><td>16.300</td><td>16.300</td><td>—</td><td>23.200</td><td>24.100</td><td>24.200</td><td>24.280</td><td>24.280</td><td>—</td><td>16.750</td><td>17.312</td><td>18.780</td><td>18.700</td><td>18.700</td><td>—</td><td>I.D. for both Stiffness and Weight - in.</td></tr>
<tr><td>1</td><td>1</td><td>1</td><td>1</td><td>2</td><td>2</td><td>2</td><td>2</td><td>2</td><td>2</td><td>2</td><td>2</td><td>3</td><td>3</td><td>4</td><td>4</td><td>5</td><td>5</td><td>6</td><td>6</td><td>6</td><td>6</td><td>7</td><td>7</td><td>7</td><td>7</td><td>7</td><td>8</td><td>9</td><td>9</td><td>9</td><td>9</td><td>9</td><td>10</td><td>10</td><td>10</td><td>10</td><td>Material No. (Ref. to Computer Input)</td></tr>
<tr><td colspan="4">90</td><td colspan="8">130</td><td colspan="2">310</td><td colspan="2">330</td><td colspan="2">430</td><td colspan="4">540</td><td colspan="5">680</td><td>980</td><td colspan="4">1000</td><td>880</td><td colspan="4">800</td><td>Temperature of the Shaft - °F</td></tr>
<tr><td colspan="22">Assumed to be similar to Magnesium Casting Alloy EZ33A</td><td colspan="11">Assumed to be similar to Hastelloy X</td><td colspan="4">Similar to A-286</td><td>Material of the Shaft</td></tr>
<tr><td colspan="4">6.54</td><td colspan="8">6.46</td><td colspan="2">6.29</td><td colspan="2">6.03</td><td colspan="2">5.82</td><td colspan="4">5.60</td><td colspan="5">25.3</td><td>24.1</td><td colspan="4">23.4</td><td>24.1</td><td colspan="4">24.8</td><td>E — (10)⁶ psi.</td></tr>
<tr><td colspan="22">0.0664</td><td colspan="11">0.297</td><td colspan="4">0.296</td><td>ρ — lbs./in.³</td></tr>
<tr><td colspan="4">1.82</td><td colspan="8">1.79</td><td colspan="2">1.78</td><td colspan="2">1.68</td><td colspan="2">1.62</td><td colspan="4">1.58</td><td colspan="5">6.92</td><td>6.55</td><td colspan="4">6.37</td><td>6.55</td><td colspan="4">6.68</td><td>G — (10)⁶ psi.</td></tr>
</table>

MTI
0264-45333-500

Sheet 1 of 4; Rotor No. 1 with □ Stations

Mathematical Rotor Model of T-55 Engine Casing

Fig. 4-1 T55 Engine Casing Model

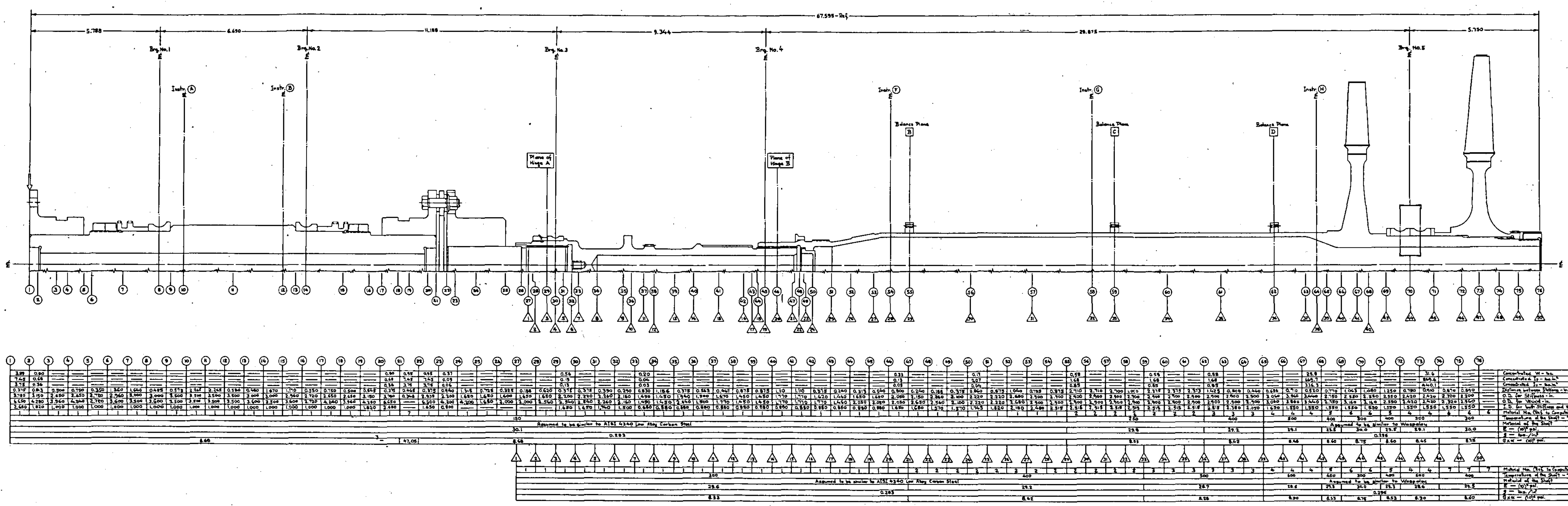

Bearing Data for Balancing Rig Analysis

Brg. No.	Total Estimated Radial Stiffness to Foundation K - lbs./in.	Damping B lbs.sec./in.
1	1,500,000	1.0
2	1,500,000	1.0
3	1,000,000	1.0
4	1,000,000	1.0
5	200,000	1.0

MTI
0264-45333-500

Sheet 2 of 4: Rotor No. 2 with △ Stations
Rotor No. 3 with ○ Stations

Mathematical Models of T-55 Power Turbine Balancing Rig Rotor Assembly

Fig. 4-2 T55 Balancing Rig Rotor and Engine Rotor Models

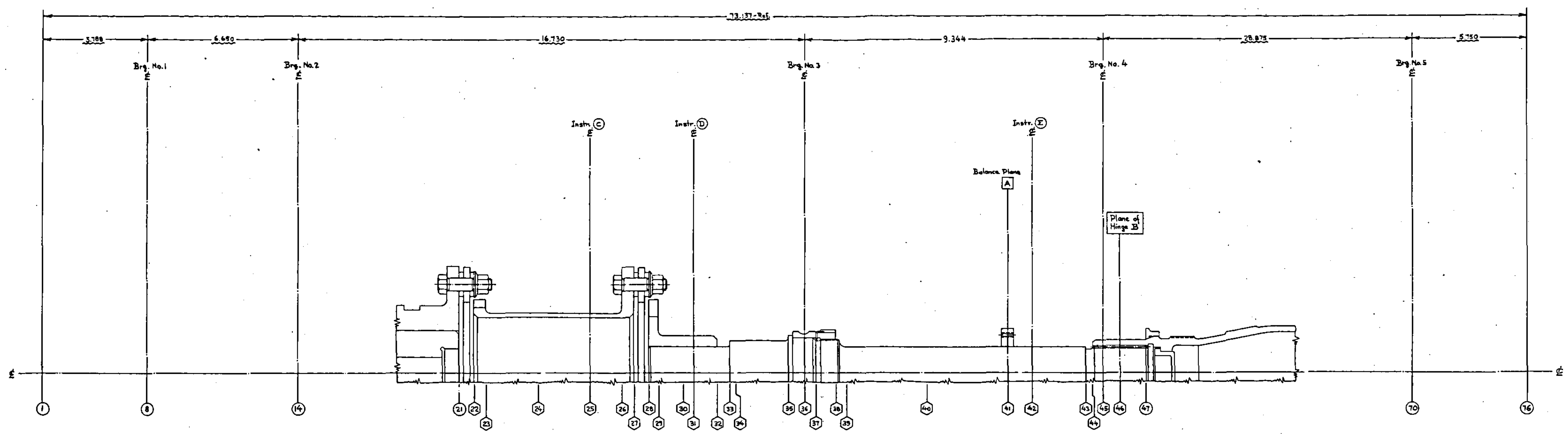

Station	22	23	24	25	26	27	28	29	30	31	32	33	34
Concentrated W – lbs.	0.95	—	—	—	—	0.95	0.95	0.19	—	—	—	—	—
Concentrated I_P – lbs.in.^{2}	7.45	—	—	—	—	7.45	7.45	0.07	—	—	—	—	—
Concentrated I_T – lbs.in.^{2}	3.75	—	—	—	—	3.75	3.75	0.04	—	—	—	—	—
Distance between Stations – in.	0.375	1.650	1.650	1.010	0.375	0.465	0.300	0.770	0.320	0.760	0.395	0.190	1.645
O.D. for Stiffness – in.	4.100	3.750	3.750	3.750	4.100	0.[illegible]48	2.800	1.950	1.650	1.650	1.650	1.870	2.000
O.D. for Weight – in.	4.500	3.750	3.750	3.750	4.500	—	4.250	2.340	2.340	2.340	1.650	2.000	2.000
I.D. for both Stiffness and Weight – in.	3.500	3.500	3.500	3.500	3.500	—	1.650	—	—	—	—	—	—
Material No. (Ref. to Computer Input)	1	1	1	1	1	7	1	1	1	1	1	1	1
Temperature of the Shaft – °F	150												
Material of the Shaft	Assumed to be similar to AISI 4340 Low Alloy Carbon Steel												
E — $(10)^6$ psi.	30.1												
ρ — lbs./in.^{3}	0.283												
G × α — $(10)^6$ psi.	8.68					47.05	8.68						

Station	35	36	37	38	39	40	41	42	43	44	45	46
Concentrated W – lbs.	—	—	—	—	—	—	0.14	—	—	—	—	0.56
Concentrated I_P – lbs.in.^{2}	—	—	—	—	—	—	0.18	—	—	—	—	0.19
Concentrated I_T – lbs.in.^{2}	—	—	—	—	—	—	0.09	—	—	—	—	0.13
Distance between Stations – in.	0.500	0.345	0.630	0.320	2.542	2.542	0.750	1.665	0.225	0.325	0.525	0.815
O.D. for Stiffness – in.	2.200	2.200	2.100	1.900	1.650	1.650	1.650	1.650	1.450	1.650	1.650	2.050
O.D. for Weight – in.	2.500	2.560	2.700	1.900	1.650	1.650	1.650	1.650	1.450	2.050	2.050	1.650
I.D. for both Stiffness and Weight – in.	—	—	—	—	—	—	—	—	—	—	—	1.650
Material No. (Ref. to Computer Input)	1	1	1	1	1	1	1	1	1	1	1	1

MTI
0264-45333-500

Sheet 3 of 4: Rotor No.4 with ⬡ Stations

Mathematical Model of T-55 Power Turbine
Modified Balancing Rig Rotor Assembly

Paul G. Barzatay
July 12, 1978

Fig. 4-3 T55 Modified Balancing Rig Rotor Model

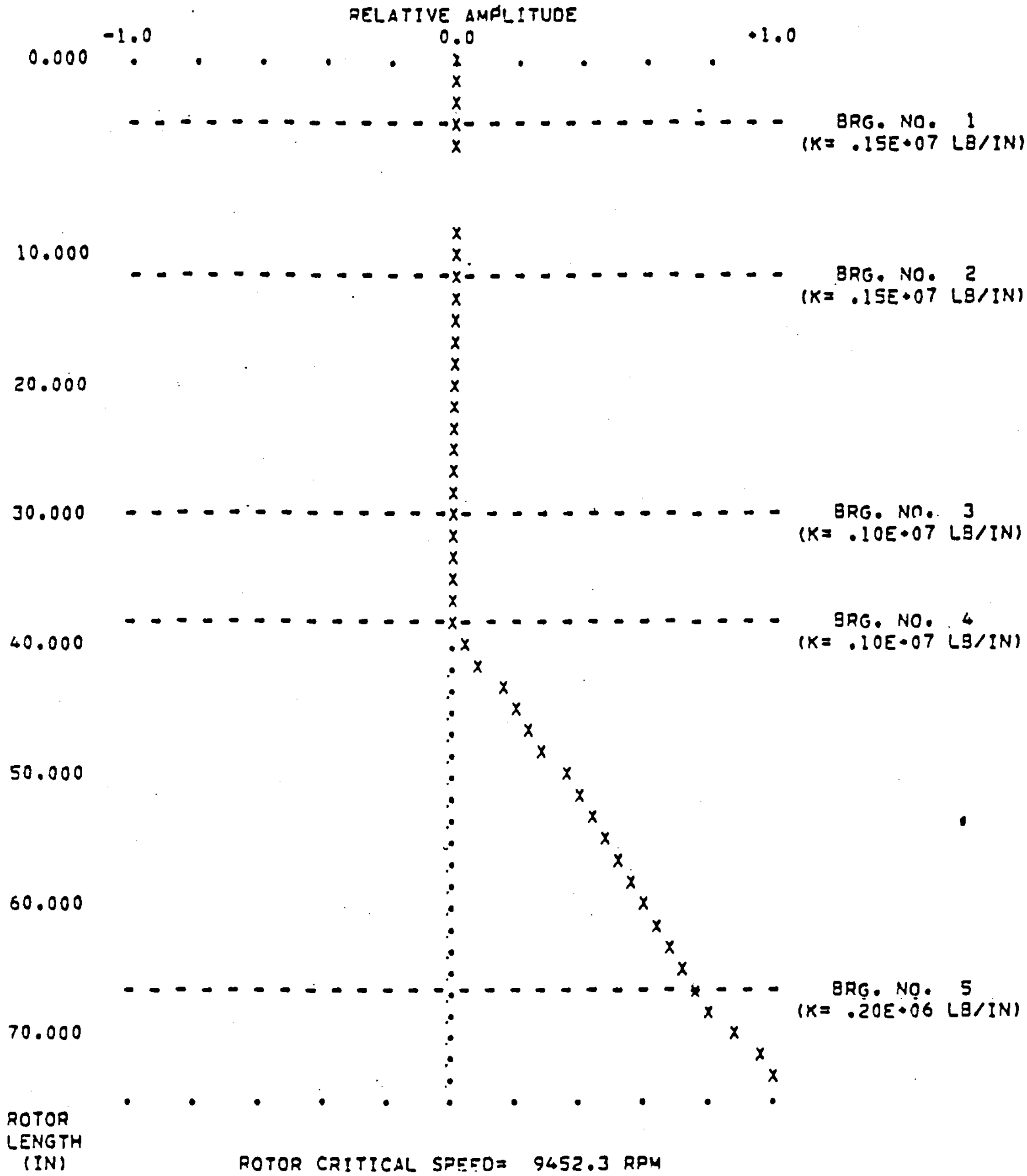

82686

FIG. 3.4.4 POWER TURBINE FIRST CRITICAL (CASE 4)

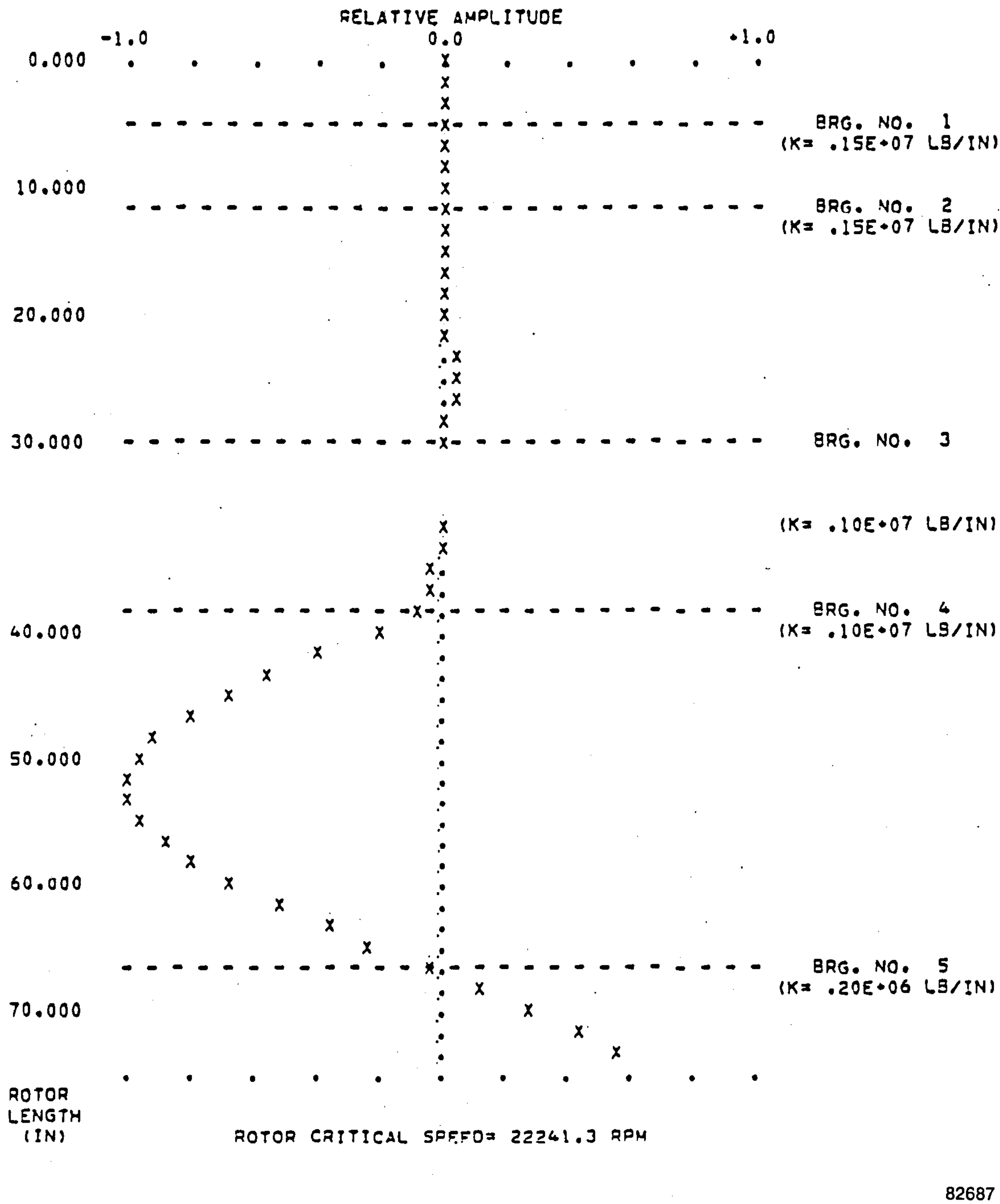

FIG. 3.4.5 POWER TURBINE SECOND CRITICAL (CASE 4)

MECHANICAL TECHNOLOGY INCORPORATED

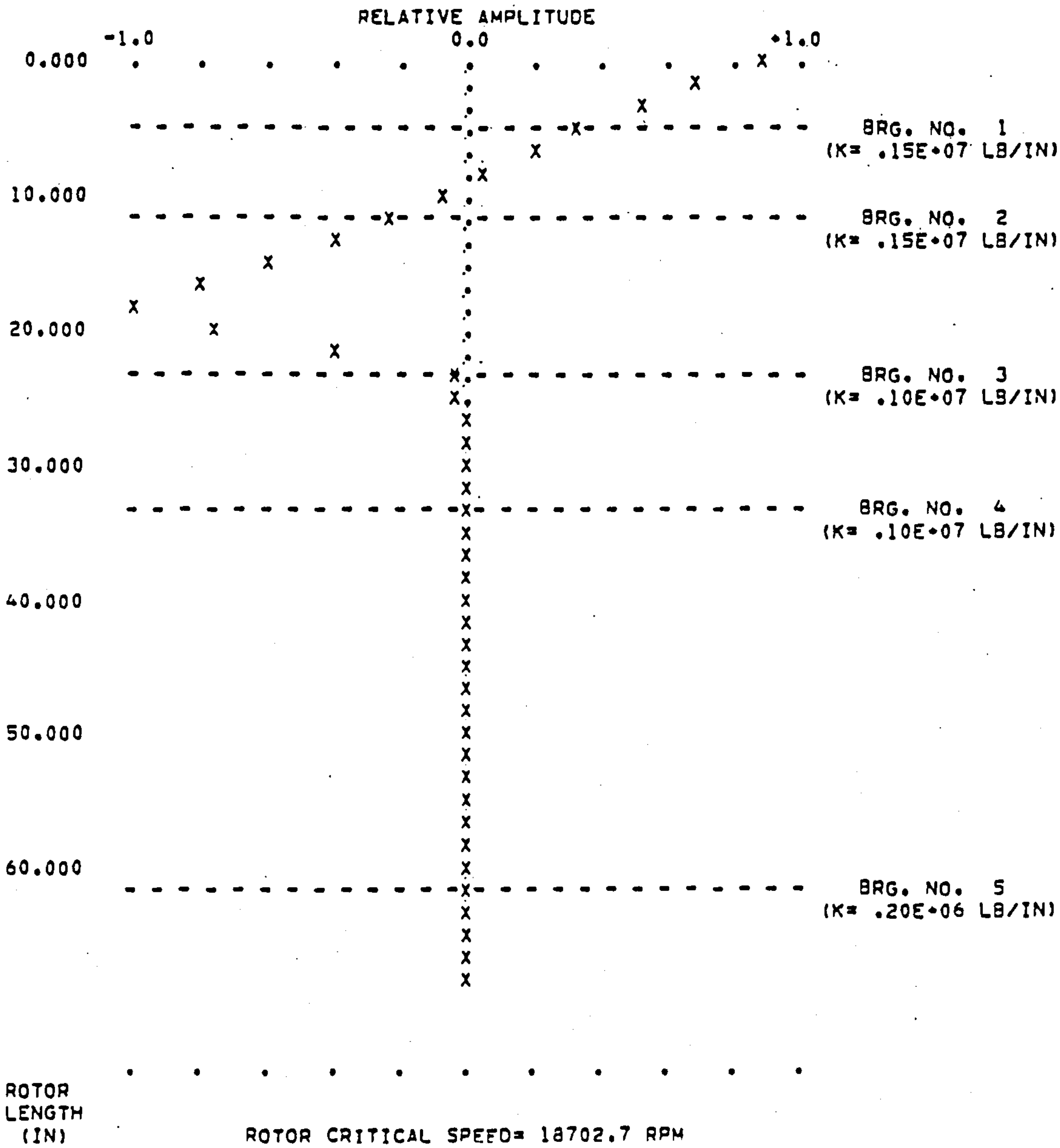

82695

FIG. 3.4.6 RIG CRITICAL (CASE 4)

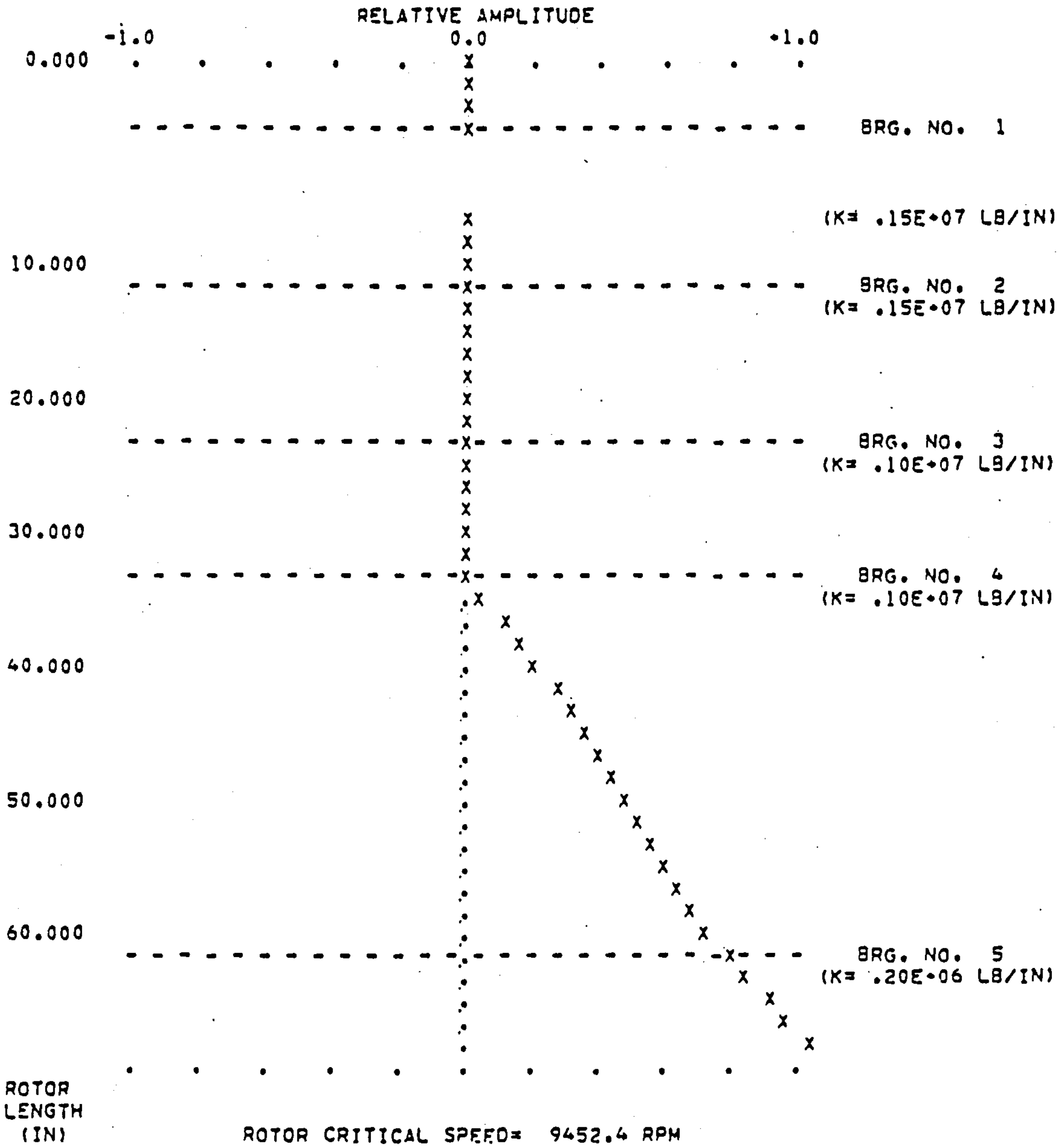

82697

FIG. 3.4.7 POWER TURBINE FIRST CRITICAL (CASE 6)

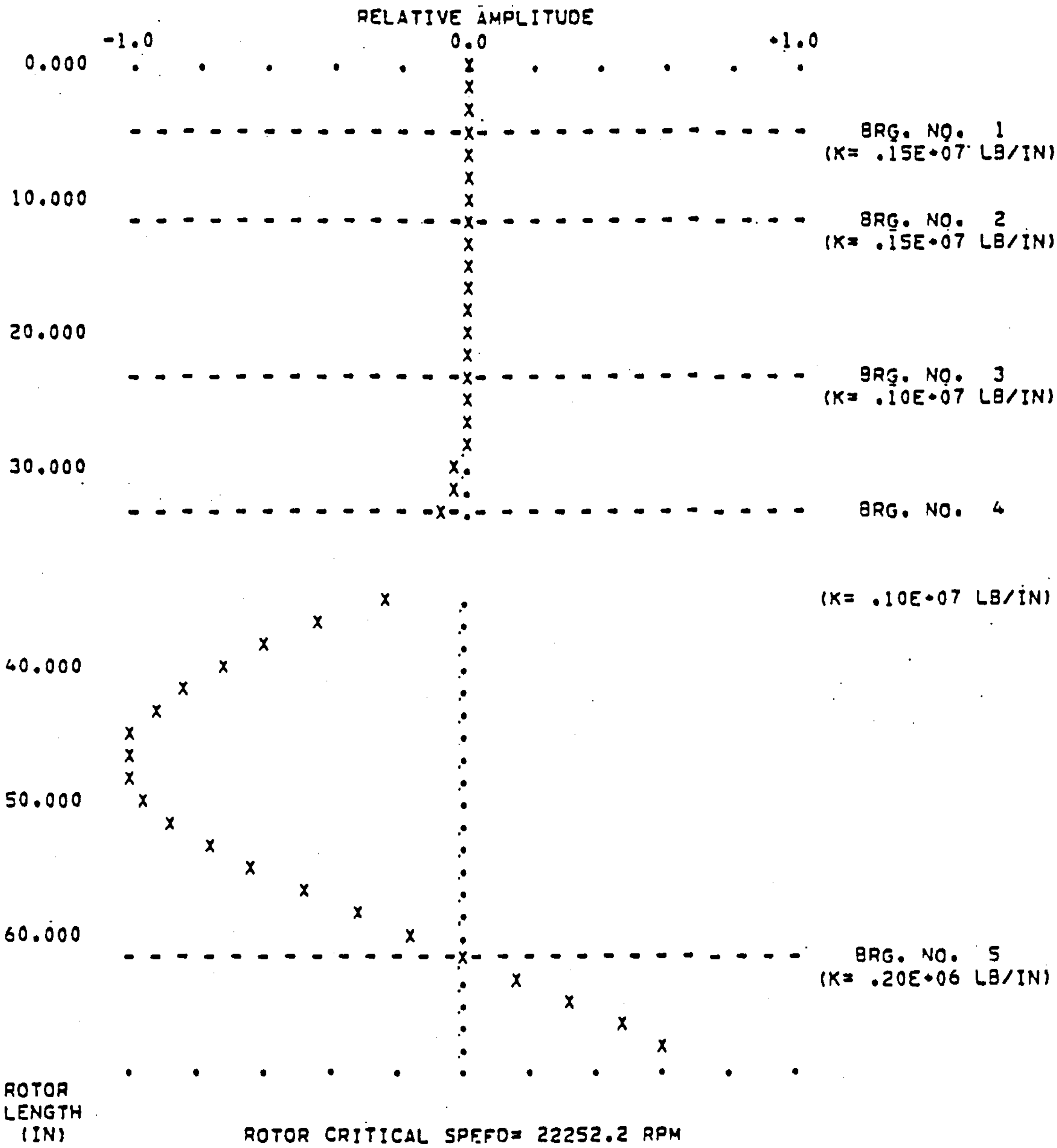

82696

FIG. 3.4.8 POWER TURBINE SECOND CRITICAL (Case 6)

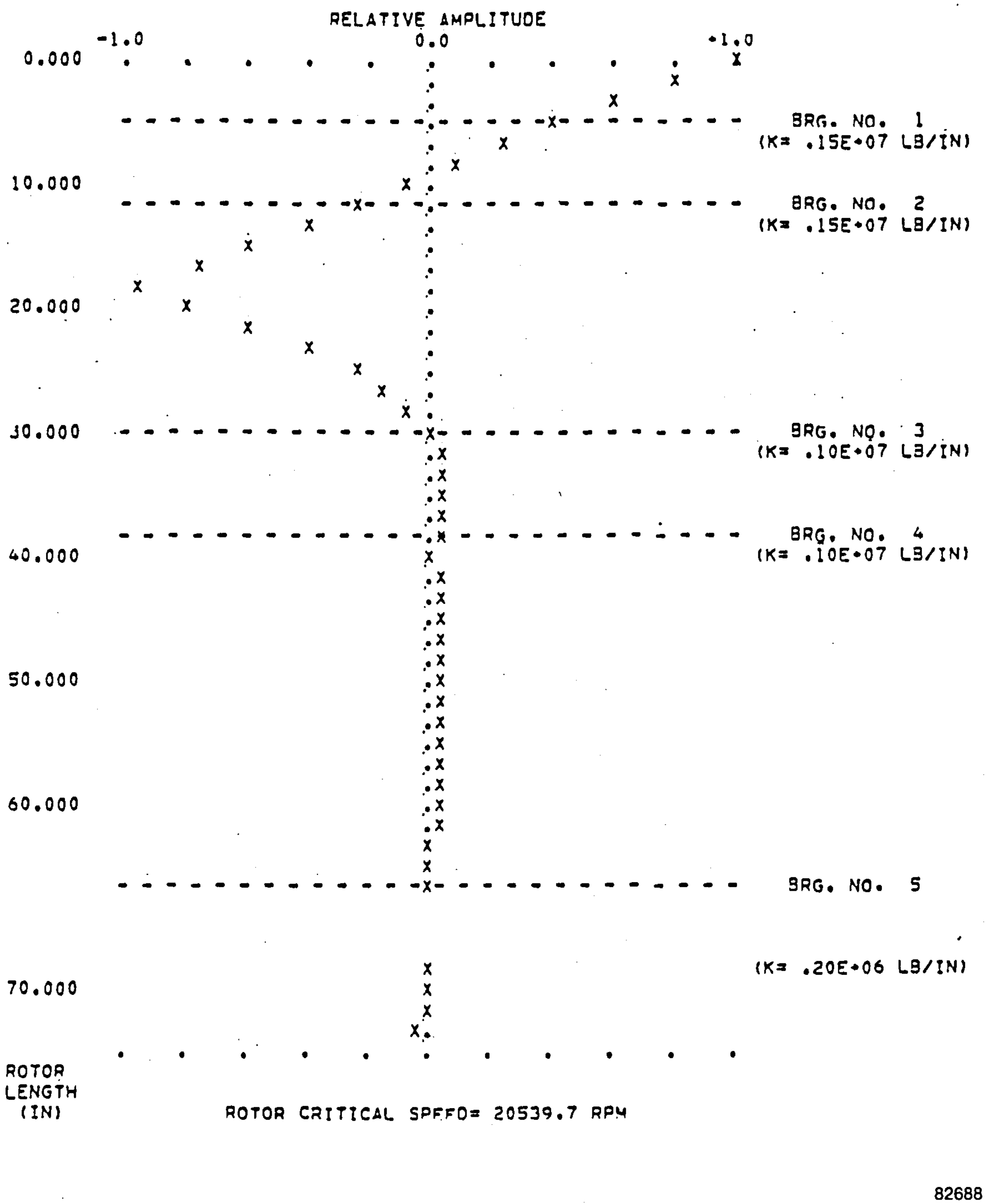

FIG. 3.4.9 RIG CRITICAL (CASE 6)

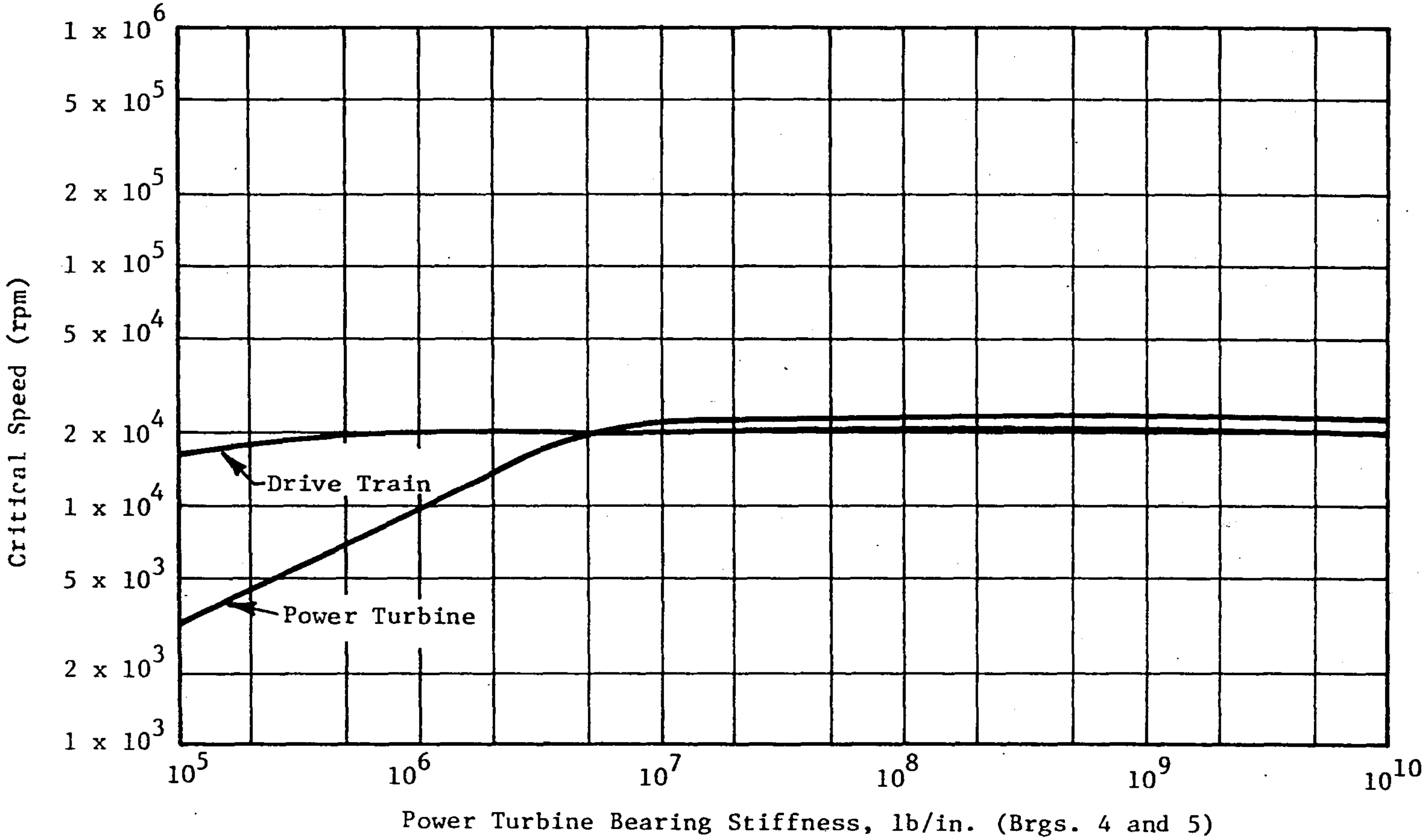

FIG. 3.4.10 POWER TURBINE CRITICAL SPEED MAP

801373

MECHANICAL TECHNOLOGY INCORPORATED

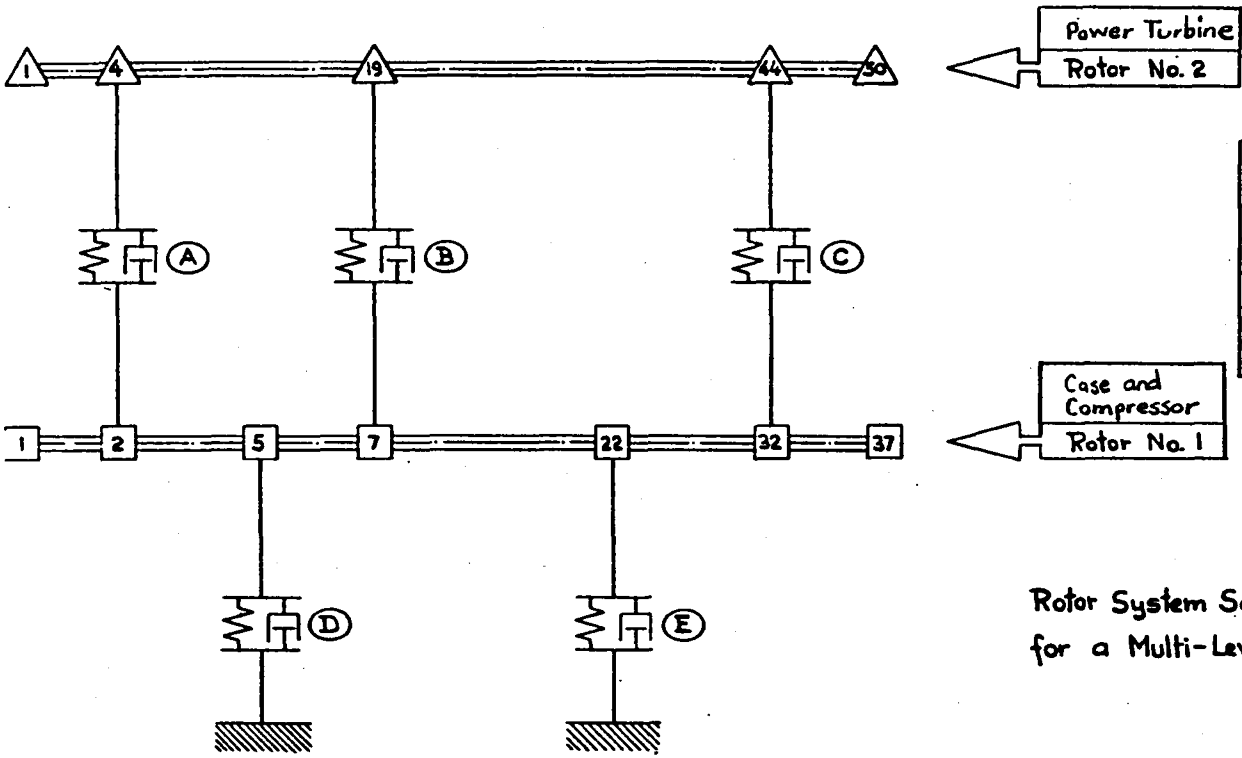

Data of Interconnections:

Ident.	Total Estimated Radial Stiffness K- lbs./in.	Damping B lbs.sec./in.
A	750,000	1.0
B	1,250,000	1.0
C	200,000	1.0
D	250,000	—
E	25,000	—

MTI
0264-45333-500

Sheet 4 of 4: System Schematic
Rotor System Schematic of the T-55 Power Turbine for a Multi-Level Rotordynamic Analysis

Paul J. Berzatzy
July 10, 1978

791728-1

FIG. 3.4.11 SYSTEM SCHEMATIC FOR MULTI-LEVEL ROTORDYNAMIC ANALYSIS

Casing

MODE SHAPE - ROTOR NO. 1

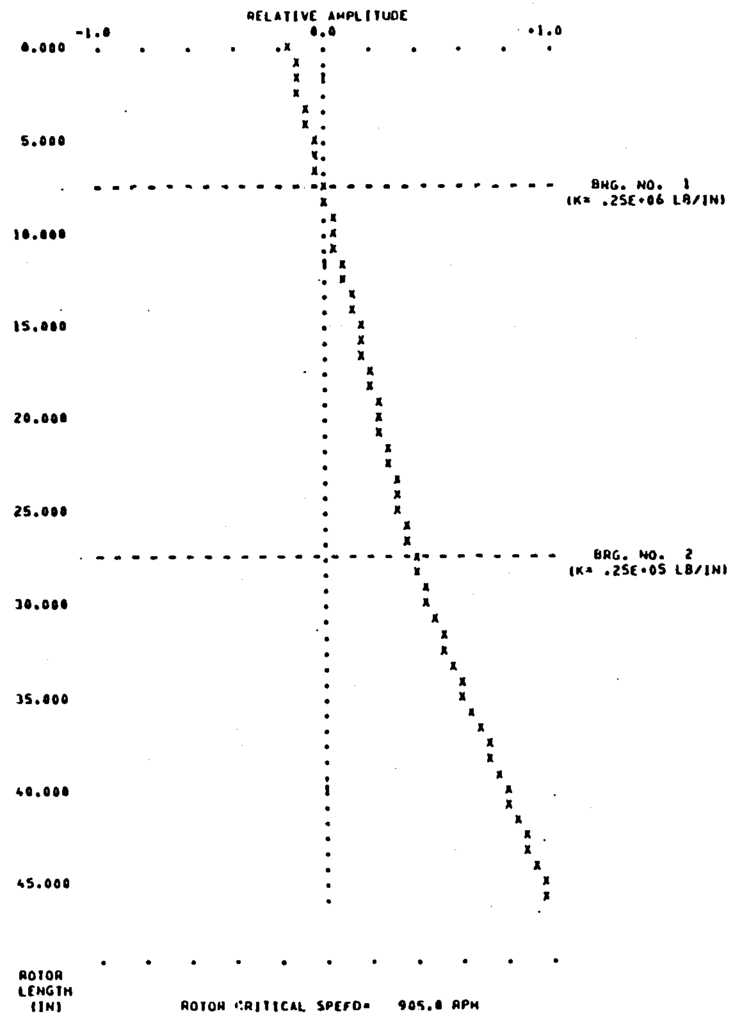

Power Turbine Rotor

MODE SHAPE - ROTOR NO. 2

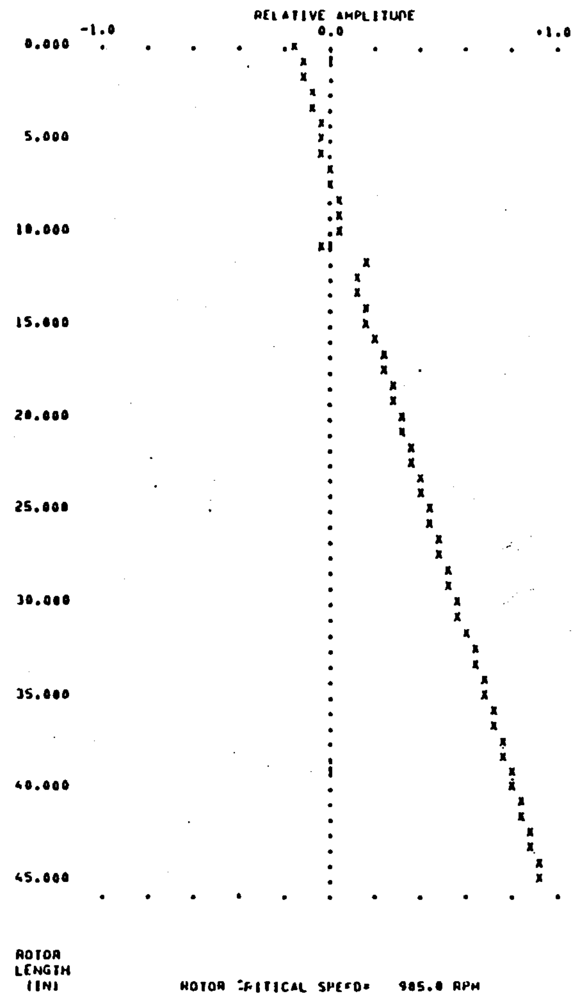

82689

FIG. 3.4.12 ENGINE CRITICAL SPEED OF 905 RPM

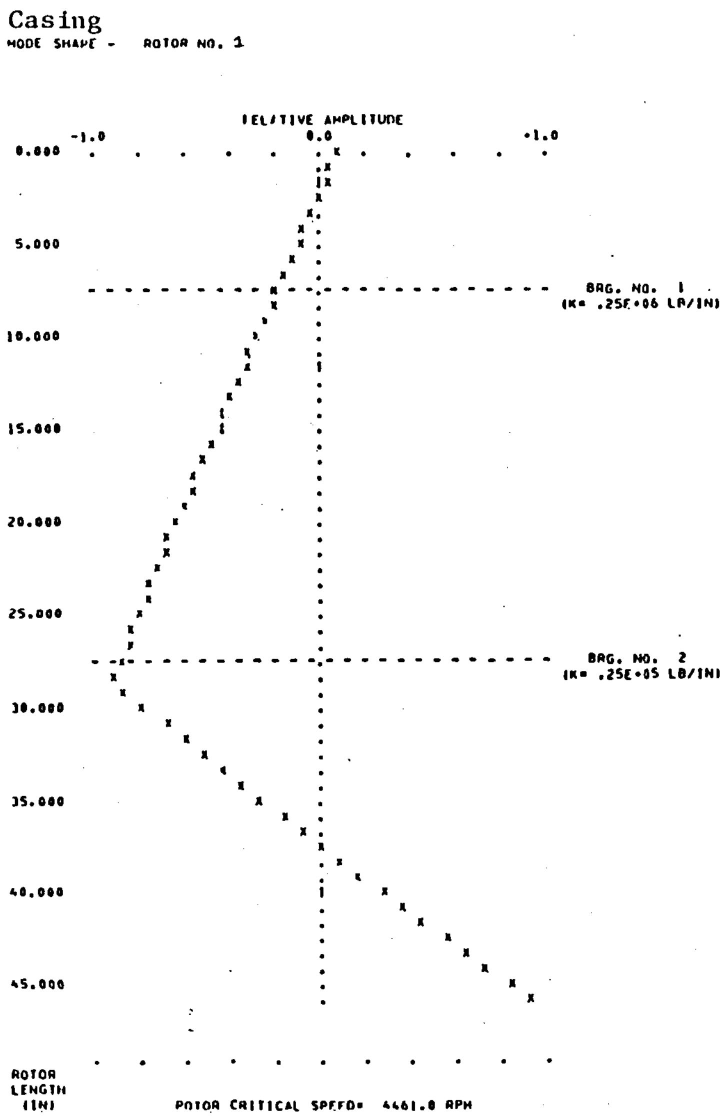

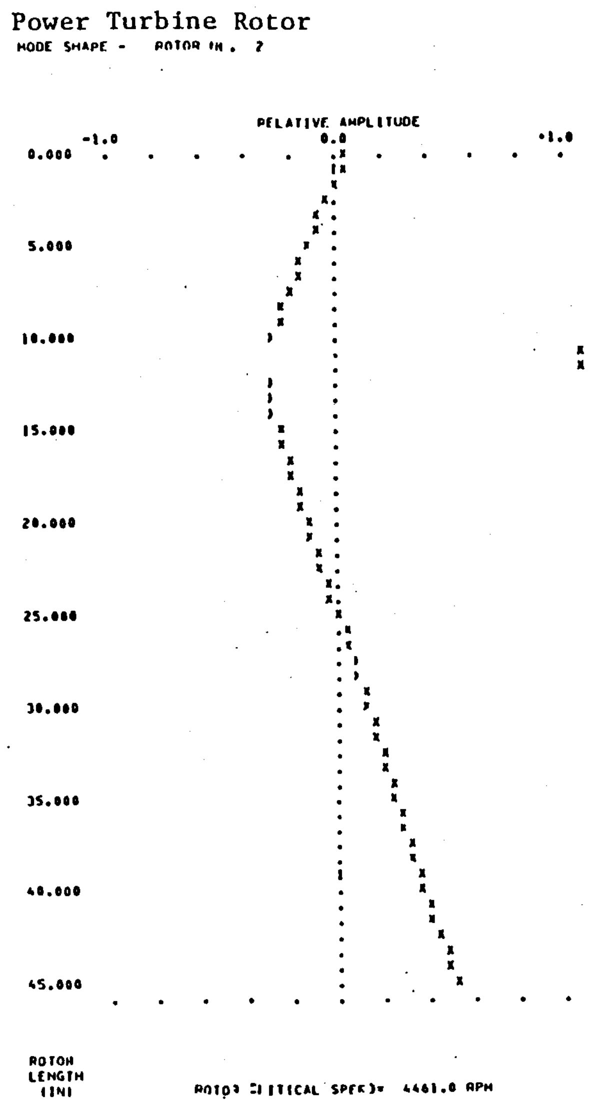

82690

FIG. 3.4.13 ENGINE CRITICAL SPEED OF 4461 RPM

MECHANICAL TECHNOLOGY INCORPORATED

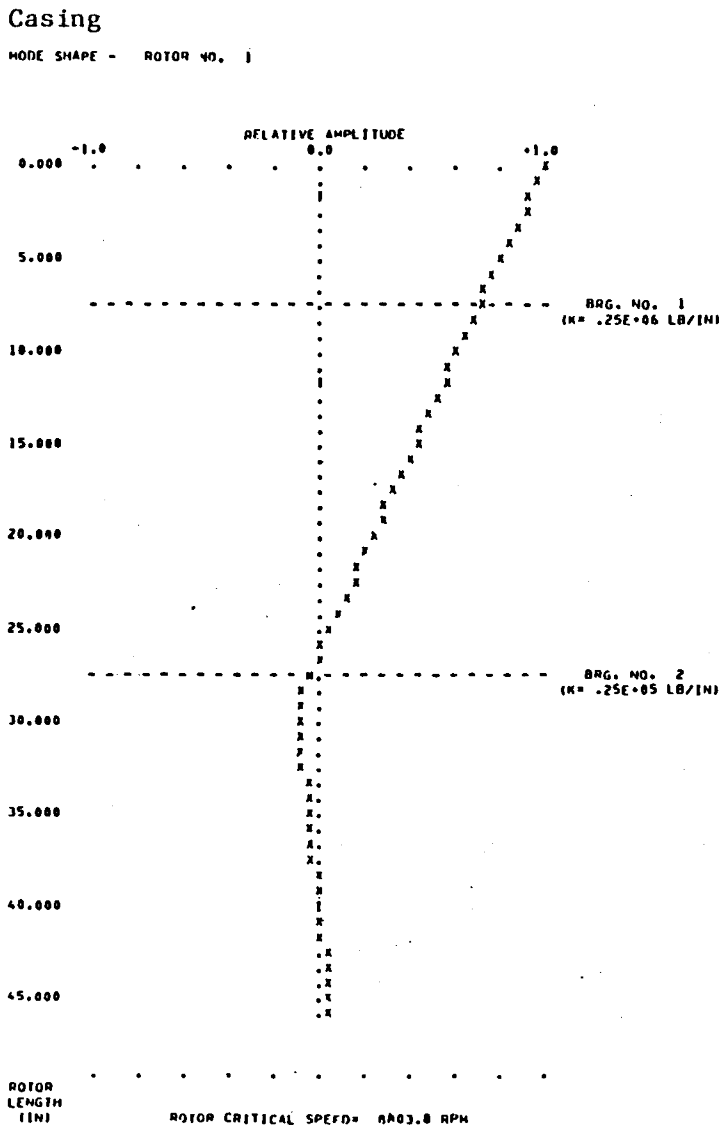

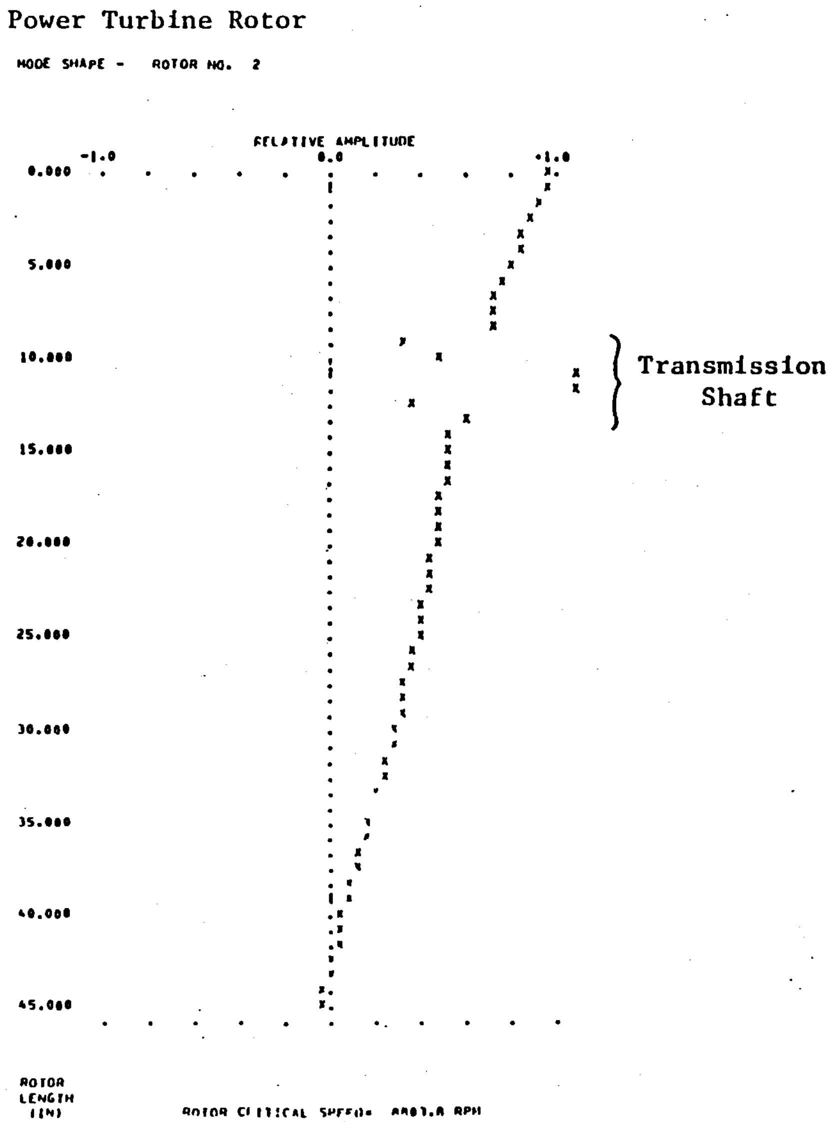

82691

FIG. 3.4.14 ENGINE CRITICAL SPEED OF 8804 RPM

MECHANICAL TECHNOLOGY INCORPORATED

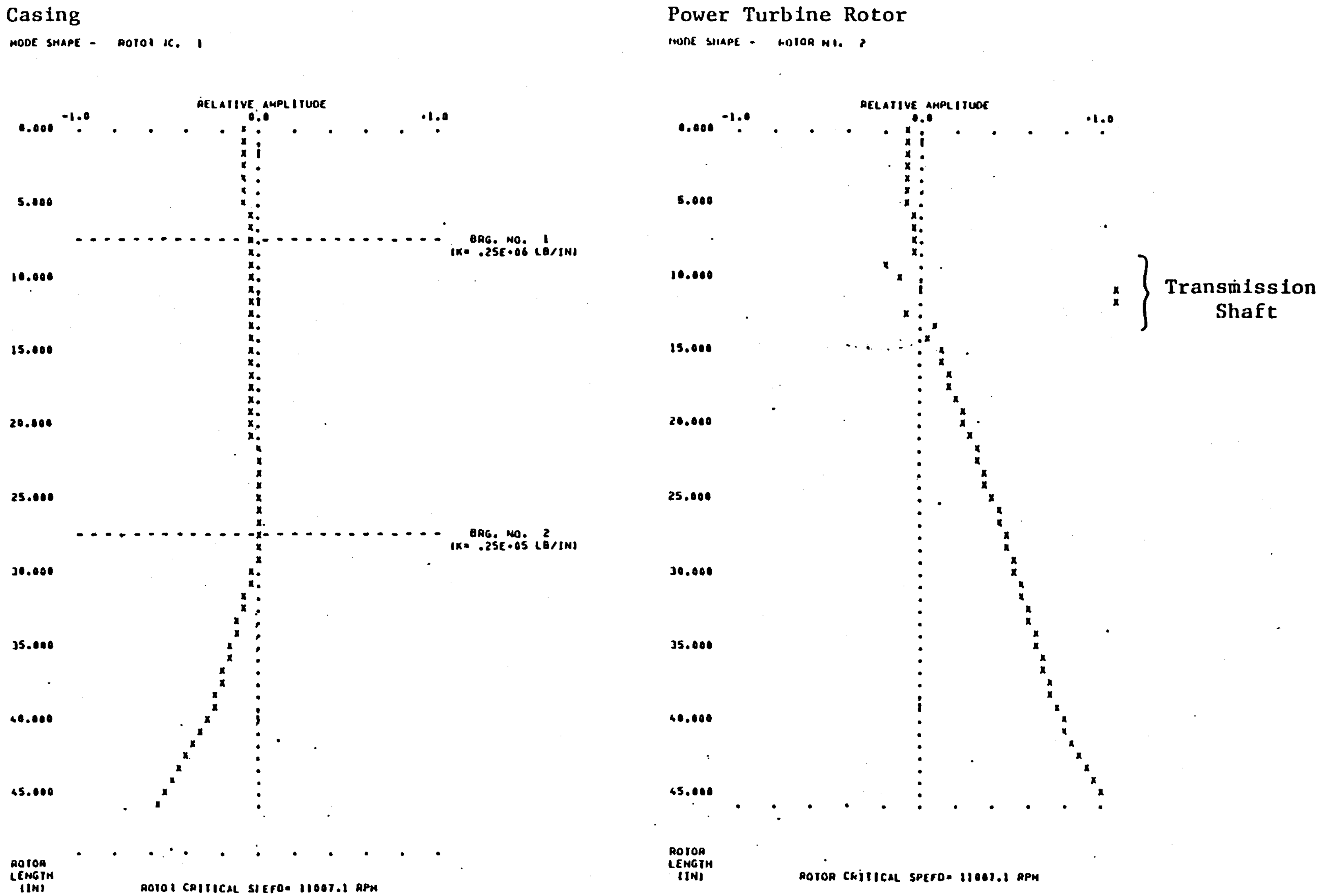

82692

FIG. 3.4.15 ENGINE CRITICAL SPEED OF 11007 RPM

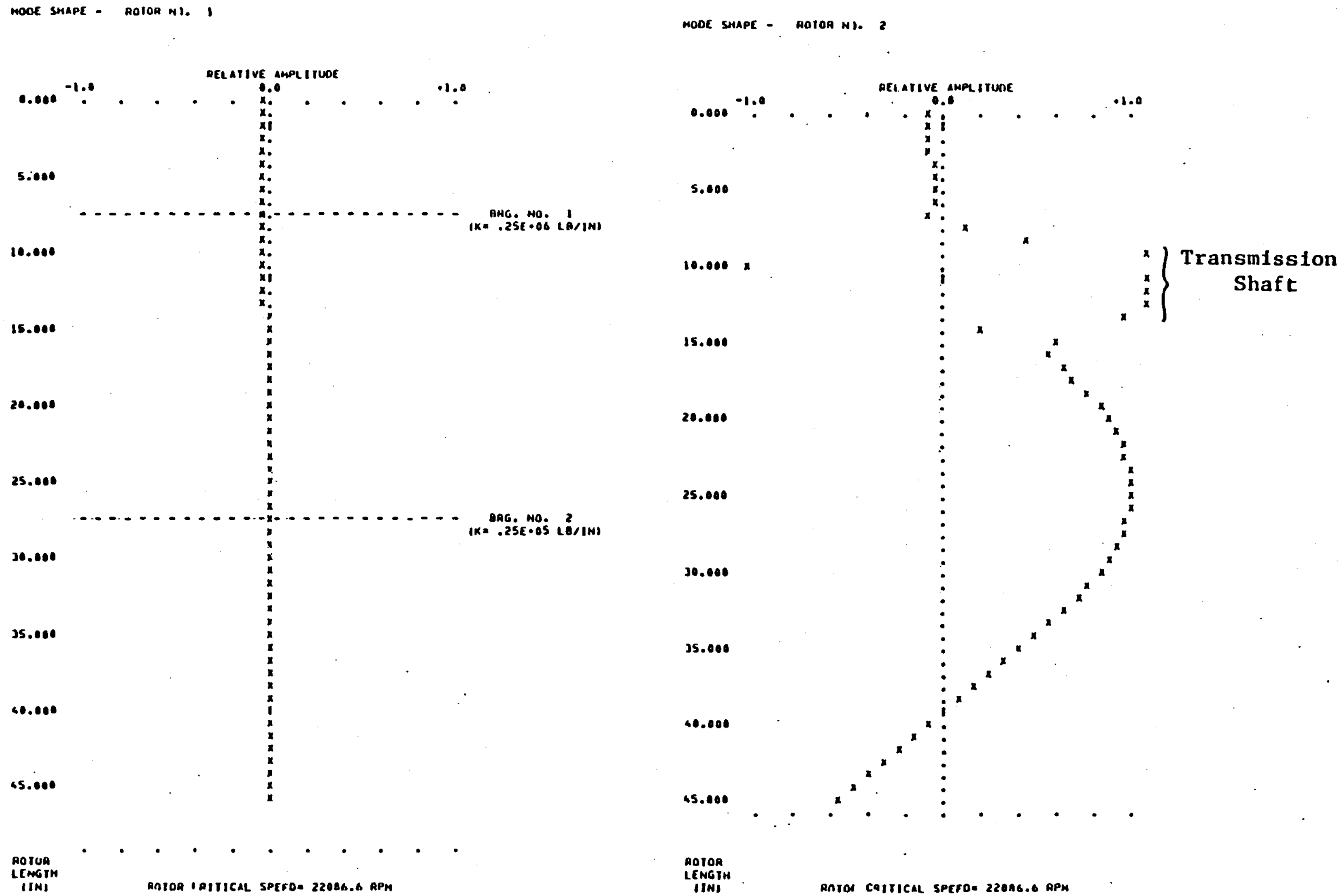

82693

FIG. 3.4.16 ENGINE CRITICAL SPEED OF 22087 RPM

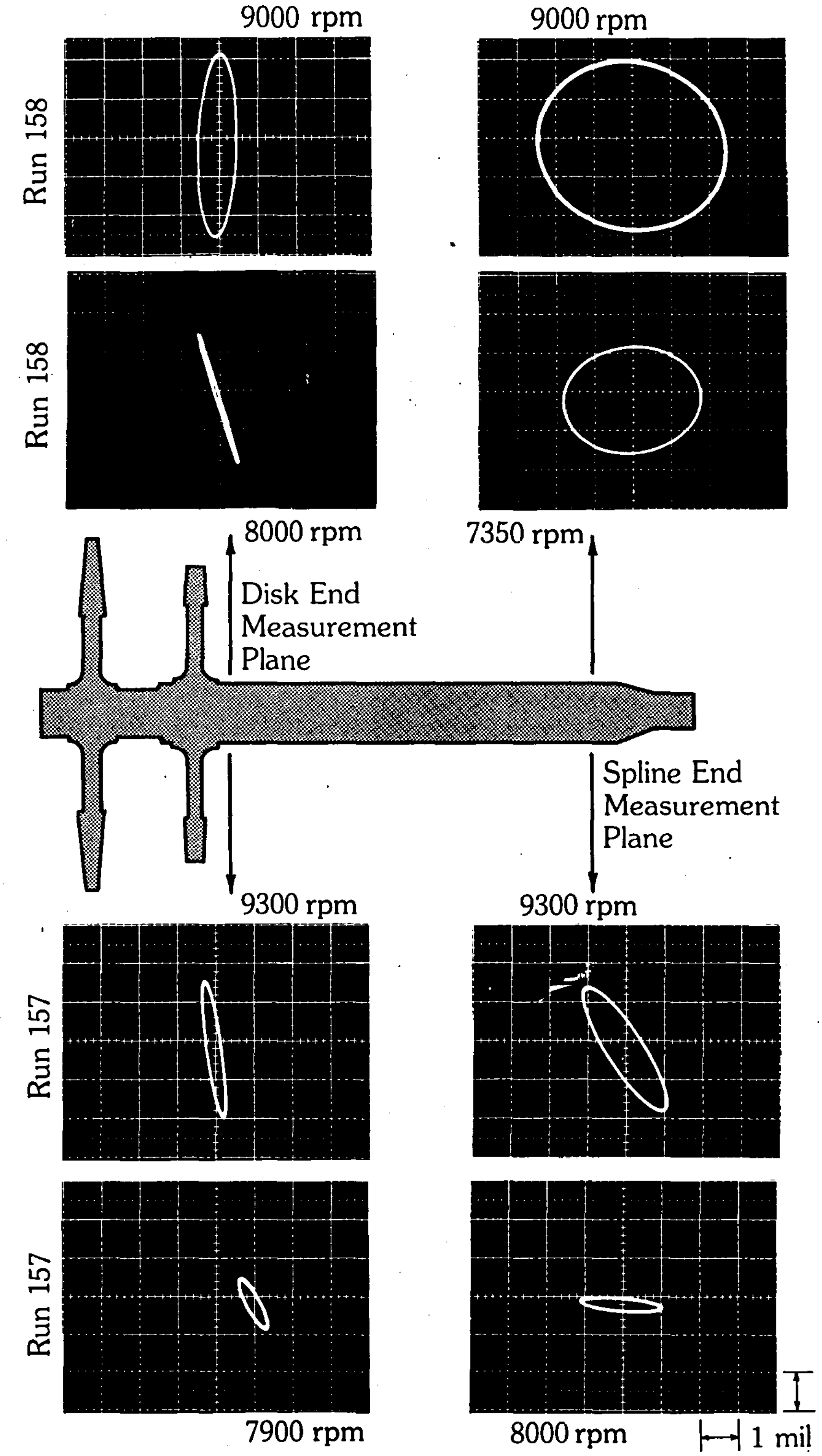

FIG. 3.4.17 EXPERIMENTAL NET ORBITS AT CRITICAL SPEEDS

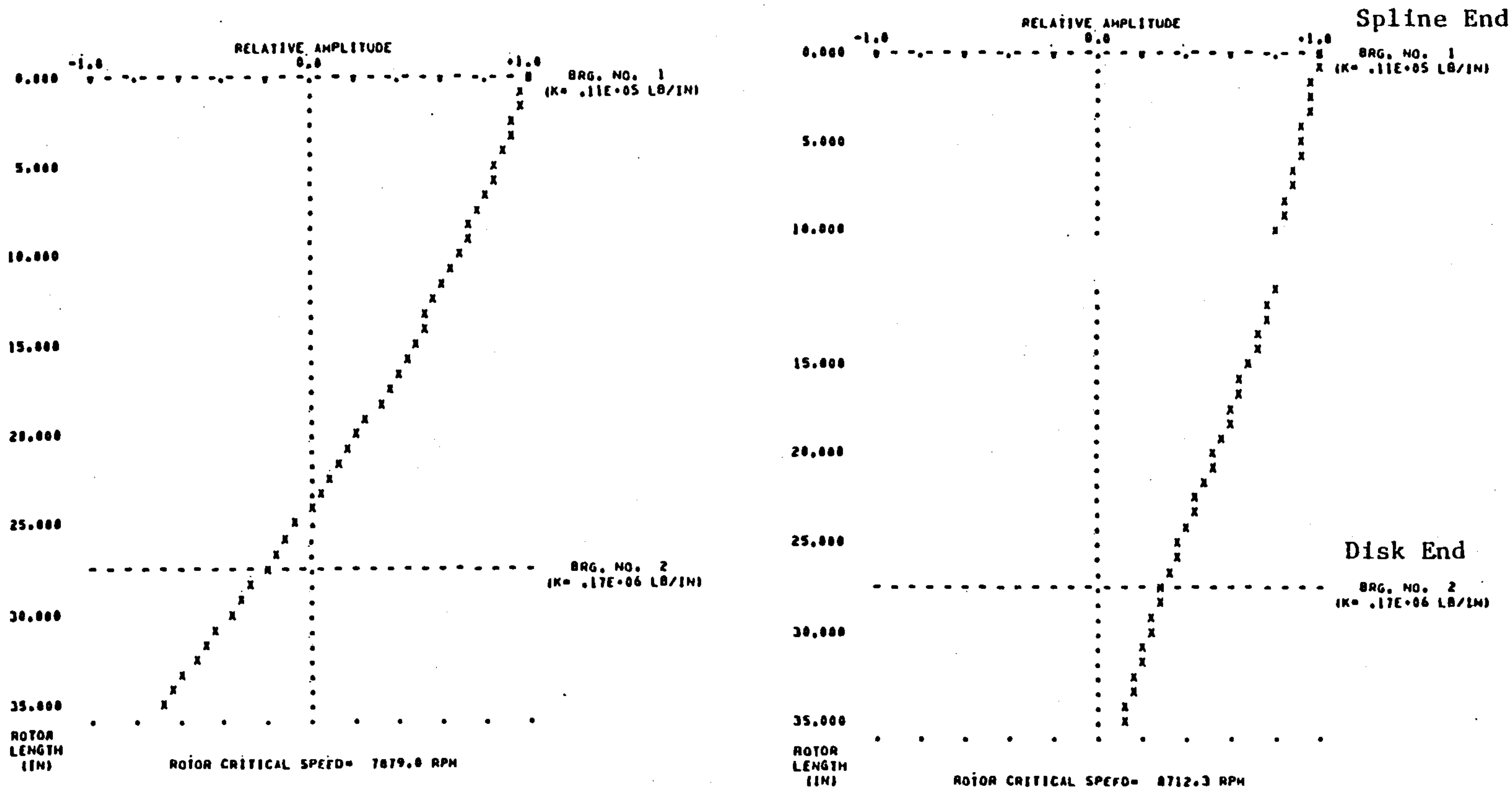

FIG. 3.4.18 THEORETICAL MODE SHAPES IN A VERTICAL PLANE

82694

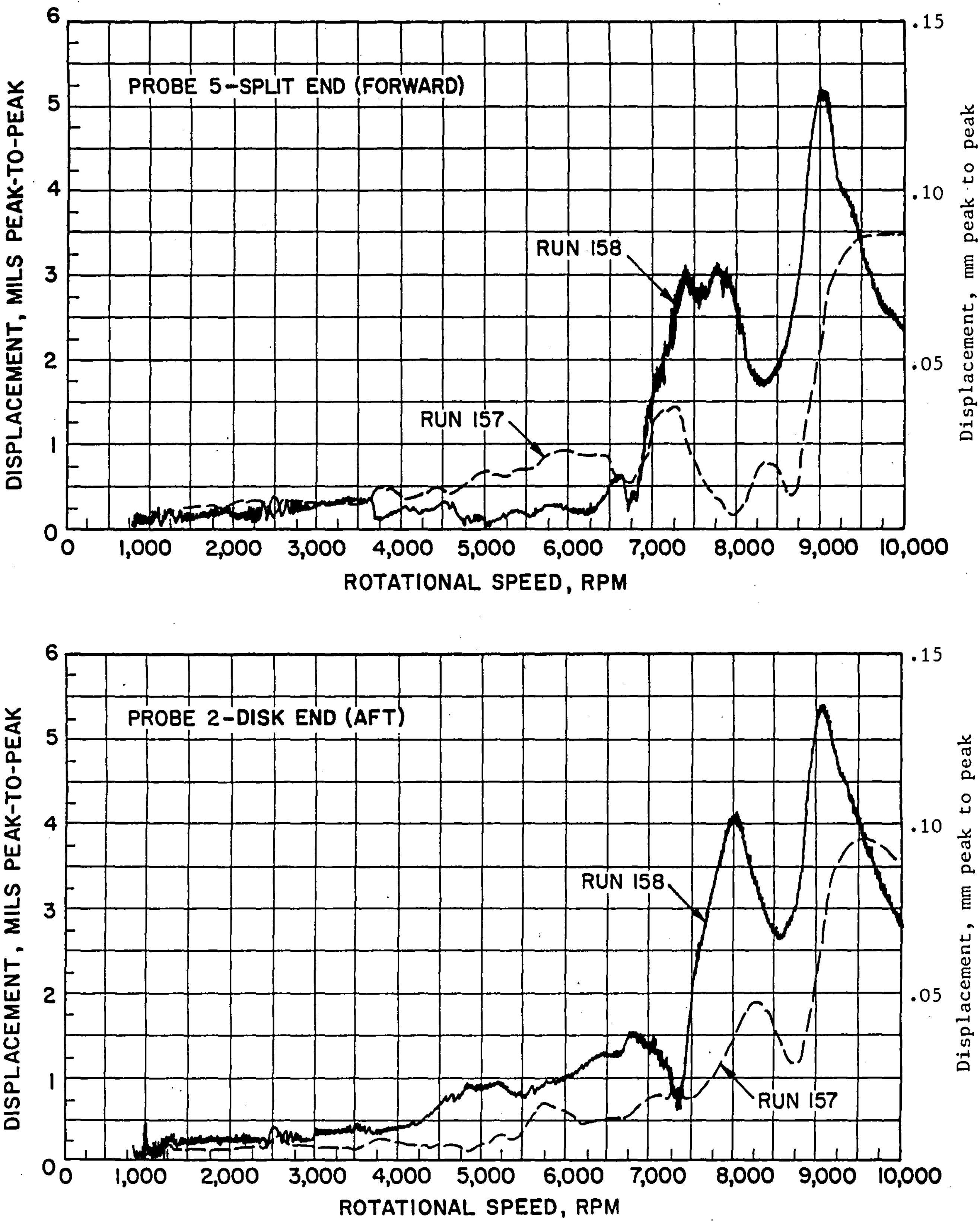

FIG. 3.4.19 VARIATION IN VIBRATION RESPONSE - VERTICAL SENSORS

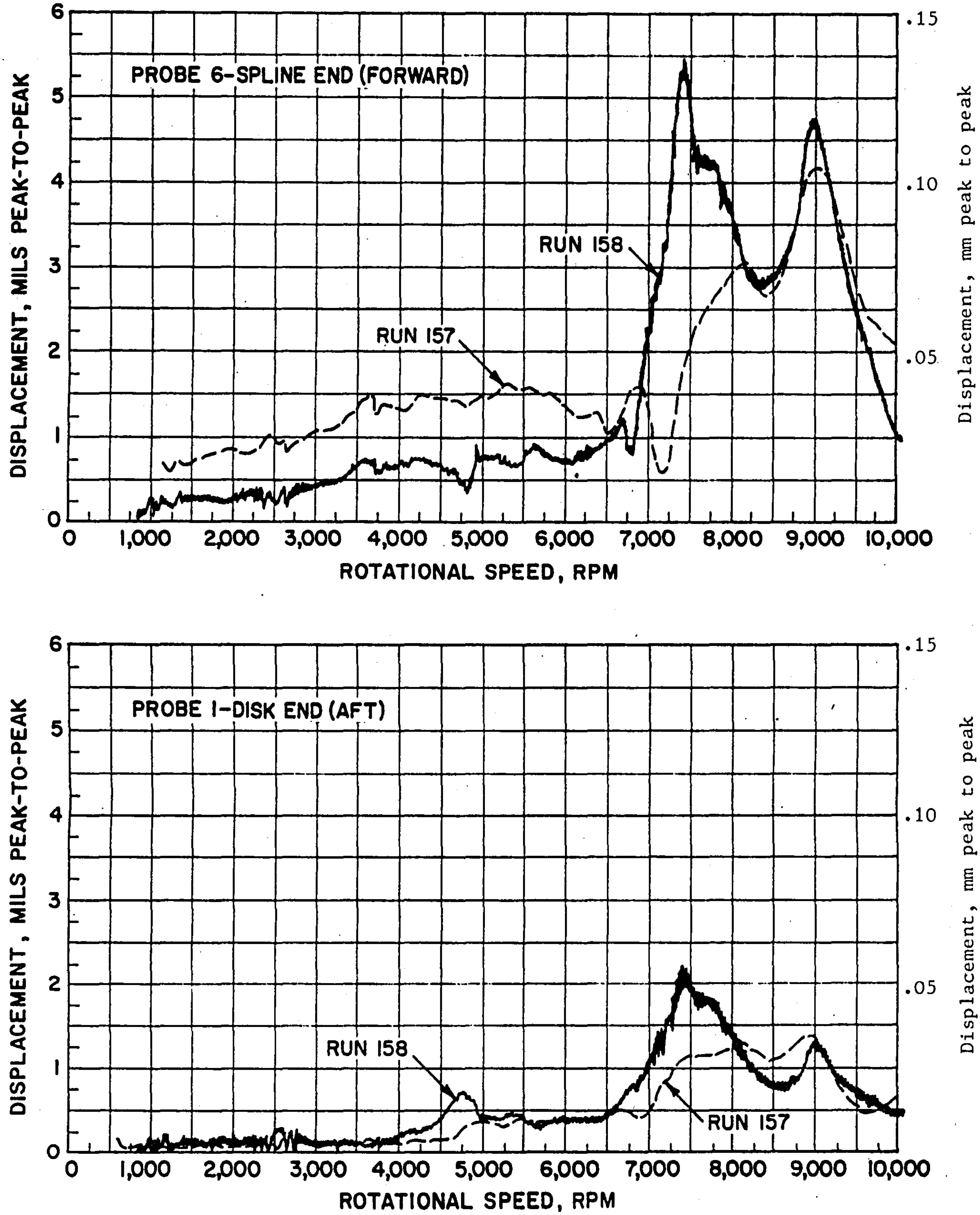

FIG. 3.4.20 VARIATION IN VIBRATION RESPONSE - HORIZONTAL SENSORS

TABLE 3.4.1

ROTOR DYNAMIC ANALYSIS FOR PREVIOUS AND CURRENT RIGS

TWO LEVEL MODEL (CASING & POWER TURBINE)

PREVIOUS RIG (FIGURE 3.4.2)

CRITICAL SPEEDS	SPEED IN RPM NO HINGES (CASE 1)	HINGE @ PLANE A (CASE 2)	HINGE @ PLANE B (CASE 3)	BOTH HINGED (CASE 4)
1st Lateral (Rigid Conical @ Disk)	9502	9500	9452	9452
2nd Lateral (Rotor Bending)	23531	23461	22254	22252
Rig Critical (Rigid Spindle)	20408	18703	20356	18703

CURRENT RIG (FIGURE 3.4.3)

CRITICAL SPEEDS	SPEED IN RPM NO HINGES (CASE 5)	HINGE @ PLANE B (CASE 6)
1st Lateral (Rigid Conical @ Disk)	9505	9452
2nd Lateral (Rotor Bending)	23660	22241
Rig Critical (Rigid Spindle)	20546	20540

TABLE 3.4.2
ROTOR DYNAMICS ANALYSIS FOR T55 ENGINE

ENGINE (FIGURES 3.4.1 & 3.4.2)

	SPEED IN RPM				
	NO HINGES			HINGE @ PLANE B	
CRITICAL SPEEDS	TOTAL ENGINE CASE 8	CASING CASE 9	TURBINE CASE 10	TOTAL ENGINE CASE 11	TURBINE CASE 12
1st Lateral (Rigid, Conical)	11034	-	9499	11007	9452
2nd Lateral (Rotor Bending)	23255	-	23385	22087	22099
Casing	909	1053	-	905	-
	4546	5119	-	4461	-
	8845	9613	-	8804	-

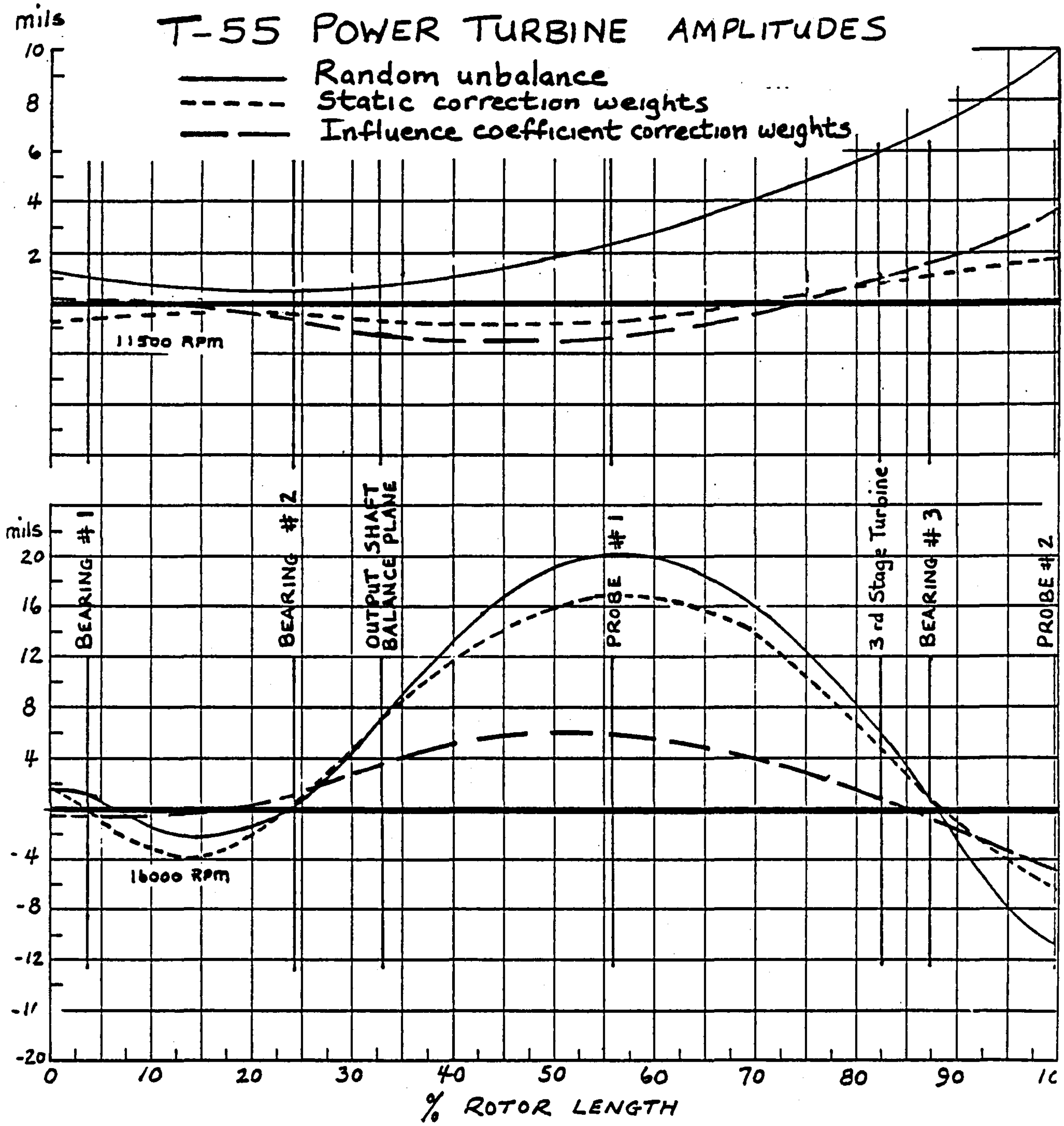

FIG. 3.5.1

82720

POWER TURBINE AMPLITUDES, MILS (PEAK)

UNBALANCE Amount & Location	Shaft End	Brg. 1	Brg. 2	Midspan	Brg. 3	Turbine End
71.8 gm cm (1 in oz)  4th stage	.022 mm .86 mils	.024 mm .94 mils	.011 mm .43 mils	.132 mm 5.18 mils	.215 mm 8.47 mils	.269 mm 10.59 mils
71.8 gm cm (1 in oz) 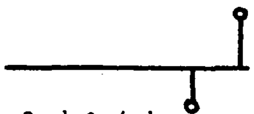 3rd & 4th stage	.014 mm .57 mils	.019 mm .76 mils	.010 mm .41 mils	.164 mm 6.64 mils	.138 mm 5.44 mils	.157 mm 6.17 mils
143.6 gm cm (2 in oz) 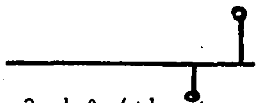 3rd & 4th stage	.029 mm 1.13 mils	.038 mm 1.51 mils	.021 mm .81 mils	.337 mm 13.28 mils	.276 mm 10.87 mils	.313 mm 12.33 mils
11,500 RPM						
71.8 gm cm (1 in oz)  4th stage	.003 mm .11 mils	.009 mm .35 mils	.003 mm .12 mils	.297 mm 11.71 mils	.068 mm 2.69 mils	.067 mm 2.62 mils
71.8 gm cm (1 in oz) 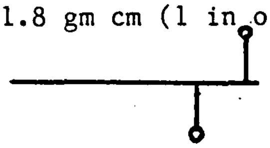 3rd & 4th stage	.005 mm .20 mils	.020 mm .80 mils	- .015 mils	.648 mm 25.5 mils	.076 mm 2.99 mils	.087 mm 11.62 mils
143.6 gm cm (2 in oz) 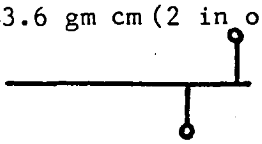 3rd & 4th stage	.010 mm .40 mils	.041 mm 1.61 mils	.001 mm .030 mils	1.295 mm 51. mils	.152 mm 5.99 mils	.590 mm 23.24 mils

16,000 RPM

T55 POWER TURBINE SENSITIVITY TO FOURTH TURBINE STAGE UNBALANCE

TABLE 3.5.1

T55 BEARING LOADS

UNBALANCE Amount & Location	Brg. 1	Brg. 2	Brg. 3
71.8 gm cm (1 in oz) @ 4th stage	3120 N 701.5 lbf	2376 N 534.2 lbf	7531 N 1693. lbf
71.8 gm cm (1 in oz) couple 3rd & 4th stage	2521 N 566.7 lbf	2259 N 507.8 lbf	4836 N 1087.2 lbf

11,500 RPM

	Brg. 1	Brg. 2	Brg. 3
71.8 gm cm (1 in oz) @ 4th stage	1169 N 262.8 lbf	66 N 14.9 lbf	2396 N 538.7 lbf
71.8 gm cm (1 in oz) couple 3rd & 4th stage	2682 N 603. lbf	83 N 18.7 lbf	2663 N 598.7 lbf

16,000 RPM

TABLE 3.5.2

CASE RESPONSE TO

4TH TURBINE STAGE UNBALANCE

mm peak/mils peak

UNBALANCE Amount & Location	Shaft End	Brg. 1	Midspan	Brg. 2		Turbine End
1 in oz (71.8 gm cm) 4th stage	.023 mm .89 mils	.017 mm .66 mils	.006 mm .25 mils	.004 mm .16 mils	.051 mm 1.99 mils	.153 mm 6.01 mils
1 in oz (71.8 gm cm) 3rd & 4th stage	.020 mm .77 mils	.014 mm .57 mils	.005 mm .18 mils	.002 mm .08 mils	.032 mm 1.27 mils	.099 mm 3.89 mils

11,500 RPM

UNBALANCE Amount & Location	Shaft End	Brg. 1	Midspan	Brg. 2		Turbine End
1 in oz (71.8 gm cm) 4th stage	.008 mm .30 mils	.005 mm .21 mils	.003 mm .11 mils	.002 mm .09 mils	.005 mm .21 mils	.026 mm 1.03 mils
1 in oz (71.8 gm cm) 3rd & 4th stage	.018 mm .69 mils	.012 mm .48 mils	.005 mm .20 mils	.004 mm .14 mils	.006 mm .25 mils	.028 mm 1.11 mils

16,000 RPM

TABLE 3.5.3

POWER TURBINE AMPLITUDES

FOR STATIC CORRECTION WEIGHTS

(mm, peak/mils peak)

UNBALANCE	Shaft End	ST. 4 Brg. 1	ST. 19 Brg. 2	ST. 32 Midspan	ST. 44 Brg. 3	Turbine End
Random Unbalance	1.25 mils .032 mm	1.09 mils .028 mm	.60 mils .015 mm	1.91 mils .049 mm	6.95 mils .177 mm	9.99 mils .254 mm
Corrected @ ST. 29 & 3rd Stage	.77 mils .020 mm	.63 mils .016 mm	.39 mils .010 mm	.68 mils .017 mm	.95 mils .024 mm	1.78 mils .045 mm
Corrected @ ST. 33 & 3rd Stage	.68 mils .017 mm	.55 mils .014 mm	.38 mils .010 mm	1.96 mils .050 mm	.82 mils .021 mm	2.25 mils .057 mm
Corrected @ ST. 36 & 3rd Stage	.65 mils .017 mm	.53 mils .013 mm	.37 mils .009 mm	2.66 mils .068 mm	.75 mils .019 mm	2.80 mils .071 mm
11,500 RPM						
Random Unbalance	1.55 mils .039 mm	.92 mils .023 mm	.19 mils .005 mm	20.26 mils .515 mm	.51 mils .013 mm	11.05 mils .281 mm
Corrected @ ST.29 & 3rd Stage	1.52 mils .039 mm	.80 mils .002 mm	.17 mils .004 mm	16.44 mils .418 mm	.80 mils .020 mm	6.52 mils .166 mm
Corrected @ ST. 33 & 3rd Stage	1.78 mils .045 mm	.60 mils .015 mm	.18 mils .005 mm	35.9 mils .912 mm	2.11 mils .054 mm	14.15 mils .359 mm
Corrected @ ST. 36 & 3rd Stage	1.90 mils .048 mm	.77 mils .020 mm	.19 mils .005 mm	44.66 mils 1.134 mm	3.07 mils .078 mm	19.45 mils .494 mm

16,000 RPM

TABLE 3.5.4

POWER TURBINE AMPLITUDES

FOR INFLUENCE COEFFICIENT BALANCE

(mm peak/mils peak)

	SHAFT END	Brg. 1	Brg. 2	MIDSPAN	Brg. 3	ROTOR END
Random Unbalance	1.25 mils .032 mm	1.09 mils .028 mm	.6 mils .015 mm	1.91 mils .049 mm	6.95 mils .177 mm	9.99 mils .254 mm
2 Plane Balance	.16 mils .004 mm	.09 mils .002 mm	.48 mils .012 mm	1.43 mils .036 mm	1.84 mils .047 mm	3.73 mils .095 mm
11,500 RPM						
Random Unbalance	1.55 mils .039 mm	.92 mils .023 mm	.19 mils .005 mm	20.26 mils .515 mm	.51 mils .013 mm	11.05 mils .281 mm
2 Plane Balance	.30 mils .008 mm	.24 mils .006 mm	1.11 mils .028 mm	5.98 mils .152 mm	.96 mils .024 mm	4.82 mils .122 mm

16,000 RPM

TABLE 3.5.5

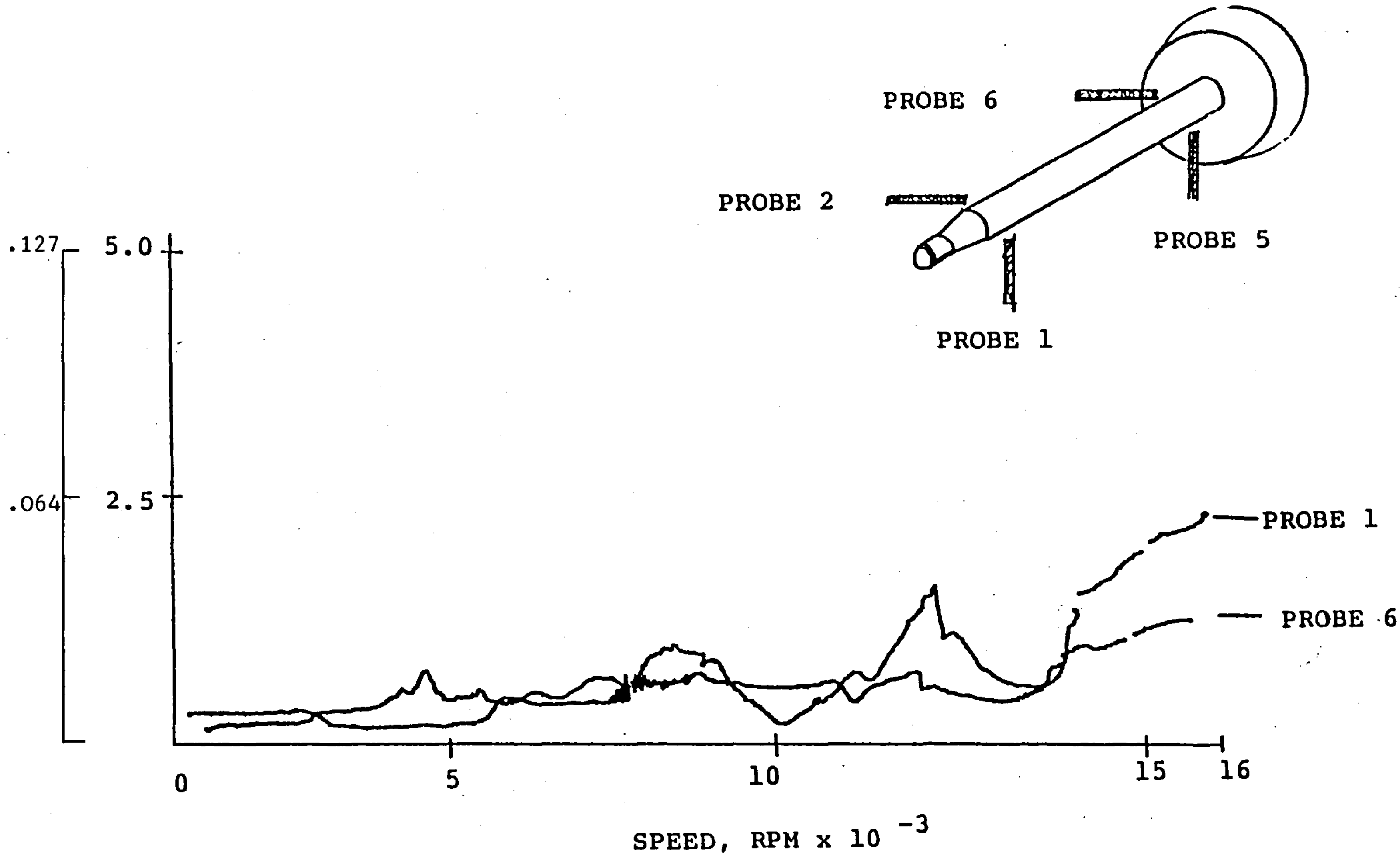

82685

FIG. 3.6.1 T55 SN 268922 VIBRATION AFTER BALANCING

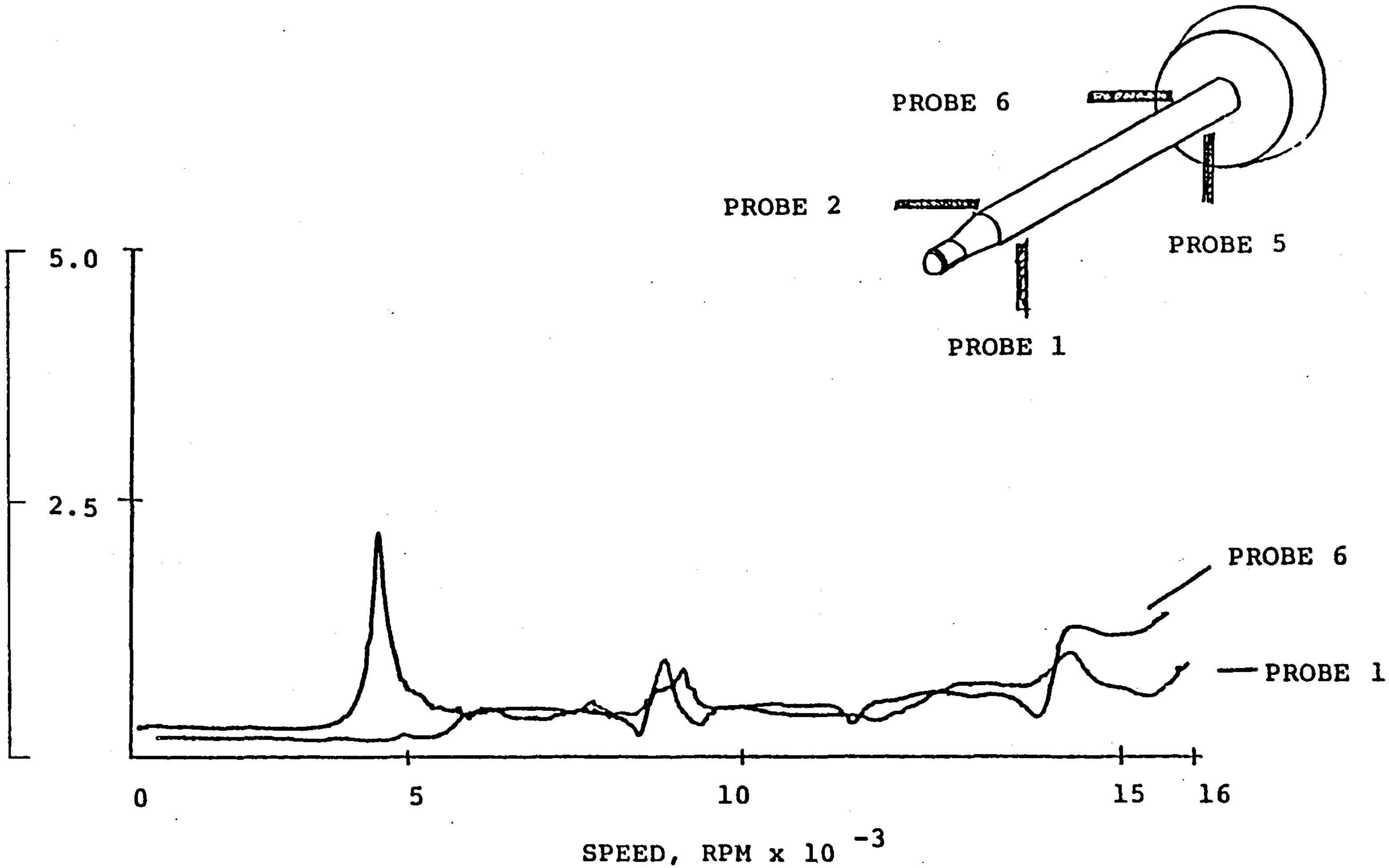

82684

FIG. 3.6.2 T55 SN U00559 VIBRATION AFTER BALANCING

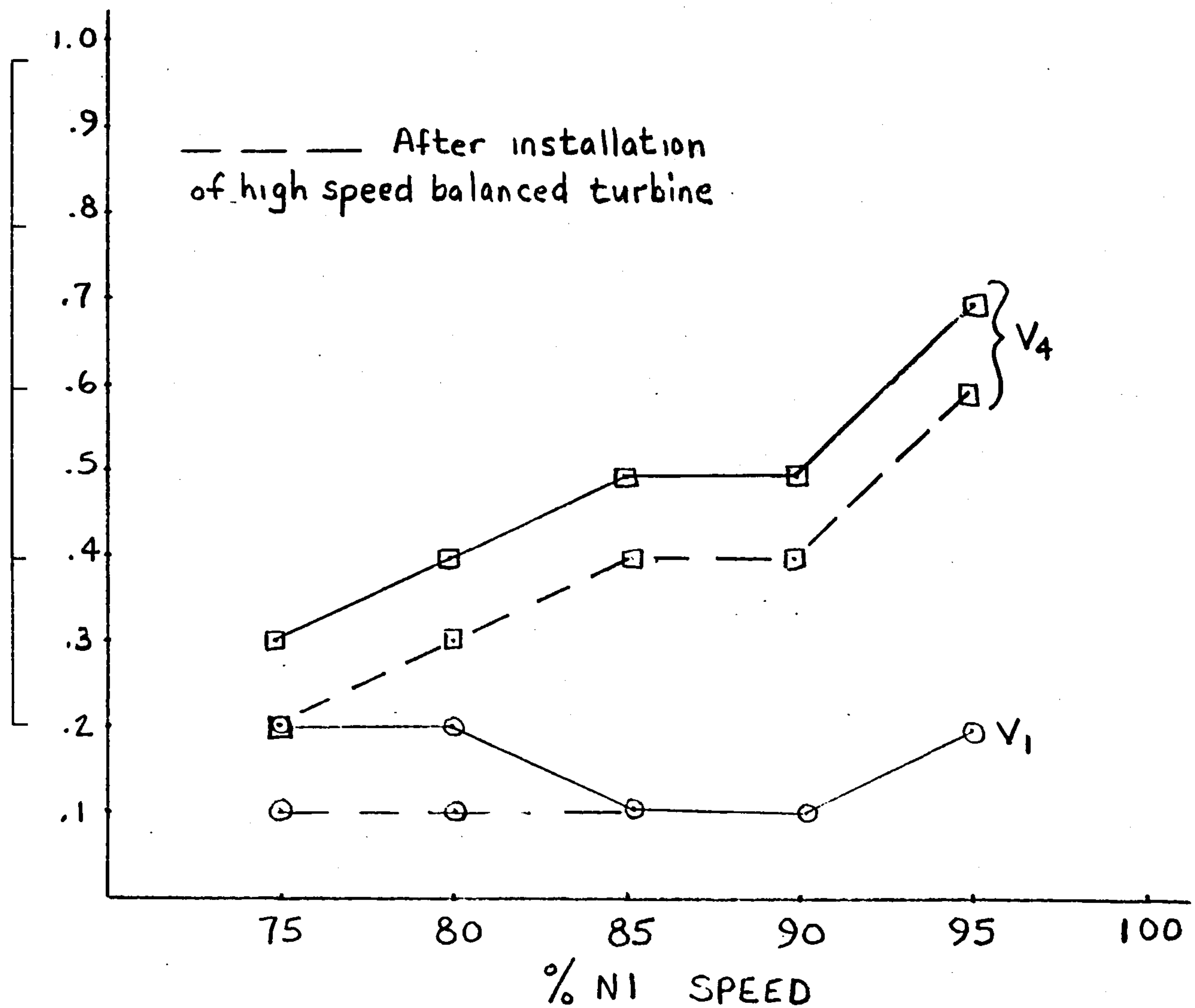

82683

FIG. 3.6.3

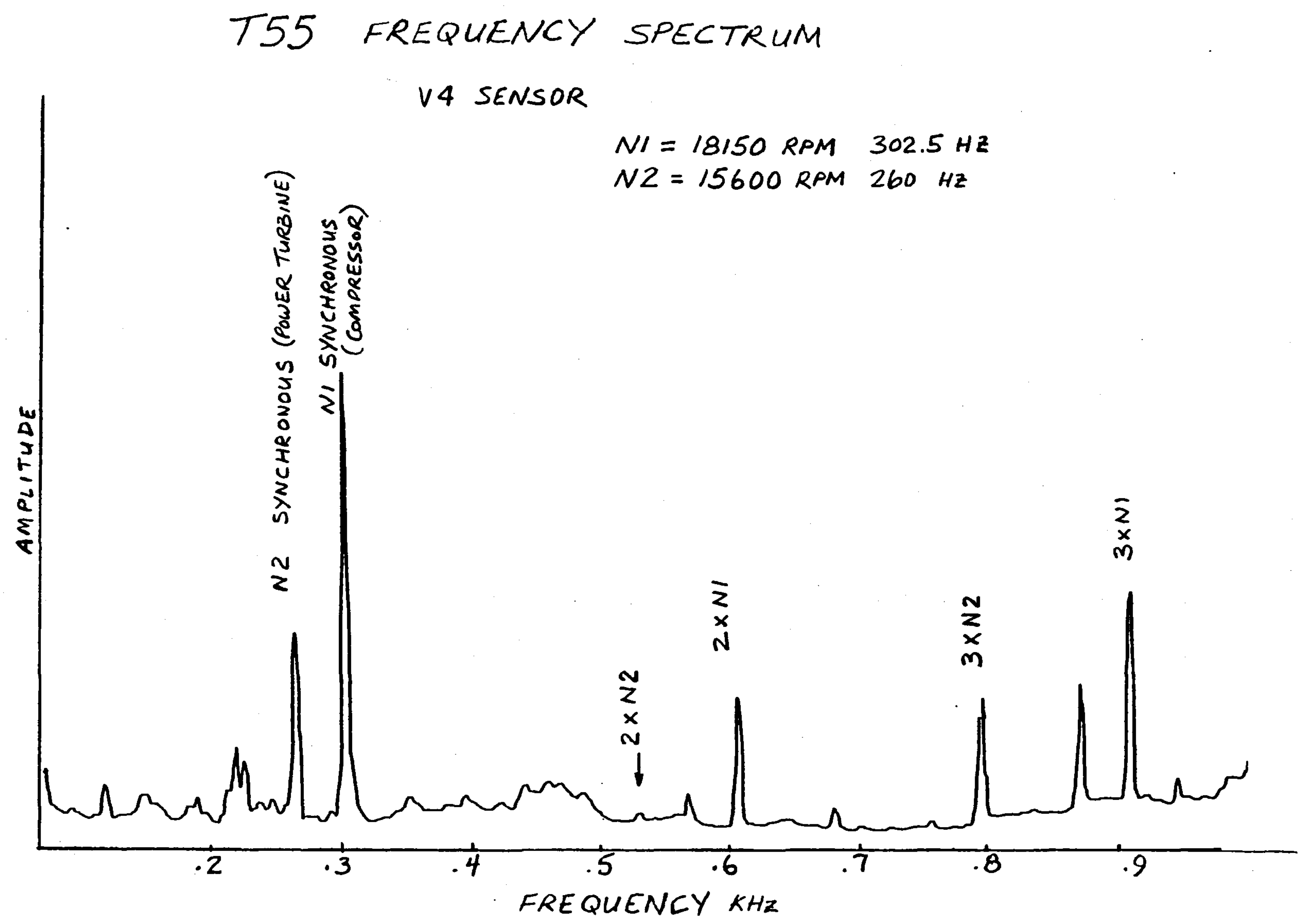

FIG. 3.6.4

82729

RIN:T02RJ30024Z GAS TURBINE ENGINE TEST LOG SHEE

SER.NO.LE19650 SEQ.NO.0843.9088 REC NO. 9 F/C S/N 68250 F/F DEVIAT
CURVE TECH DATA SET* 11 LIMIT TECH DATA SET* 11 LIMIT MODIFICATIO

S/S	START	STOP	START	STOP	START	STOP
MGT	1112		1230			
ET	19.0	34.4	16.9	45.3		
TOD	1321	1323	1327	1400		

OS GOV STOPS %NI %NII WF TEMP PB TOD ET
HIGH:
LOW:

ACCEL CHECKS %NI SECS MGT DECEL SECS TOD ET
GI TO
FI TO
FI TO

VIB %N1	%NII	V1	V2	V3	V4	TOD	ET
75.3	94.0	.20	.20	1.10	.20	1354	:04
79.8	94.9	.10	.20	.90	.20		
84.9	94.2	.10	.20	.90	.30		
90.1	89.5	.10	.30	.90	.40		
90.1	95.4	.10	.20	.90	.40		
90.2	99.7	.10	.30	1.10	.50		
93.0	101.3	.10	.50	1.10	.80		
94.8	94.6	.20	.40	.90	1.20		

SURGE CHECK NOT OK
OIL CONSUMPTION OK
CUSTOMER AIR CHECK NOT OK
BLEED BAND CLOSES AT .0 %N1

ANY QUESTIONS CONCERNING THIS ENGINE LOG SHEET MAY BE DIRECTED TO AUTOVON 8

FIG. 3.6.5

Engine Test Data with High Speed Balanced Turbine

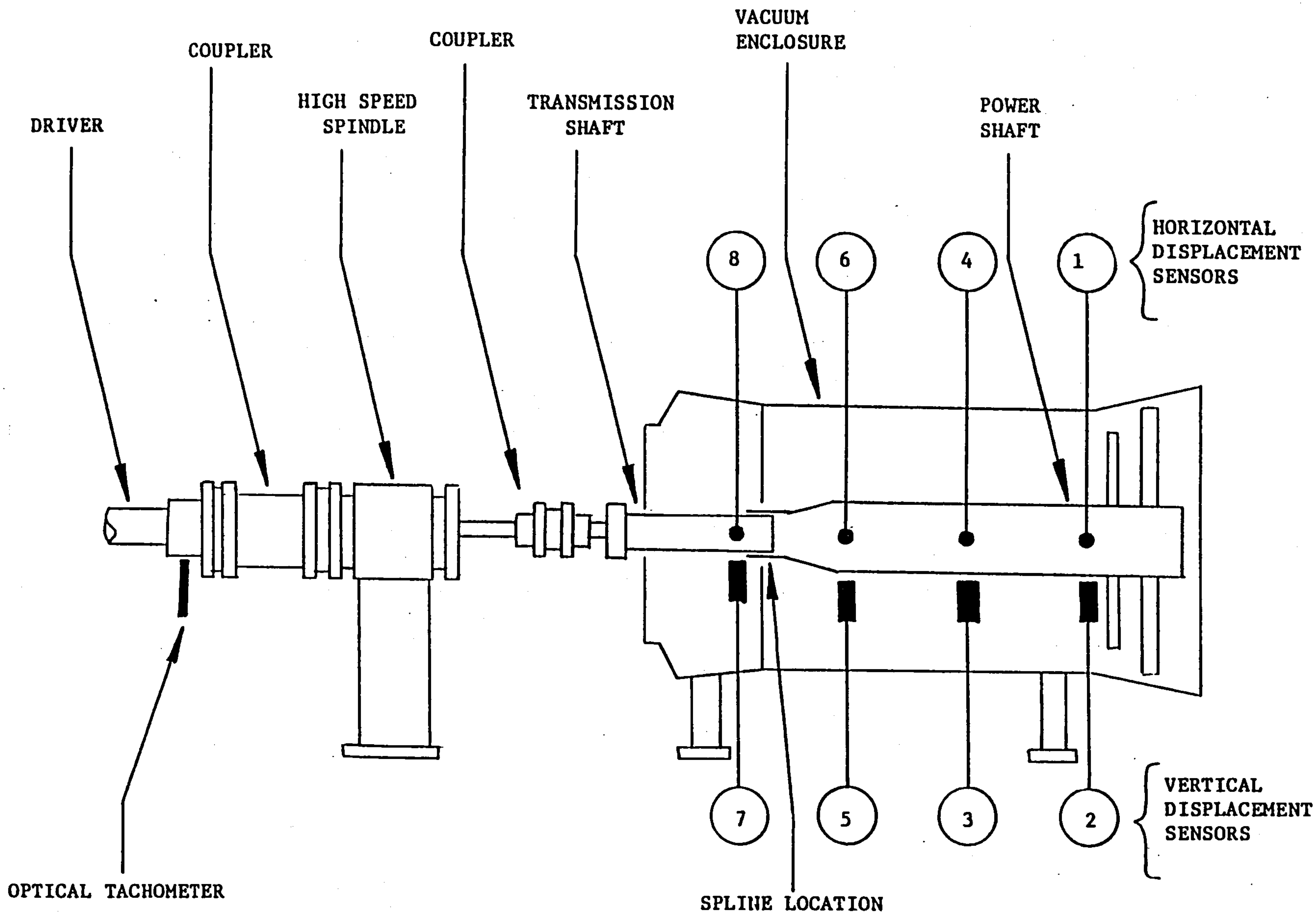

82682

FIG. 3.7.1 SPLINE TEST HARDWARE AND INSTRUMENTATION LOCATION

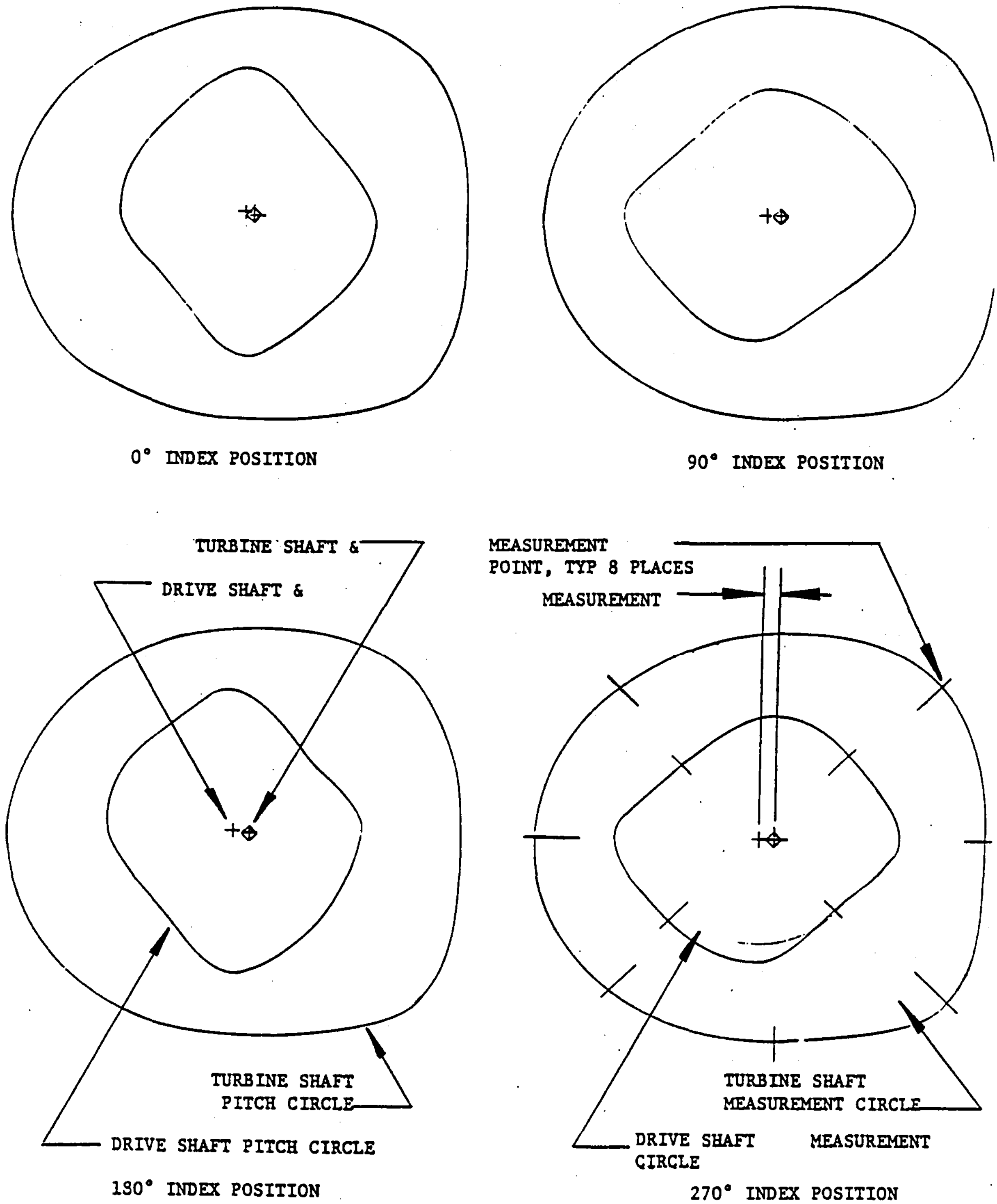

FIG. 3.7.2 PITCH CIRCLE SCHEMATICS FOR TURBINE SN 265503

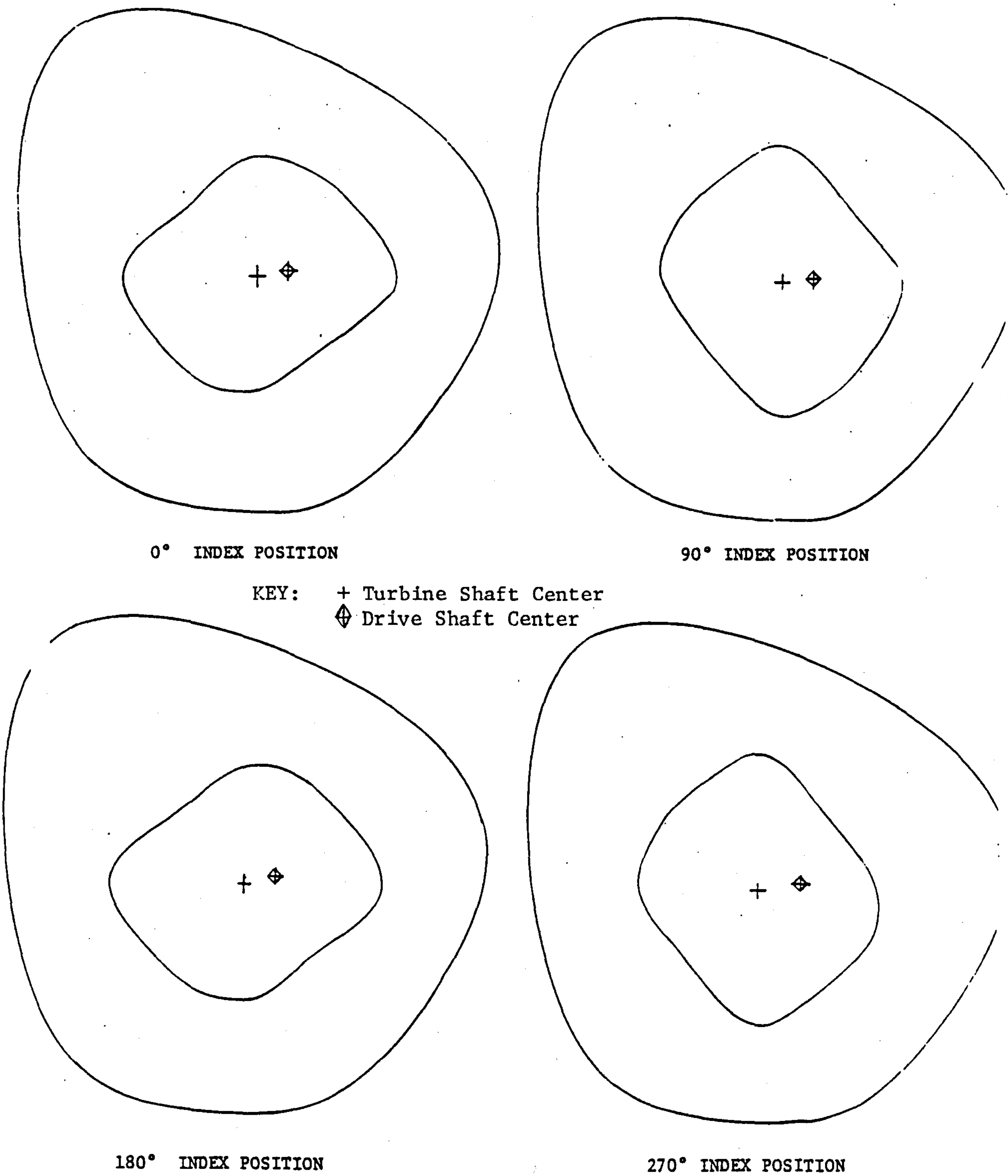

FIG. 3.7.3 PITCH CIRCLE SCHEMATICS FOR TURBINE SN U00257

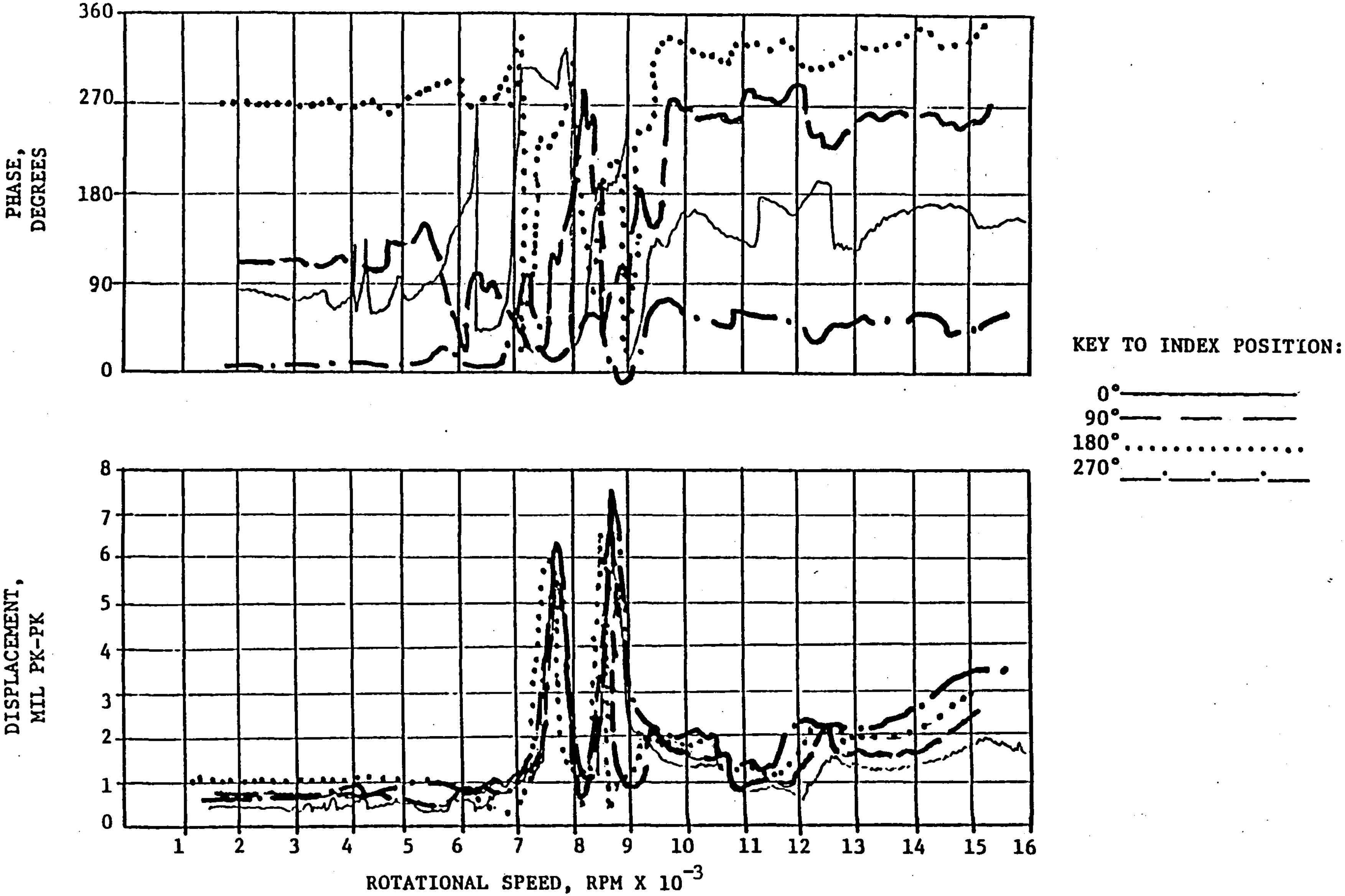

82681

FIG. 3.7.4 POWER SHAFT VERTICAL VIBRATION, PROBE 5, SN265503

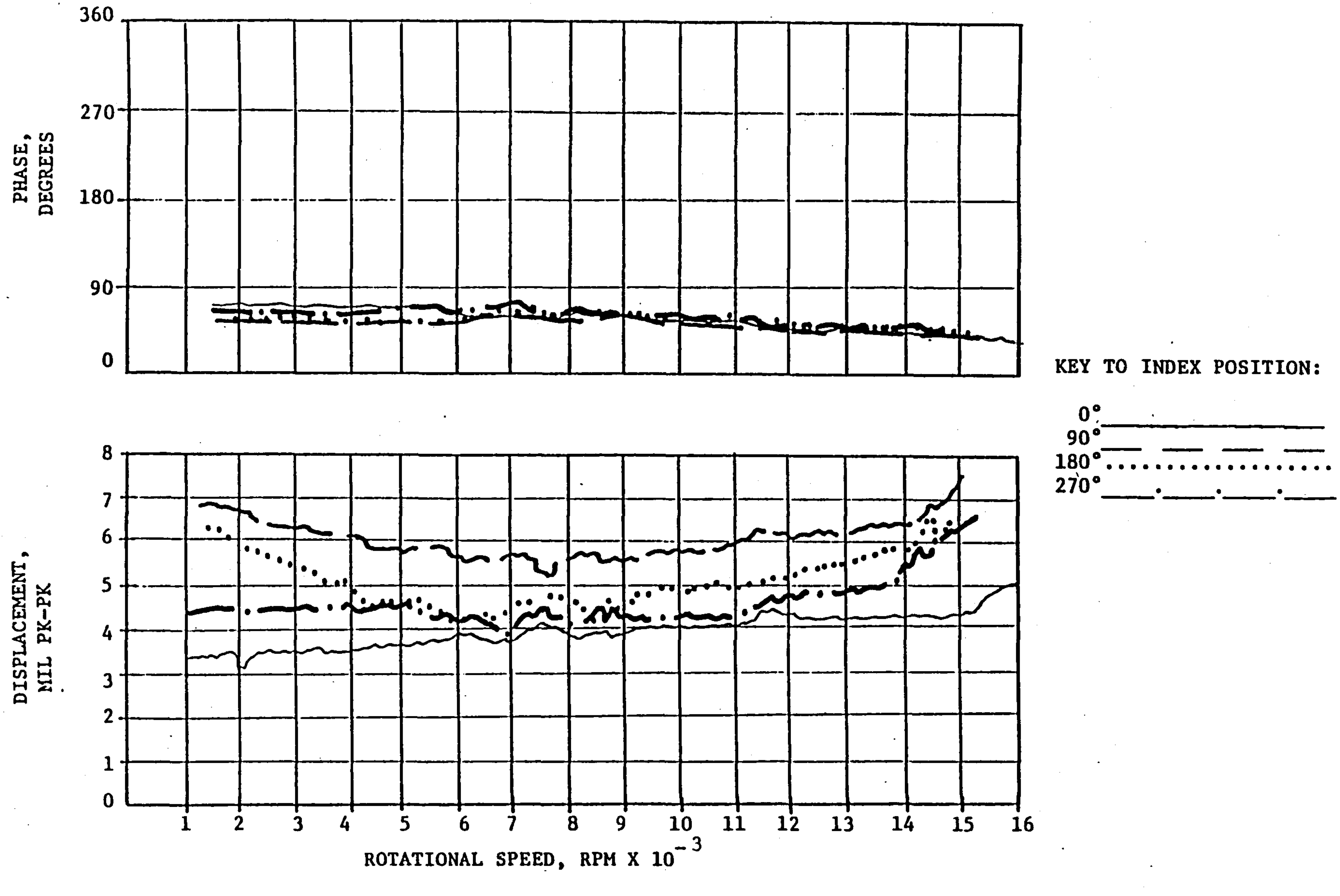

FIG. 3.7.5 TRANSMISSION SHAFT VERTICAL VIBRATION, PROBE 7, SN 265503

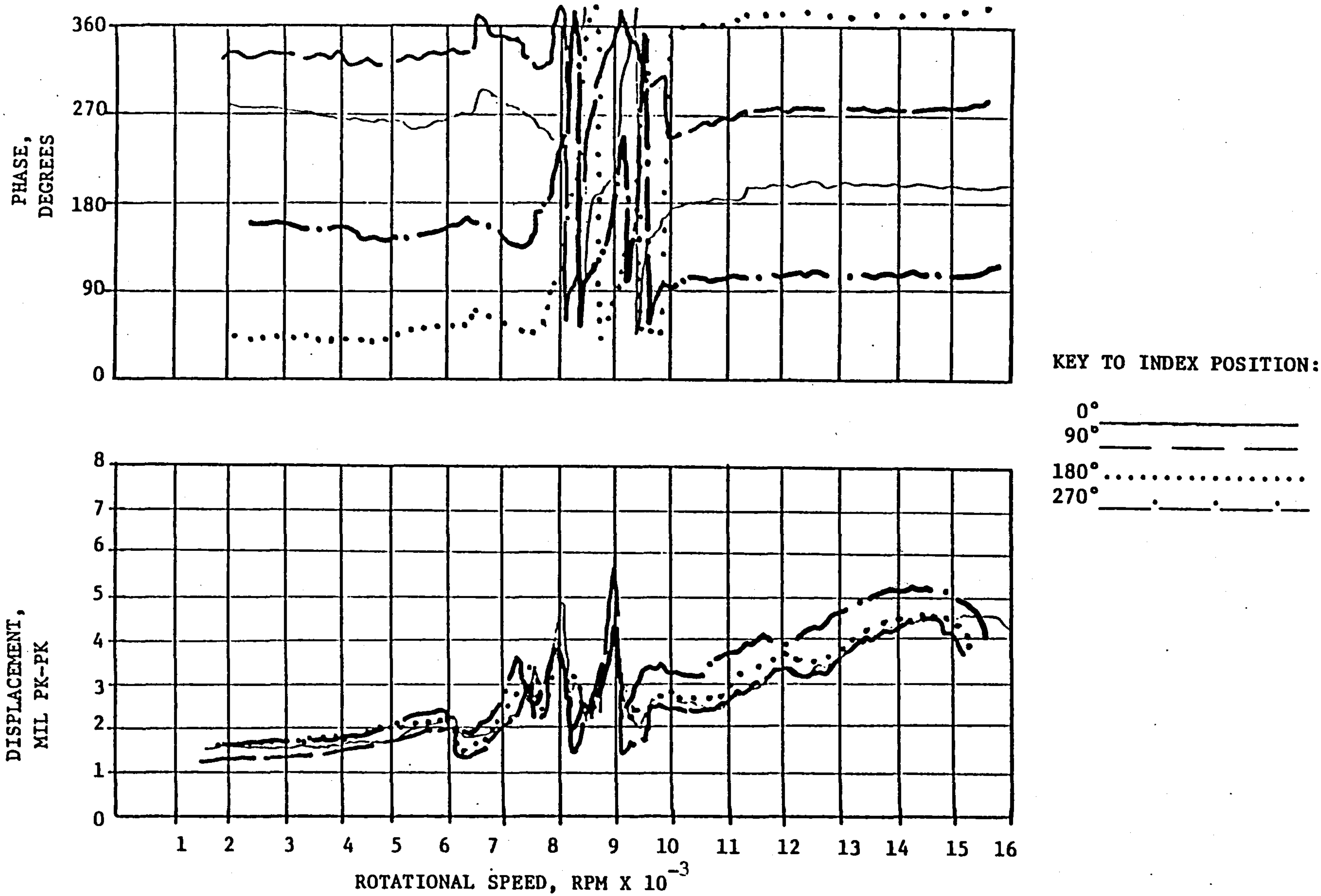

82679

FIG. 3.7.6 TURBINE DISK VERTICAL VIBRATION, PROBE 2, SN 265503

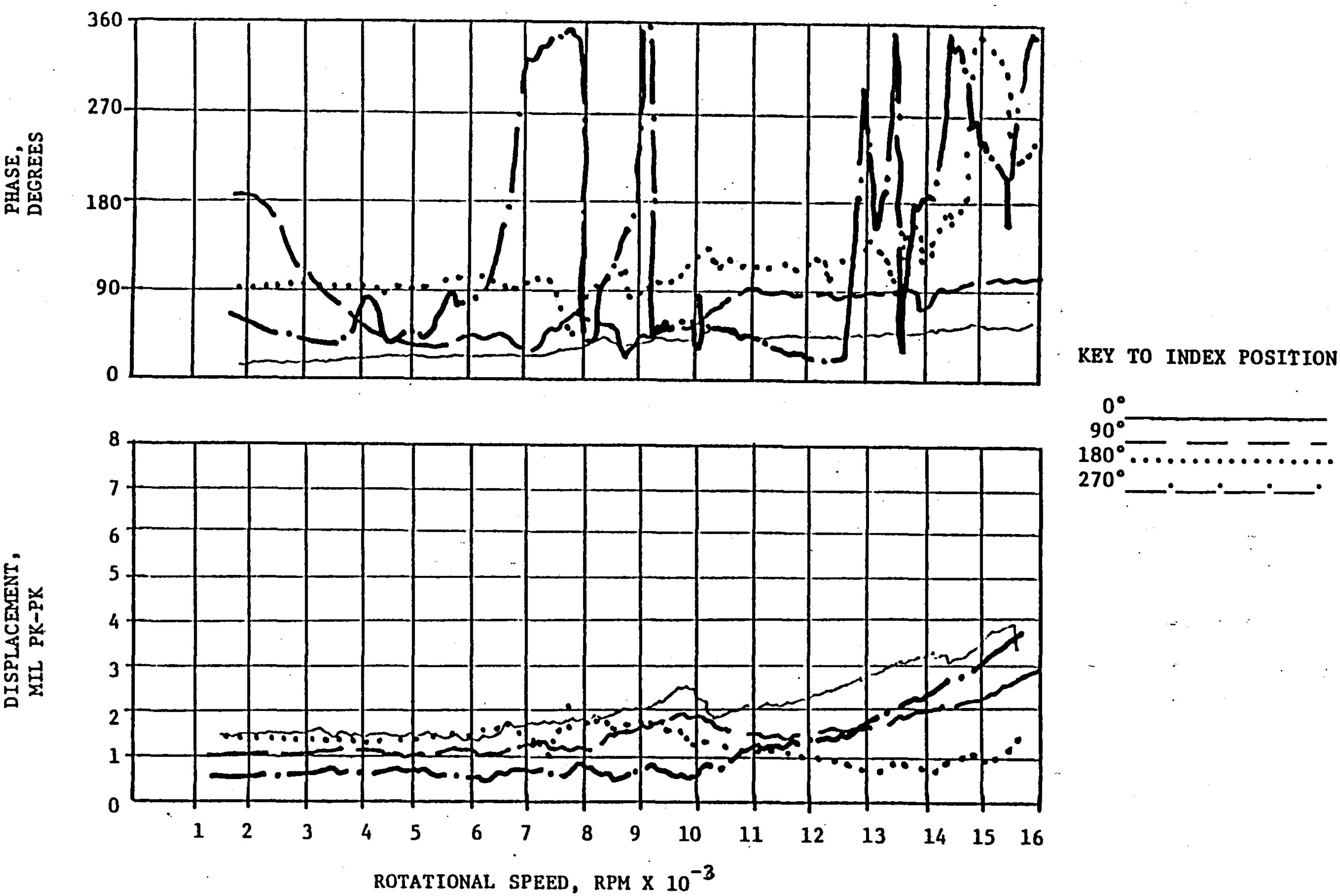

82678

FIG. 3.7.7 POWER SHAFT VERTICAL VIBRATION, PROBE 5, SN U00257

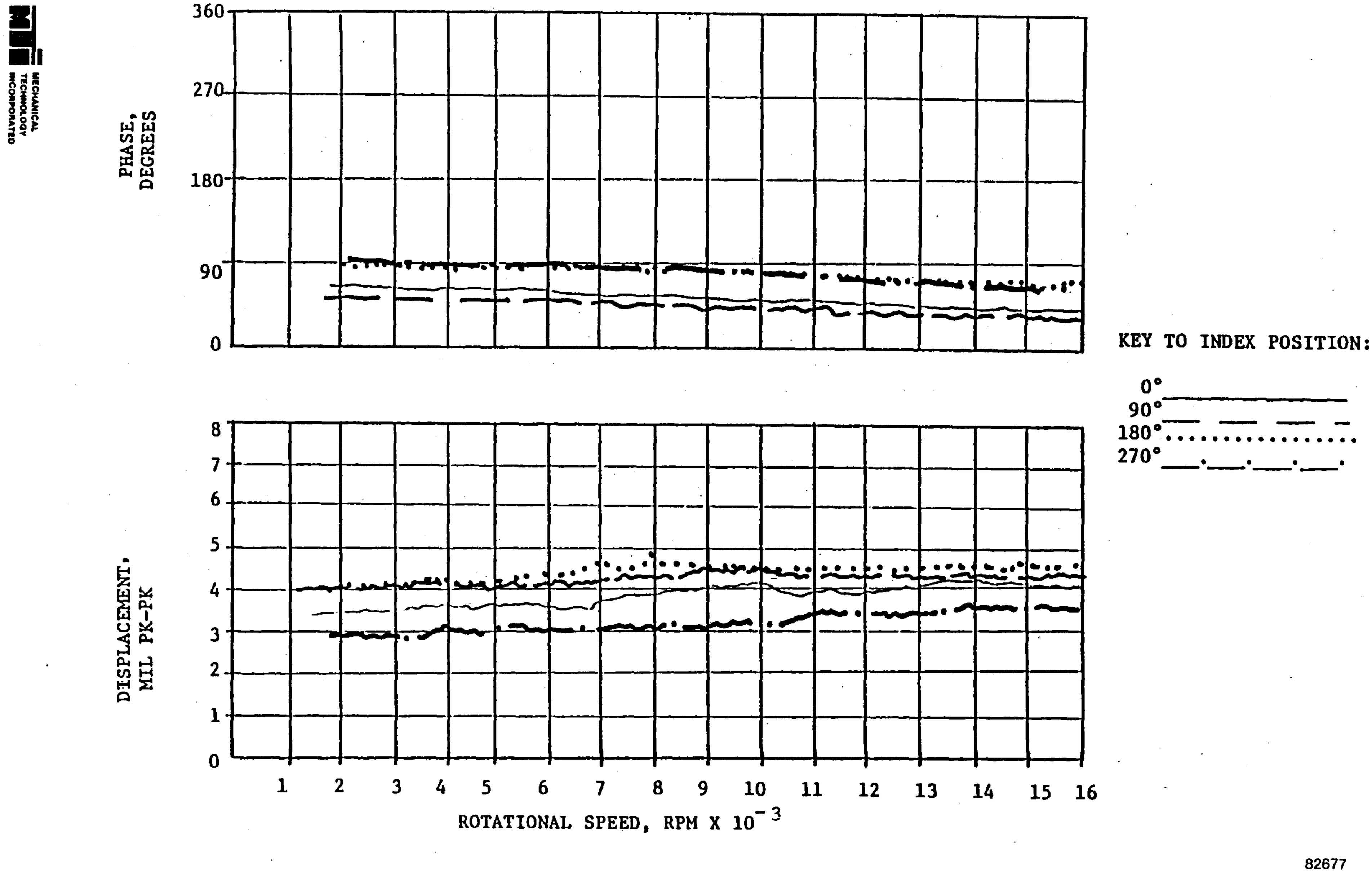

FIG. 3.7.8 TRANSMISSION SHAFT VERTICAL VIBRATION, PROBE 7, SN U00257

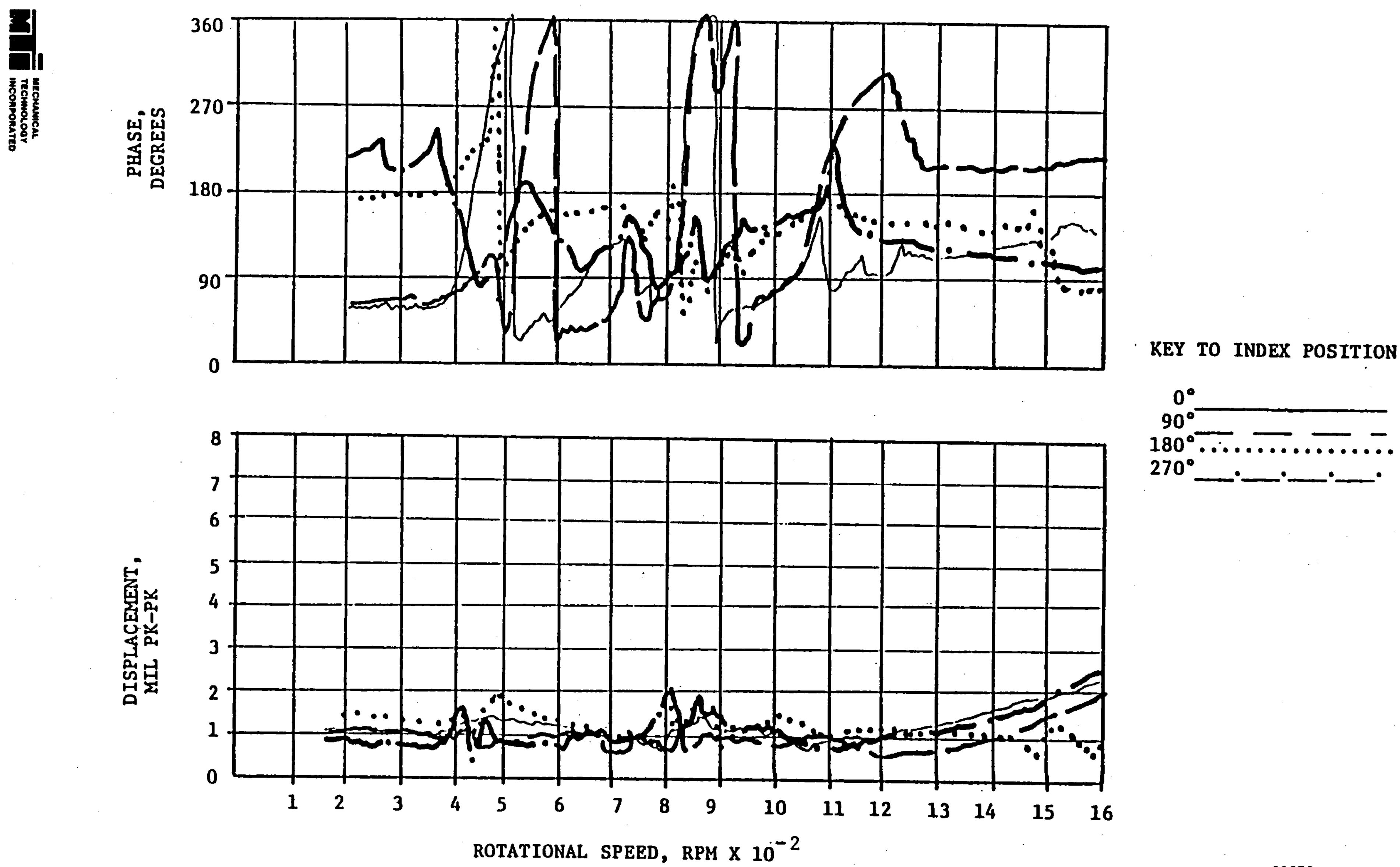

FIG. 3.7.9 TURBINE DISK VERTICAL VIBRATION, PROBE 2, SN U00257

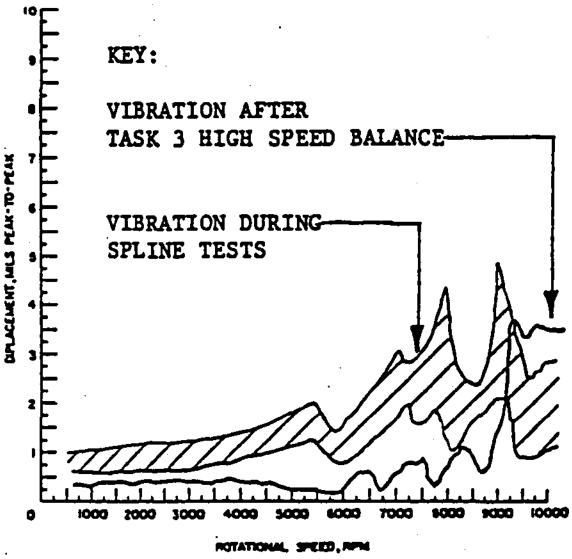

PROBE 2, TURBINE SN 265503

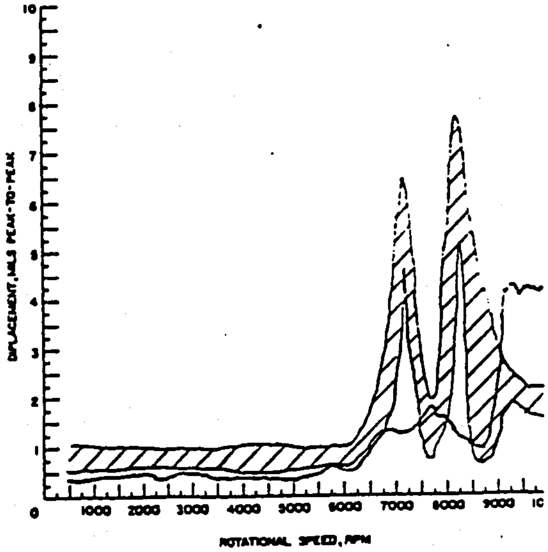

PROBE 5, TURBINE SN 265503

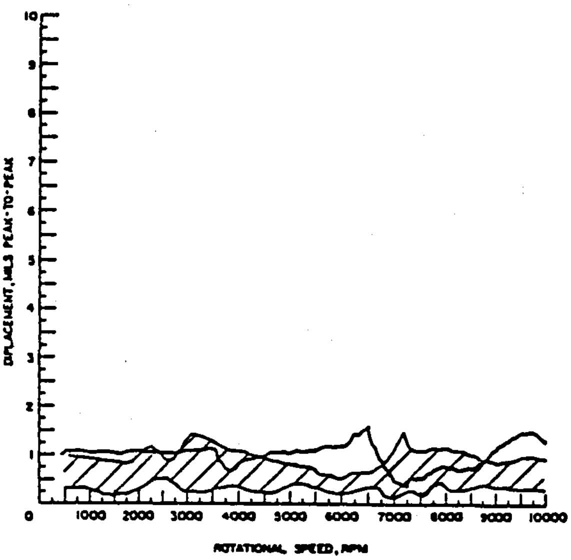

PROBE 2, TURBINE SN U00257

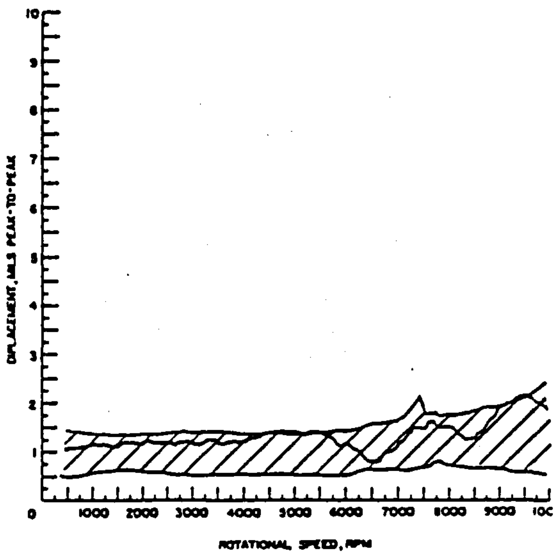

PROBE 5, TURBINE SN U00257

FIG. 3.7.10 VIBRATION RESPONSE AFTER HIGH SPEED BALANCE AND DURING SPLINE TESTS

TABLE 3.7.1 MEASURED SPLINE CLEARANCE

SN U00257			SN 265503		
INDEX POSITION	DIRECTION	CLEARANCE MIL-PK	INDEX POSITION	DIRECTION	CLEARANCE MIL-PK
0°	0°	4	0°	0°	6
	45	4		45	5
	90	5		90	5
	135	4		135	5
	180	5		180	5
	225	4		225	6
	270	4		270	5
	315	3		315	6
90°	0°	4	90°	0°	5
	45	5		45	5
	90	4		90	4
	135	4		135	4
	180	4		180	4
	225	5		225	5
	270	5		270	4
	315	5		316	5
180°	0°	5	180°	0°	5
	45	5		45	5
	90	4		90	5
	135	3		135	4
	180	4		180	4
	225	4		225	5
	270	5		270	5
	315	5		315	4
270°	0°	5	270°	0°	5
	45	5		45	5
	90	5		90	5
	135	4		135	5
	180	5		180	5
	225	5		225	5
	270	5		270	6
	315	5		315	6

End of Document